BOSTON UNIVERSITY

COLLEGE OF ENGINEERING

Dissertation

MODELING BY MANIPULATION – ENHANCING ROBOT PERCEPTION

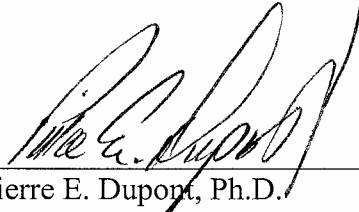**THROUGH CONTACT STATE ESTIMATION**

by

THOMAS DEBUS

B.S., University of Versailles, 1995
M.S., Boston University, 2000

Submitted in partial fulfillment of the

requirements for the degree of
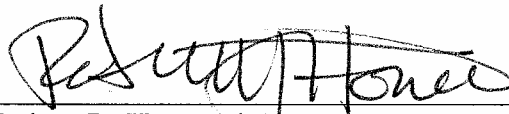
Doctor of Philosophy
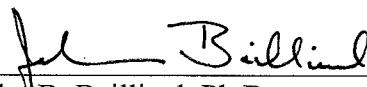
2005

Approved by

Advisor:

Pierre E. Dupont, Ph.D.
Associate Professor, Aerospace and Mechanical Engineering

Second Reader:
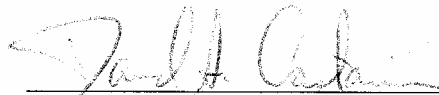
Robert D. Howe, Ph.D.
Gordon McKay Professor of Engineering,
Harvard University, Division of Engineering and Applied Scien

Third Reader:

John B. Baillieul, Ph.D.
Professor, Chairman, Aerospace and Mechanical Engineering

Fourth Reader:

David A. Castañon, Ph.D.
Professor, Electrical and Computer Engineering

Acknowledgements

First and foremost, I would like to thank Professor Pierre E. Dupont. His guidance and support have been invaluable, and his constant encouragements have allowed me to stay positive and determined in my research. Above all, he showed faith in my work and my ideas; without him, I could not have written this thesis.

I would like to express my gratitude to Professor Robert D. Howe for his enthusiasm, great insights and support. Not only did he contribute greatly with his ideas and knowledge, but he also opened the doors to his biorobotics laboratory. I would also like to thank Professor John B. Baillieul and Professor David A. Castañon for being my committee members.

Thanks to my many friends and colleagues at Boston University over the years. In particular I want to thank my fellow members of the Intelligent Mechatronics Laboratory. Special thanks to Jeff Stoll for the many valuable discussions about contact state estimation. I would also like to extend thanks to the entire staff of the Aerospace and Mechanical Engineering for their help and kindness.

Finally, I would like to thank my mother and brother for their unconditional love, encouragements, and support for many years. This dissertation is dedicated to them.

MODELING BY MANIPULATION – ENHANCING ROBOT PERCEPTION THROUGH CONTACT STATE ESTIMATION

(Order No.   )

THOMAS DEBUS

Boston University College of Engineering, 2005

Major Professor: Pierre E. Dupont, Ph.D., Associate Professor of
Aerospace and Mechanical Engineering.

ABSTRACT

Autonomous task performance is the ultimate goal of robotics. To this end, enhancing robot perception, the ability of a robot to recognize and model its environment, is essential. This thesis presents design tools for contact-based perceptual systems applicable to manipulation tasks which can be described by sequences of contact states between rigid objects. The fundamental component of such systems is a contact state estimator. This estimator uses sensor data collected as objects are manipulated to determine the sequence of actual contact states from a network of possible contact states. In the process, it also estimates the parameters, e.g., geometric parameters, of the individual contact state models.

In this thesis, a rigorous approach to contact state estimator design is proposed which involves characterizing four properties of a given contact state network, set of sensors, and associated contact state models. These properties are: (1) the distinguishability of contact states, (2) the observability of each contact state inside the state network, (3) the

identifiability of each contact state model's parameters, and (4) the excitability of the sensor inputs to permit estimation of all the parameters associated with a contact state model. The first two properties address the feasibility of contact state estimation, while the last two address the feasibility of estimating the parameters of the individual contact states.

The major contribution of this thesis is the development of a unified analytic approach to testing the distinguishability of contact states and the identifiability of their parameters. The testing method is applicable to any contact state model regardless of the chosen sensing modality. The concept of contact observability is also introduced as a forward projection of the parameter history associated with the execution of the task. The effect of the sensor signals on the parameters is analyzed by studying the invertibility of an excitability matrix representing the relationship between the structure of the contact states and the sensor signals. Finally, an implementation of a contact state estimator is presented using a hidden Markov model to combine a nonlinear least squares estimator with prior information from a contact state network.

Table of Contents

List of Tables

List of Figures

Chapter 1

Introduction

Robotic systems are used in a variety of manipulation tasks ranging from computer chip assembly to undersea connector mating. A vast majority of these systems can be classified into three categories: a) teleoperated systems, b) semi-autonomous systems, and c) autonomous systems, as illustrated in Fig. 1.1. Each of these systems is defined by two capabilities. The first is perception, which includes sensing and modeling the environment in which the robot operates. The second is action, which includes planning the sequence of motor commands to accomplish the task and controlling their execution. The discriminating factor between these three systems is whether the human or the machine is in charge of perception and action. Teleoperated and semi-autonomous systems are commonly used to perform manipulation tasks in poorly known environments since humans can adapt and react quickly to unplanned situations (e.g., space exploration, nuclear material handling, undersea oil development). Autonomous

systems, on the other hand, are currently restricted to assembly tasks in well-modeled environments (e.g., part mating assembly) since machine perception is limited in poorly known environments.
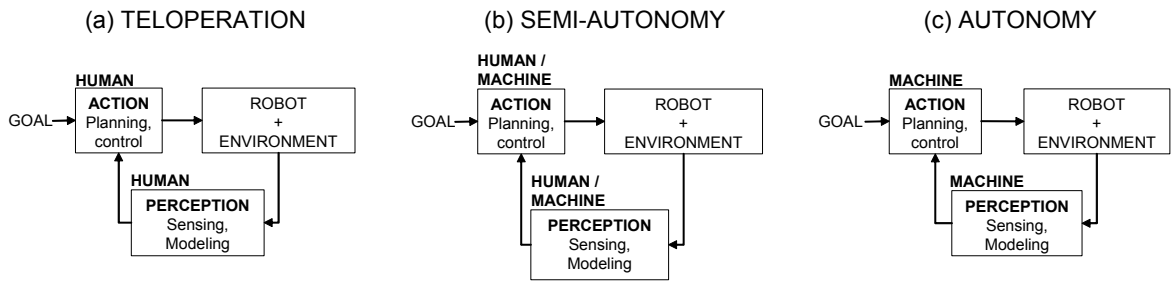
Figure 1.1: Robot classification.

A central goal of robotics research is the creation of robotics systems that can perform tasks autonomously in poorly known environments. To this end, enhancing the ability of a robot to perceive and model its environment is essential. In manipulation tasks, this level of perception depends on the fundamental ability of the system to detect and control contacts between manipulated objects. At each step of task execution, motion planning and control involve moving from one contact state to another. In these situations, the robot must be able to recognize and distinguish among all of the contact states involved in task execution. Furthermore, in order to implement contact-based motion planning and control laws, it is necessary to estimate during contact the parameters (e.g., geometric parameters) describing the contact. These two problems of contact state estimation and parameter estimation constitute the core of perceptual systems applicable to manipulation

tasks. In such systems, a fundamental tool to solve this dual estimation problem is a contact state estimator. This estimator uses sensor data collected as objects are manipulated to determine the sequence of actual contact states from a network of possible contact states. In the process, it also estimates the parameters of the individual contact state models.

The objective of this thesis is to provide design tools that assess the feasibility of implementing a contact state estimator given a set of sensors, a list of parameterized contact state models, and a contact state network representation of the task. This research addresses four important properties required for the implementation of the estimator. These properties are: (1) the distinguishability of contact states, (2) the observability of each contact state inside the state network, (3) the identifiability of each contact state model's parameters, and (4) the excitability of the sensor inputs to permit estimation of all the parameters associated with a contact state model.

This chapter provides an overview of the construction of a contact state estimator. In particular, it is shown that the design and implementation of an estimator requires the solution to nine sub-problems, seven of which are part of the design process. The next section introduces and defines these sub-problems. The following section lists the assumptions on the contact models utilized in this thesis and defines the concept of *poorly known environments* with respect to these assumptions. An outline of the work presented in this thesis is described at the end of the chapter.

1.1 Contact State Estimator

Manipulation tasks can be represented as collections of contact states that describe how the manipulated object is in contact with objects in the environment. As an example, Fig. 1.2 illustrates a possible sequence of contact states associated with a planar peg-in-hole insertion task. The number of contact states corresponds to the number of possible contacts between the features of the manipulated peg and its environment (e.g., vertices, edges). In this example, the set of all possible states comprises all the one-point contacts, two-point contacts and line contacts between the peg and the hole. Note that Fig. 1.2 shows one possible contact state sequence; however, other sequences exist.
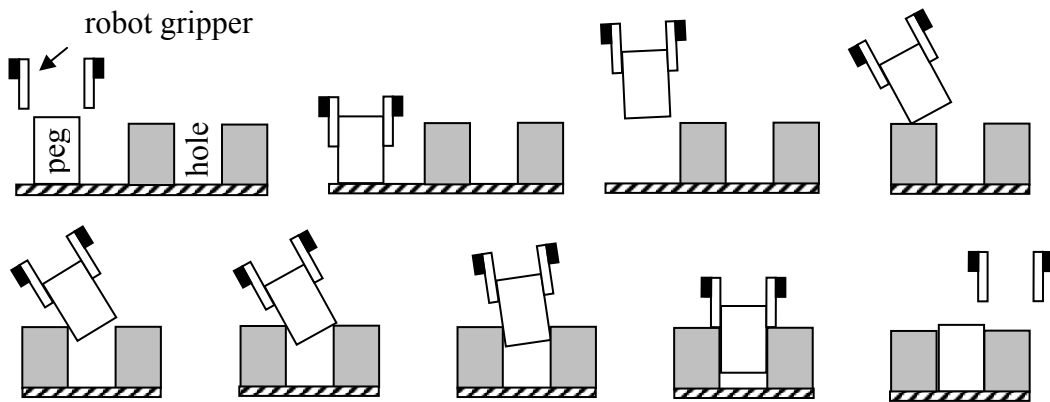
Figure 1.2: Peg-in-hole insertion decomposed into a sequence of contact states.

The completion of the peg-in-hole insertion task shown in Fig. 1.2 requires a control algorithm that depends on the nature of the contact states as well as the parameters characterizing these contacts (e.g., location of the hole, dimension of the peg). For example, different control laws must be applied whether the peg is inside or outside the

hole. Similarly, the gains of the controller must be set differently if the hole is tilted or not. In the context of poorly known environments; however, this information is partially known and needs to be accurately estimated using a contact state estimator. As shown in Fig. 1.3, contact state estimation in a poorly known environment is a dual problem involving the estimation of contact parameters as well as contact states, given a task description and a set of sensors. These two estimates can then be used in a control algorithm and a motion planner to achieve robot autonomy.
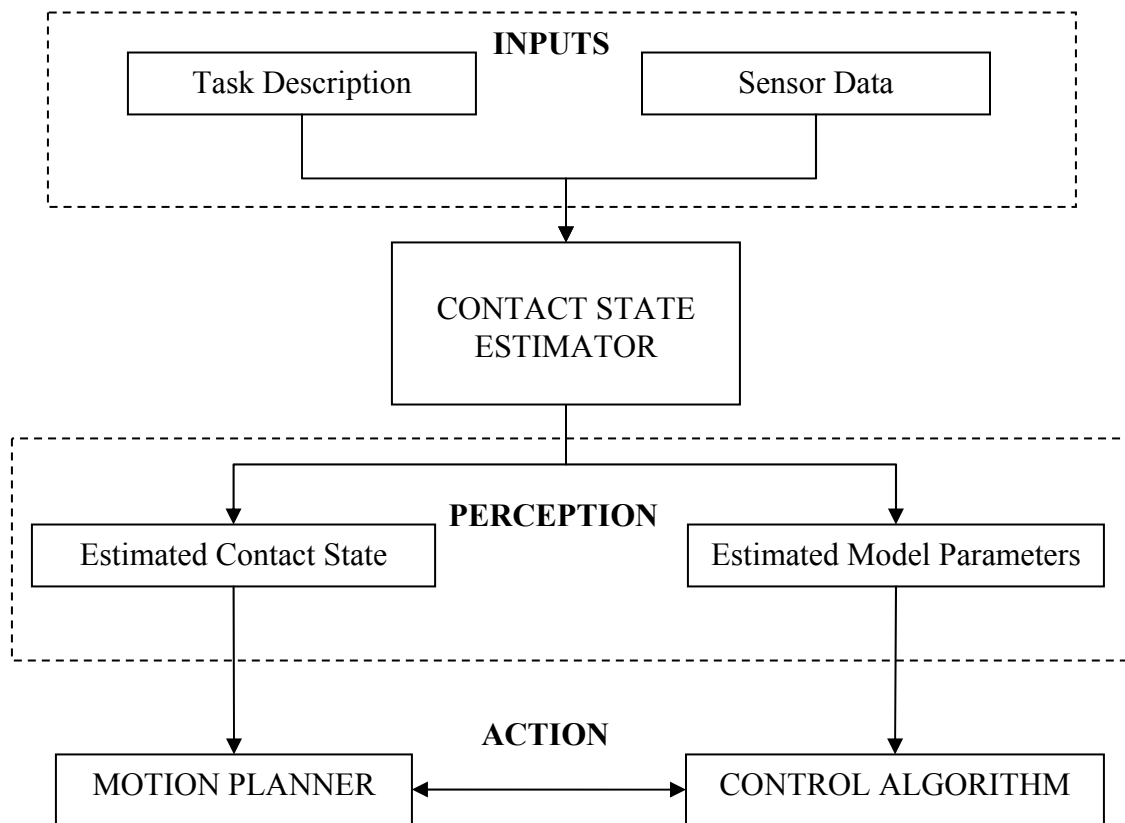
Figure 1.3: Perceptual system applicable to manipulation tasks.

1.1.1 Design of a Contact State Estimator

Given a manipulation task (e.g., pick-and-place, peg-in-hole insertion) and a list of contact states describing the possible geometric interactions among the objects in contact (i.e., contact topology), the goal of the design process is: 1) to encode the task into a network of states in which each node represents a possible contact state, and 2) to model each contact state as an equation that relates the sensors of the manipulating robot and the parameters of the objects in contact. As illustrated in Fig. 1.4, seven problems need to be solved when designing a contact state estimator: 1) task representation, 2) contact state modeling, 3) task encoding, 4) contact state identifiability, 5) data excitation, 6) contact state distinguishability and 7) contact state observability. Contact state modeling and task encoding constitute the outputs of the design process. The last four problems of Fig. 1.4 are used to verify that these two outputs satisfy the conditions of identifiability, excitability, distinguishability, and observability necessary to the implementation of a contact state estimator. As noted in the figure, detailed descriptions of these seven problems are presented in various chapters of the thesis. Brief definitions of the problems are as follows:

1) Task representation: The objective of this step is to resolve the task into a sequence of contact states between the manipulated object and the fixed objects in the environment. This procedure is divided into two parts. First a list of elementary contact states (i.e., contact topology) representing the possible contact interaction between the objects in the task is chosen. Then, these elements are used to decompose the task into a graph of possible contact state sequences.

2) <u>Contact state modeling:</u> Mathematical models are needed for each contact state. This modeling problem is addressed by finding constraint equations that are used to relate the sensor data, $s(t)$, and the parameters p characterizing the objects in contact.

3) <u>Task encoding:</u> The goal of the encoding phase is to find a mathematical way of representing the information associated with the task. The proposed solution is to represent the contact state graph using a probability transition matrix in which each element corresponds to the likelihood of transition between states.

4) <u>Contact state identifiability:</u> The identifiability test verifies that the parameters associated with each contact state model can be estimated from the available sensing modalities.

5) <u>Data excitation:</u> Sensor data need to be sufficiently exciting to estimate all the parameters associated with a contact state model. The objective of the data excitation step is to find sensor paths that can ensure the estimation of all the parameters associated with a given contact model.

6) <u>Contact state distinguishability:</u> Distinguishability tests if the proposed contact state models and associated sensors are sufficient to disambiguate each contact state from the others in a given list of elementary contact states. For a given task, the result is to assemble contact states into subsets which are distinguishable from each other.

7) <u>Contact state observability:</u> Observability verifies that each state in a given contact state network is distinguishable using sensor and task information. This implies that task information is sufficient to disambiguate the contact states within each distinguishable subset of states.

robot gripper

peg hole

TASK

1. TASK REPRESENTATION

Contact Topology *(chapter 3)*   Task Decomposition *(chapter 5)*

C_1 C_2 C_3 ... C_1 C_2 C_4 ...

2. CONTACT STATE MODELING
(chapter 3)

$$C_1: f_1\big(s(t), p_1\big) = 0$$
$$C_2: f_2\big(s(t), p_2\big) = 0$$
$$\vdots$$

3. TASK ENCODING
(chapter 5)

a_{11} a_{22} a_{33} a_{44}

$\mathbf{C_1}$ $\begin{matrix}a_{12}\\a_{21}\end{matrix}$ $\mathbf{C_2}$ $\begin{matrix}a_{23}\\a_{32}\end{matrix}$ $\mathbf{C_3}$ $\begin{matrix}a_{34}\\a_{43}\end{matrix}$ $\mathbf{C_4}$

$\begin{matrix}a_{13}\\a_{31}\end{matrix}$ $\begin{matrix}a_{24}\\a_{42}\end{matrix}$

$\begin{matrix}a_{14}\\a_{41}\end{matrix}$

4. CONTACT STATE

IDENTIFIABILITY

(chapter 4)

6. CONTACT STATE

DISTINGUISHABILITY

(chapter 4)

5. DATA

EXCITATION

(chapter 6)

7. CONTACT STATE

OBSERVABILITY

(chapter 5)

Figure 1.4: The seven design steps of a contact state estimator.

As illustrated in Fig. 1.4, the sub-problems associated with the design of a contact state estimator can be interdependent. For example, distinguishability, identifiability, and data excitation use analytical techniques that are based on the equations provided by the modeling step of the design process. Observability analysis requires distinguishability testing to investigate the distinguishability of every contact state inside a given contact state graph. Similarly, the data excitation step utilizes contact state models that have been shown to be identifiable since the parameters associated with an unidentifiable contact models cannot be estimated regardless of the chosen sensor path.

Contact state modeling and task encoding result in mathematical representations of both the contact states and the contact state graph that are then utilized in the implementation of the estimator. As shown in Fig. 1.4, the design of the contact state models and the design of the contact state network are iterative processes that depend on the results of the identifiability test, data excitation test, and observability test. For example, if contact models are shown to be unidentifiable, then they need to be remodeled (e.g., alternate sensing modality) or removed from the list of candidate contact states. Similarly, an unobservable contact state network must be modified until it satisfies the observability property.

1.1.2 Implementation of a Contact State Estimator

Given a set of sensors, a list of parameterized contact state models, and a contact state network representation of the task, the implementation phase focuses on building a contact state estimator that generates the most likely sequence of contact states

corresponding to the data as well as the states' associated parameters. As illustrated in Fig. 1.5, this filter requires an estimation algorithm and a detection algorithm. These are defined as follows:

8) Multiple Model Estimation: Given a sequence of sensor data points and a contact state network obtained from the design phase, a multiple model estimation algorithm is implemented to estimates the parameters and residual associated with each contact model of the state network. The implementation of a multiple model estimation algorithm using sliding nonlinear least squares is presented in Chapter 6.

9) Contact State Estimation: The decision algorithm is built around a decision test that requires two inputs. First, estimation residuals are used to judge how well a portion of the data stream fits the possible contact states. Second, conditional probability theory is used to adjust these results to account for knowledge of prior and anticipated contact states as embodied in the task's contact state network created in the design phase. A decision test based on hidden Markov model is discussed in Chapter 7.

Contact State Modeling   **Sensor Data**   **Task Encoding**

MULTIPLE MODEL ESTIMATION

Contact model

$C_1 : f_1(s(t), p_1) = 0$

Contact model

$C_2 : f_2(s(t), p_2) = 0$

Contact model

$C_n : f_n(s(t), p_n) = 0$

8. ESTIMATION ALGORITHM
(chapter 6)

Parameter estimate p_1
and residual ε_{p_1}

Parameter estimate p_2
and residual ε_{p_2}

Parameter estimate p_n
and residual ε_{p_n}

CONTACT STATE ESTIMATION

9. DECISION
ALGORITHM
(chapter 7)

a_{11} a_{22} a_{33} a_{44}

C_1 C_2 C_3 C_4

PERCEPTION

Estimated Model Parameters

Estimated Model Parameters

ACTION

MOTION PLANNER

CONTROL ALGORITHM

Figure 1.5: Implementation schematic of a contact state estimator.

1.2   Assumptions

Without loss of generality, contact models are considered for pairs of objects. One object, termed the manipulated object, is assumed to be gripped and manipulated by a robot. The second object is called the environment object. The concept of a *poorly known environment* is defined by the following assumptions:

- Objects are rigid polygons or polyhedrons of known shapes but unknown dimensions.
- The manipulated object does not slip in the gripper.
- The environment object is fixed with respect to a world coordinate frame.
- In the most general case, the configuration (position and orientation) of the manipulated object with respect to the gripper is unknown and the configuration of the environment object with respect a world frame is unknown. The parameters associated with the objects' configurations (6 for polygonal models and 12 for polyhedral models) constitute unknown parameters in the contact models.
- Contact models are comprised of nonlinear equalities involving configuration parameters and sensor variables. Inequality constraints (e.g., overlap constraint and non-penetration constraint) are not considered.
- Uncertainty in sensor variables (noise) is not considered in the design phase of the estimator; however, it is considered in its implementation phase.

These assumptions can be directly related to the four types of uncertainties typically considered in the literature: sensing uncertainty, manufacturing uncertainty (i.e., uncertainty in the shape and dimension), uncertainty in the location of the manipulated object inside the gripper, and uncertainty in the location of the static objects inside the environment (Rosell et al. 2001). In this thesis, sensing uncertainties are implicitly considered in the implementation of the contact estimator but not in its design. The effect of manufacturing on the shape of the objects is not considered (i.e., a flat surface is not considered as a curved surface due to manufacturing uncertainties). The last two types of uncertainties are considered since the locations of the manipulated and fixed objects are assumed to be unknown.

1.3 Outline of the Thesis

Chapter 2 presents a literature survey on contact estimation and discusses its relevance to contact state estimation in poorly known environments. First, prior work on contact state estimation is reviewed with respect to the nine sub-problems presented in Fig. 1.4 and Fig. 1.5. Next, the limitations of the prior work in the context of poorly known environments are discussed and related to the contributions of this thesis.

Figures 1.4 and 1.5 provide a map for the organization of this thesis and illustrate how the construction of a contact state estimator is analyzed throughout the chapters of this document. Chapter 3 starts by reviewing the contacting topology used to describe contact states geometrically. The second part of this chapter describes the modeling of contact

states using pose, velocity and force measurements. In particular, it is shown how contact states can be modeled as homogeneous nonlinear algebraic equations parameterized by time-dependent sensor data and time-independent parameters representing the unknown locations and positions of the two objects in contact. An illustration of the three modeling techniques is provided at the end of the chapter.

Chapter 4 defines the problems of distinguishability and identifiability in the context of contact state estimation. Both problems are based on finding sets of time-independent parameters that can satisfy the contact models simultaneously. As one of the major contributions of this thesis, a unified solution to the two problems is proposed using Taylor series expansion. In this framework, the structure of the contact models is decomposed as sets of algebraic equations given by the Taylor coefficients. Distinguishability and identifiability of contact state models are then analyzed by solving these sets of equations for the time-independent unknowns parameterizing the contact states. This technique is implemented for several contact states modeled using kinematic sensing. A complexity analysis, based on the structural properties of the kinematic equations is presented at the end of the chapter.

Chapter 5 addresses the problem of task feasibility in poorly known environments. To this end, the observability of the contact state graph representing the task is analyzed. A solution to this problem is given by combining distinguishability testing with the information contained in the history of the estimated parameters associated with the

execution of the task. Once the contact state graph is shown to be observable, the encoding of the task is addressed using a probability transition matrix.

Chapters 6 and 7 focus on the implementation of a contact state estimator. The realization of an estimation algorithm suited to parameter estimation in poorly known environments is discussed in Chapter 6. First, the Levenberg-Marquardt, a nonlinear least squares technique shown to be robust to poorly known initial conditions is reviewed as well as the excitation condition necessary to its implementation. Thereafter, an explicit estimation scheme based on multiple differentiations and nullspace analysis is presented. This method proves to be fast, but too sensitive to noise to be practically implemented. However, the analytical nature of the technique provides valuable insights on the type of exciting paths necessary for the estimation of the parameters associated with the contact state models.

Chapter 7 focuses on the implementation of a contact state detection algorithm. The assessment is performed by a Hidden Markov Model (HMM), which combines a measure of how well each set of contact equations fit the sensor data with the probability of specific contact state transitions. The approach is illustrated for a three dimensional peg-in-hole insertion using a tabletop manipulator robot. Contact states are modeled by pose equations parameterized by time-dependent sensor data and time-independent object properties. At each sampling time, multiple model estimation coupled with an HMM are

used to assess the most likely contact state. Using only position sensing, the contact state

sequence is successfully estimated without knowledge of nominal parameter values.

Chapter 8 concludes the thesis by summarizing its contribution to the field of contact

state estimation. Suggestions for future research are also presented at the end of the

chapter.

Chapter 2

Prior Work

Contact state estimation has been applied to a variety of applications, including model-based compliant motion (De Schutter et al. 1999, Lefebvre et al. 2003), fine manipulation (McCarragher and Asada 1996, Eberman 1997), task monitoring (McCarragher and Asada 1993, Hannaford and Lee 1991), man-machine cooperation (Dupont et al. 1999, Debus et al. 2000) and robot learning (Pook and Ballard 1993, Skubic and Volz 2000). The contact state estimators used in these applications are designed and implemented using analytical and numerical tools that can provide solutions to one or several of the sub-problems illustrated in Fig. 1.4 and Fig. 1.5. This chapter presents an overview of these tools and discusses their limitations in the context of poorly known environments.

The first section reviews prior work on contact state estimation and its associated sub-problems. This section is divided into two parts. First, a review of contact state estima-

tors available in the literature is presented. Then the most relevant techniques found in the robotic literature with respect to each of the sub-problems defined in Chapter 1 are reviewed. The next section summarizes the limitations of the current techniques applicable to contact state estimation. Based on these limitations, the objectives of this thesis are presented at the end of the chapter.

2.1 Contact State Estimator

Using contact states to perform manipulation tasks is not a new concept. The concept originated from work in fine motion planning and force control in which researchers quickly realized that a task is a contact-driven process that requires appropriate parameter-dependent control laws at each of its contact phases. One of the first papers to propose a solution to this problem is due to Asada and Hirai (1989). Their work formalized the concept of contact state estimation by reducing it to three components: symbolic representation of assembly processes (i.e., task representation in this text), contact state modeling, and contact state classification (contact state detection in this text). This technique was implemented successfully to monitor ten contact states during a frictionless quasi-static part-mating assembly task (Hirai 1994). The approach was limited to tasks with a known geometry (i.e., object shape and size were known, the location of the object inside the gripper was known, the locations of the objects in the environment were known).

Recent works on parameter-based contact state estimation are focusing on relaxing these constraints. In this context, contact state estimation becomes a dual coupled

estimation problem in which both contact states and their parameters are estimated. Progress in contact state modeling and parameter estimation has been driven by research in model-based compliant motion (e.g., Bruyninckx 1995, De Schutter et al. 1999, and Lefebvre et al. 2003). In Bruyninckx for example, twist and wrench measurement equations are utilized to model contact states as virtual mechanisms parameterized by the first and second order geometric properties of the contact surfaces. These parameterized models are then used as the measurement equations of a Kalman filter (De Schutter et al. 1999). Contact transitions are detected by monitoring the consistency of the filter's innovations using a statistical threshold. In Eberman (1997), contact state estimation is performed using a statistical observer. The observer uses maximum likelihood to estimate the parameters associated with linear contact models, and then a sequential hypothesis tester based on the estimation's log-likelihood is utilized to detect contact state transitions. This approach presents the advantage of using a common language (i.e., probability) to model and detect the contact states. As a result, contact models can be easily augmented without changing the detection algorithm (e.g., add probabilistic impact model, add probabilistic vibration model).

Both of these approaches assume relatively small uncertainty and good nominal values for the parameters. Therefore, these techniques cannot be used in a poorly known environment; nevertheless, they provide a good foundation upon which to build a contact state estimator.

Many of the concepts presented in this thesis have been defined in the context of fine motion planning in semi-structured environments. The objective of the next sections is to

list the most relevant techniques with respect to the sub-problems defined in Chapter 1 (i.e., task representation, contact modeling, task encoding, contact state identifiability, contact state distinguishability, contact state observability, data excitation, parameter estimation, and contact state estimation).

2.1.1 Task Representation

Two major approaches are commonly used to represent tasks: the explicit approach and the model-based approach (Park 1977). In the explicit approach, the task is represented by the actions that are needed to bring it to completion (e.g., grasp, move, insert). In the model-based approach, the task is described in terms of the geometric objects involved in its completion (e.g., polygons, polyhedrons). The lack of detail in the explicit approach can leave some flexibility in the representation that can lead to multiple representations. On the other hand, the model-based approach offers a level of detail that can be used to represent tasks uniquely and automatically (e.g., Lozano-Perez 1981, Asada and Hirai 1989). This section only reviews prior work on model-based task representation. Geometric and force representations are reviewed with an emphasis on geometric representation.

Geometry-based Task Representation

Two questions must be addressed when representing a task using geometry: what are the geometric 'building blocks' utilized in the representation? How can they be used to

discretize the task? These two issues are commonly defined in the literature as contact topology and task decomposition.

Contact Topology

In the context of motion planning, tasks are typically described using rigid concave or convex polygons or polyhedrons (e.g., Ambler and Popplestone 1975, Lozano-Perez 1981). This assumed geometry of the task allows for its natural decomposition into sets of primitive geometric constraints called contact states in Asada and Hirai (1989), elemental contacts in Desai and Volz (1989), or principal contacts in Xiao (1993). Several contacting topologies have been proposed in the literature to describe contact states in terms of contacting elements such as vertex, edge, and face (e.g., Lozano Perez 1983, Desai and Volz 1989, and Xiao 1993). The most complete topology is provided by Xiao (1993). In this approach, contact states primitives are called principal contacts and are described as pairs of contacting elements which are not part of the boundaries of other contacting elements. For example, a face-face contact is considered as a single face-face contact and not as a combination of vertex-face or edge-face contacts. In this framework, Xiao showed that a task can be decomposed into contact formations that can be described by combining four principal contacts in the polygonal case and ten principal contacts in the polyhedral case.

The contact state decomposition of manipulation tasks involving curved objects remains an open problem. Recent progress has been made by Luo et al. (2004). In this

work, the concept of principal contact has been extended to curved objects by segmenting their curvature into curve segments and surface patches.

Task Decomposition

While task topology deals with the problem of defining a set of possible contact states that can be used to describe a task, task decomposition looks at the possible connections between contact states. This step is at the root of any motion planning approach since it provides a map of the possible strategies that can lead to task completion. A common tool used in motion planning is the concept of configuration-space obstacles introduced by Lozano-Perez (1981, 1983). In this representation, the configurations (i.e., positions and orientations) of the manipulated block in the Cartesian space correspond to points in the configuration space. The end result of a configuration space obstacle is a manifold that corresponds to all the possible configurations that result in contacts between a manipulated object and its environment. In a contact state point of view, this manifold can be partitioned into regions that correspond to the different contact states composing the task (e.g., C-surface in Mason 1981). Computation of configuration spaces has been an important research topic in the motion planning community, and as a result many algorithms are available (e.g., gross motion planning survey by Hwang and Ahuja 1992). Nevertheless, the complexity of the computation is such that computing configuration spaces for complex 3D models remains an open problem.

As an alternative to configuration spaces, contact state graphs can also be utilized to decompose tasks (e.g., Asada and Hirai 1989, Desai and Volz 1989, Hirukawa et al.

1994, and Xiao and Ji 2001). This concept, introduced by Asada and Hirai (1989),

reduces a task to a discrete representation given by a graph in which each node represents

a contact state and each link represents a possible transition from a contact state to

another. In contrast to configuration space representations that result in a continuous

representation of the task, contact state graphs result in a discrete representation of the

task in the Cartesian space. This discretization allows for fast computation even for

complex 3D models. This representation permits motion planning by searching paths in

the graph that lead to a specified goal given a specified starting contact state. Xiao and Ji

(2001) have made a significant contribution to contact state graph computation. In their

approach, contact state graphs are built by merging subgraphs that are obtained by

repeatedly decreasing the level of constraint associated with the desired final contact

formation. This method allows for fast and automatic generation of contact state graphs

for complex 3D polyhedra.

Force-based Task Representation

Task representation using force analysis has been little studied in the literature. Brost

and Mason (1989) present a graphical method in which a line of force maps to point in

the plane, a friction cone maps to a line segment and multiple friction contacts map to a

convex polygon. This mapping is defined as the force-dual space. This space is built

using three topological elements: the combination of the plane of positive moments, the

plane of negative moments, and the line of zero moments. This technique has been

implemented as a contact distinguishability tool by Rosell et al. (2001) for analyzing

planar motion feasibility under uncertainty. No extension to three dimensions is known to the author.

A combined force and geometric representation of tasks is presented by Erdmann (1994). In this approach, the concept of C-space is augmented by incorporating the constraints that represent the effect of the friction cone. This approach is useful to determine the possible motions of an object subjected to force and torque.

2.1.2 Contact State Modeling

A considerable literature on deriving closed-form expressions to characterize contact states appears in the contexts of motion planning (e.g., Ambler and Popplestone 1975, Farahat et al. 1995a, Hirai and Asada 1993, McCarragher and Asada 1993, Xiao and Zhang 1997), grasping (i.e., Cai and Roth 1987, Montana 1988), and model-based compliant motion (i.e., Bruyninckx et al. 1995, De Schutter et al. 1999). This section reviews how contact states have been modeled in the literature. The first part of this section addresses prior work on physics-based representations of contact states, whereas the second part reviews the literature on probabilistic-based representations of contact states.

Physics-Based Modeling of Contact States

Three types of modeling techniques have been commonly used in the literature to represent contact states: kinematic models, quasi-static force models, and dynamic force models.

Kinematic Representation

In terms of kinematic representation of the contact states, Popplestone et al. (1980) is an early reference in which configuration constraints between objects are extracted from the spatial relationships among the objects' features (e.g., face, edge). In Farahat et al. (1995a), the contacts between a polygonal workpiece manipulated by two or three active polygons are represented as a set of homogeneous kinematic equations parameterized by the configurations of the contacting objects. Closed-form expressions for the possible configurations of the grasped object are then derived by solving the set of kinematic equations. Xiao and Zhang (1997) extended the analysis of polygonal contact states by providing an exhaustive description of all the possible kinematic equality constraints, overlap constraints, and non-penetration constraints characterizing the contacts.

The above kinematic representations only deal with objects defined using first order geometric properties (i.e., orientation of contact normals and location of contact points). The kinematic description of objects exhibiting second order geometric properties (i.e., curvatures) can be found in the grasp literature. For example, a kinematic description of the relative motion of two bodies undergoing point contact is studied in the work of Cai and Roth (1987) and Montana (1988).

Quasi-Static Force Representation

Force representation of contact states has been extensively studied in a quasi-static point of view. Whitney (1982) presents one of the earliest and most complete works on

the kinematic and force characterization of the three different phases associated with a chamfered peg-in-hole assembly task (i.e., chamfer crossing, one-point contact, two-point contact). Desai and Volz (1989) use static equilibrium conditions to describe the contact forces associates with planar contact states. The resulting equality equations are then transformed into inequalities to model the effects of sensing uncertainties. Hirai and Asada (1993) utilize the concept of polyhedral convex cones to characterize the range of forces that satisfies the unidirectional constraints due to contacts between polyhedral objects. The same reasoning is also applied to describe the range of admissible displacement sets. Moreover, Hirai (1994) showed that both cones are dual to each other when the constraints are unidirectional.

The effects of friction have been extensively investigated in the task assembly literature (e.g., peg-in-hole insertion). Two early and much-cited references on the effect of friction forces during a peg-in-hole insertion are Simunovic (1979) and Whitney (1982). In the context of contact state estimation, however, friction is often neglected. This simplification is due to the estimation complexity added by the nonlinear effect of friction. An exception is the work of Farahat et al. (1995b) in which friction forces obeying Coulombs law are linearized and represented as an extra constraint on the quasi-static equilibrium conditions that characterize the contact formations. One way to avoid the modeling complexity of friction is to encode it as a probabilistic disturbance (e.g., Eberman 1995, De Schutter et al. 1999).

Bruyninckx and co-workers present a systematic and unifying approach to contact state modeling in a series of papers on model-based compliant motion (Bruyninckx 1995,

Bruyninckx et al. 1995, De Schutter et al. 1999, Lefebvre et al. 2003). In this approach, contacts between a manipulated object and the environment are modeled as virtual mechanisms parameterized by the first and second order geometric properties of the contact surfaces. Motion freedoms and their dual sets of possible reaction forces are modeled up to second order using twist and wrench bases. Finally, reciprocity and consistency equations for the measured twist and wrench are derived using kinematic chains and the properties of the objects in contact. In a practical point of view, this approach is compelling since it eliminates the need for contact point sensors (i.e., no tactile sensing).

Dynamic Force Representation

The dynamic modeling of contact states has largely been overlooked in the contact state literature due to the assumed (and programmed) quasi-static nature of assembly tasks. An exception is the work of McCarragher and Asada (1993, 1995a, 1995b) in which the dynamics of contact states are represented by linearized equations of motion constrained by Lagrange multipliers. The multipliers are added to enforce the geometric constraints corresponding to the contact states. Eberman (1995) proposed a slightly different approach in which the Hamiltonian is used to derive the dynamics equations. This approach resulted in two sets of first order differential equations as opposed to one in McCarragher and Asada. In both works, the dynamics effect due to the impact between rigid bodies is considered by looking at the change of momentum created by an impulse representing the collision.

Probabilistic Modeling

As an alternative to physic-based models, probabilistic models have also been used to describe contact states. These techniques, although lacking the physical insights of model-based approaches, have proven to be very efficient in practice since the models are made from experimental training data. For example, Hannaford and Lee (1991) model the map between force signals and the four phases of a peg-in-hole insertion task (i.e., move, tap, insert, and extract) using Gaussian probability density functions. These models are then used in an HMM to monitor task progression in a teleoperated assembly. In the same context, Pook and Ballard (1993) use Learning Vector Quantization on finger tension signals to create four contact primitives for a tele-manipulation task (i.e., grasp, carry, press, slide). In Eberman and Salisbury (1994), four contact signals (i.e., impacts, slip, no contact, and grasping contacts) are modeled using KL-expansion, a normal white noise process, and an auto-regressive model.

2.1.3 Task Encoding

In the contact state graph utilized to decompose a task, actions are not encoded, and as a result the graph is undirected. An early approach to build directed graphs was proposed by Lozano-Perez et al. (1984). In this approach, a directed graph, defined as a reachability graph, encodes the motions between the states using a computed pre-image of the desired goal. Adding the a priori knowledge of the motion (e.g., velocity cone) augments the graph by partitioning the free space. This technique is used in Eberman (1997) to represent the possible motions inside a 2D maze.

28

In Donald and Jennings (1991) the concept of R-R graph (reachability graph of the recognizable sets) is proposed to encode the reachability relationship between the recognizability sets that partition the sensor space. This type of graph can then be included inside a lattice structure to represent the variability of the task knowledge. The bottom of the lattice is associated with small R-R graphs that represent the current limited knowledge of the task whereas the top of the lattice is associated with large R-R graphs that represent the expected full knowledge of the task.

Probabilistic approaches can also be used to encode the likelihood of transitions among the nodes of a contact state graph. The most common representations are Markov chains (e.g., Hannaford and Lee 1991) and Petrie nets (e.g., McCarragher and Asada 1995). In a Markov chain, for example, the task is encoded inside a probability transition matrix in which each element represents the likelihood of transitioning from one state to another (including self transition). The matrix can be obtained from training data (Rabiner 1989).

2.1.4 Contact State Identifiability and Distinguishability

Identifiability and distinguishability have been investigated in several fields under different names. In this document, the notion of contact distinguishability is equivalent to the notions of contact recognizability (Erdmann 1986, Xiao and Liu 1998) or contact identifiability (Rosell et al. 2001) presented in the motion planning literature. It is important to note that the concept of model identifiability presented in this thesis refers to the identifiability of the parameters used to describe the model structure and not to the

identification of the contact model. These choices of notations are inspired by the well-established nomenclature used in the state-space model literature and presented at the end of this section.

Distinguishability

The concept of distinguishability is equivalent to the early notion of recognizability introduced by Erdmann (1986) in which a state is said to be recognizable if it can be distinguished from the other states using the robot's sensors. Donald and Jennings (1991) introduce the idea of perceptual equivalence classes as distinguishable sets that partition the world based on sensor measurements. They propose an algorithm to compute the perceptual equivalence classes in the configuration space and show that the computational complexity is exponential in the dimensions of the space and polynomial in the number of points contained in the space.

As discussed in Erdmann (1986), control history and sensor history can improve distinguishability by refining the partition of the sensor space. Sensor fusion can also improve distinguishability (Donald and Jennings 1991). In this context, Xiao and Liu (1998) investigate contact recognition (i.e., distinguishability) for position/orientation and force/moment sensing in the presence of uncertainties (i.e., force can disambiguate contact states when position is not able to and vice-versa). They propose a fuzzy representation of contact states to take into account the indistinguishability nature of contact states. A recognition algorithm is discussed, but the authors do not report any implementation.

A few analytical approaches based on geometry and/or force have been implemented to test distinguishability (Xiao and Zhang 1997, Rosell et al. 2001). The concept of contact equivalence presented by Xiao and Zhang (1997) is based on analytical derivations of the equations describing the relative motions between contacting polygonal objects. This concept is used to characterize contact states that have equivalent structural equations (i.e., they are indistinguishable). Another example is presented in Rosell et al. (2001) in which tools investigating the robustness of paths generated by gross-motion planners to model uncertainty are discussed. In particular, the distinguishability of potential contact situations due to uncertainty is analyzed by computing the intersection of the generalized force domains corresponding to the possible contact states. If the domains intersect, then force measurements cannot be used to disambiguate the two contacts.

Identifiability

While distinguishability is concerned with discriminating one contact state from another based on sensor data, identifiability addresses the questions of what parameters in a particular contact state model can be estimated and, if so, how many solutions are possible. In the robot calibration literature, an identifiable model corresponds to a minimal parameterization (Gautier and Khalil 1990). In this literature, identifiability has been mostly addressed with numerical techniques (e.g., Atkeson et al. 1986, Sheu and Walker 1989). For example, analysis of the Jacobian matrix singular values (Sheu and Walker 1989) can be used tests for identifiability. Parameters are said to be unidentifiable if they

31

are associated with small singular values. An exception to numerical techniques is the work of Gautier and Khalil (1990) in which symbolic computations are used to extract the minimum set of inertial parameters used to represent the dynamic model of serial robots.

In the context of contact states, the notion of C-space equivalence defined by Eberman (1995) can be regarded as an identifiability test. This technique is applicable only if the contact model can be written as a linear function of the sensor variables. To prove identifiability, Eberman's approach was to demonstrate the uniqueness of the mapping between the coefficients of the sensor variables (typically nonlinear functions of the parameters) and the parameter values. In Bruyninckx et al. (1995), the identifiability of the geometric uncertainties parameterizing the wrench and twist Jacobians of the contact states is discussed qualitatively.

Distinguishability and Identifiability in the State-Space Model Literature

The concept of a priori testing of model distinguishability and identifiability is well established in the state-space model literature with applications related to control (Ljung and Glad 1994), biology (Chapell et al. 1990), and chemistry (Walter et al. 1985). Distinguishability has been treated in Raksanyi and Walter (1985) and Walter and Pronzato (1996) while identifiability has been examined in Chapell et al. (1990), Lecourtier et al. (1982), and Ljung and Glad (1994). In a series of papers published in the mid-eighties (i.e., Lecourtier et al. 1982, Walter et al. 1984, Walter et al. 1985) Walter and Lecourtier provided a uniform approach to testing the distinguishability and identifi-

ability of state-space models. Using models $M_i(p)$ as given in (2.1) in which X is the state vector, p is a set of unknown time-independent parameters, U is the input vector, and Y is the output vector, Walter and Lecourtier defined distinguishability and identifiability as follows:

$$M_i(p) = \begin{cases} \dot{X}(t) = f\left(X(t), U(t), p, t\right) \\ Y_i(t, p) = g\left(X(t), p, t\right) \end{cases}, X(0) = X_0, U(0) = U_0 \qquad (2.1)$$

Two state space models $M_1(p)$ and $M_2(p)$ are distinguishable if (i) for almost any q there is no p such that $Y_1(t, p) = Y_2(t, q)$ and (ii) for almost any p there is no q such that $Y_2(t, q) = Y_1(t, p)$, for any input and time in (2.1). Similarly, a state-space model $M(p)$ is globally (locally) identifiable if for almost any q there is only one (a finite number of) p such that $Y(t, p) = Y(t, q)$ for any input and time in (2.1).

Given these definitions, there exist a variety of techniques to solve for state-space model distinguishability and identifiability. For linear models, these methods include equating transfer function coefficients (Walter et al. 1984) and similarity transformations (Vajda et al. 1989). For nonlinear models, techniques include linearization (Grewal and Glover 1976), Taylor series expansions (Pohjanpalo 1978) and generating series (Walter et al. 1984).

2.1.5 Data Excitation

When addressing the problem of parameter estimation, the question of data excitation needs to be addressed. Is the input path sufficiently exciting to estimate all the parameters associated with the model? It is important to realize that this notion of sufficient excitation is different from the notion of identifiability presented in section 2.1.4. Identifiability has to do with the uniqueness of a solution while excitation has to do with the continuity of the solution on the data. This distinction is important since both problems can result in a poor estimation. In the case of unidentifiability the poor estimation is a result of a structural problem that requires an appropriate re-parameterization of the model, whereas in bad excitation the poor estimation is a result of a numerical problem that requires an appropriate re-selection of the sensor path.

The problem of data excitation has been overlooked in the contact state estimation literature where it is traditionally assumed (empirically) that the data are sufficiently exciting (e.g., De Schutter et al. 1999, Lefebvre et al. 2003, 2005). The problem, however, has been extensively investigated in the calibration literature. In this context, the excitation problem is reduced to finding measurements that result in a low condition number of the parameter Jacobian (i.e., a condition number less than 100 (Schröer et al. 1992)). Hollerbach and Wampler (1996) show how regularization techniques, such as column and row scaling of the parameter Jacobian, can be applied to reduce the condition number. Minimization of the condition number has been studied for kinematic as well as dynamic calibration. For example, Khalil et al. (1991) select the measurement configura-

tions for a simulated calibration of a TH8 robot by minimizing the condition number associated with the parameter Jacobian matrix.

In contrast to kinematic calibration where the measurements can correspond to discontinuous 'snapshots' of the system's configurations, dynamic calibration requires the continuity and smoothness of the input trajectories. This problem was first studied by Armstrong (1989) who developed a constrained nonlinear optimization technique to generate optimal robot excitation trajectories. In this approach, the condition number of an observation matrix derived from the dynamic model of the system is minimized using a Lagrangian optimization technique. The outputs of the optimization are the points of a sequence of joint accelerations. Joint velocities and joint positions are then obtained using numerical integration. In Gautier and Khalil (1992), the minimization of a cost function based on the condition number of an observation matrix derived from the energy model of the system is performed using a gradient conjugate optimization method. A discrete set of optimum position and velocity points is obtained and interpolated using a fifth-order polynomial. Swevers et al. (1997) present a statistical approach in which the determinant of the covariance matrix derived from the dynamic model of the system is minimized using a sequential quadratic programming method. The originality of the method comes from the use of a finite Fourier series to parameterize the robot trajectories.

An interesting method presented by Ljung and Glad (1990, 1994) utilizes tools from differential algebra to extract a necessary excitability condition for arbitrary nonlinear state-space models. This method, based on multiple differentiations, leads to the explicit

estimation of the time-invariant parameters of the model. This closed-form solution allows for easy extraction of a necessary condition for data excitation.

2.1.6 Contact State Observability

Observability as defined in this thesis can be directly related to the concepts of reachability and recognizability defined by Lozano-Perez et al. (1984) and Erdmann (1986). A state is observable inside a task's graph if it can be reached and recognized. This is an important concept in task planning since reaching a goal without recognizing it does not result in task completion. In Lozano-Perez et al. (1984), the notion of pre-image of the goal is introduced as a solution to this problem. The central idea is that given the known geometry of the task and sensing uncertainty bounds, pre-images of local goals that can be reached and recognized using a single compliant motion can be computed in the configuration space. Backward chaining of the local goals starting from the desired goal can then be used to develop a multi-move strategy that guarantees observability for motion planning with uncertainty. The same problem is solved by Erdmann (1986) using backward and forward projections. The backward projection solves the reachability problem while the forward projection ensures that the reachable states are also recognizable using the local history of the task. The history of the task helps to disambiguate states that are otherwise indistinguishable using only the current sensor information. As an example of forward projection, consider the four states described in Fig. 2.1. The states B and C are assumed to be distinguishable based on the current sensing, whereas the states A and D are assumed to be indistinguishable. Storing the state sequence can

help distinguished *A* and *D*. For example, if the current sensor measurement cannot disambiguate *A* from *D*, but if it is known that *B* was the previous reached state, then it can be concluded that *A* and not *D* was attained.
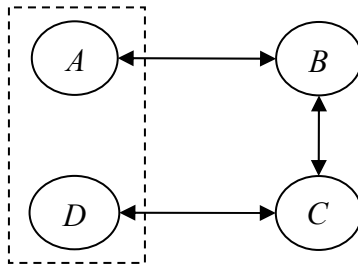
Figure 2.1: Example of forward projection associated with a four-state graph.

In the framework of contact state graph, reachability is simply reduced to path connectivity while recognizability is equivalent to complete distinguishability (i.e., all the contact states are pairwise distinguishable). In that regard, the reachable and recognizable graphs defined by Donald and Jennings (1991) ensure that the contact states are observable.

2.1.7 Parameter Estimation

An extensive body of research on parameter estimation exists in the literature. Ljung (1987), a classic reference on the subject, reviews the theory as well as many of the techniques used in parameter estimation.

Parameter estimation has been extensively studied in the contexts of robot calibration (e.g., Hollerbach and Wampler 1996 for a good overview) and fine motion planning (e.g.,

De Schutter et al. 1999, Lefebvre et al. 2003, 2005 for a recent overview). Three popular estimation techniques are the Kalman filter and its variations (e.g., extended Kalman Filter), least-squares estimation and its variations (e.g., nonlinear least squares, total least squares, weighted least squares), and maximum-likelihood estimation.

Parameter estimation has been largely utilized in fine motion planning to correct for small uncertainty errors in task assembly. Simunovic (1979) is an early reference in which a position-based Kalman filter is utilized to estimate the relative position between two mating parts given a known contact state. In the context of compliant robot motion, De Schutter and Van Brussel (1988) derive a closed-form estimate of the orientation errors between the physical and computational task frames using velocity and force measurements. In De Schutter et al. (1999), the modeling approach introduced by Bruyninckx (1995) is used to estimate the first order geometric parameters (i.e., location uncertainties on the fixed environment object and the manipulated object) associated with a cylinder-on-plane experiment. To this end, the closure-update equation as well as the wrench and twist reciprocity equations are used as the measurement equations of an extended Kalman filter. Lefebvre et al. (2003) generalize this method to the estimation of geometrical parameters of rigid polyhedra objects. In this approach, the geometry of the task allows for an automatic generation of the filter's measurement equations. This technique is then used to estimate all the grasping and environment uncertainties associated with the six contact states of a cube-in-corner placing task. Eberman (1997) provides a statistical model-based approach to building a contact state estimator. Contacts between the end-effector of a PHANToM© robot and a maze are modeled as linear

stiffness relationships between the robot configurations and the contact reaction forces. A maximum likelihood estimation technique is then used to estimate the stiffness projection matrix characterizing the contact states.

Most of the literature on contact state estimation assumes good nominal parameter values and focuses only on the estimation of small errors. This assumption allows for linearization schemes and reduces the computational difficulty of the estimation process. Solving for large initial parameter uncertainties in real time remains a difficult problem. Recent progress has been made by Lefebvre et al. (2005) in which a finite-dimensional Bayesian filter is proposed to estimate unknown parameters. The filter is based on finding a non-minimal state vector in which the measurement model is linear. A Bayesian filter is implemented to estimate the statistics of this higher dimensional state space, and then an iterative extended Kalman filter is utilized to retrieve the states associated with the original model. This technique is applied with good result to the cube-in-corner task presented in their earlier paper.

2.1.8 Contact State Estimation

Detection tests are often based on finding a threshold that can decide whether a contact state is active based on some raw or processed sensor measurements. Two families of tests are often used in the literature: deterministic and probabilistic decision tests. Prior work on both methods is presented in this section.

Deterministic Decision Test

In Hirai and Asada (1993) the geometry of the contact state models is utilized to generate a minimal set of force-based discriminant functions that are then used as boolean rules to segment force measurements into contact states. In the context of dynamic robotic assembly, McCarragher and Asada (1993) utilize quantitative reasoning to detect contact state transitions. In this framework, the raw force signals are transformed into qualitative signals that are then used to recognize the contact states and their transitions. The approach is tested successfully for a dynamic dual peg-in-hole insertion. Dupont et al. (1999) apply a similar technique by using a Boolean combination of thresholds force and motion signals to segment a pick place task.

One of the first parameter-based approaches to contact detection was proposed by Farahat et al. (1995b). In this research, a linear programming technique is used to recognize contact states. A contact state is detected as active when it satisfies the linear program associated with its parameterized model and the collected force measurements.

In the context of robot learning, Skubic and Volz (2000) use a fuzzy classifier to detect contact state patterns built from force and moment signals. The same experiment was also conducted successfully using a neural network.

Statistical Decision Test

In Eberman and Salisbury (1994), sequential hypothesis testing is used to detect and label contact events. Six statistical hypotheses are derived to describe five contact

events. The segmentation and identification of the events are performed by computing a generalized likelihood ratio test over a moving data window. In the context of compliant motion, De Schutter et al. (1999) use the Gaussian innovations of a Kalman filter to monitor contact transitions during the placing of a cube inside a corner. The sum over the normalized innovation squares (SNIS) is computed inside a window of fixed length and a threshold based on 95% confidence boundary χ^2-test is used to decide whether the innovations are consistent with the model. If the SNIS exceeds the threshold, then a transition is detected.

In the above examples, contact detection is solely based on the relationship (i.e., physics-based or probabilistic relationship) between the sensing and the contact states; however, task information can also be incorporated to improve the likelihood of contact state detection. Task information is conveniently modeled using Petri nets, neural nets, and HMM. These three techniques offer the double advantages of incorporating task knowledge and contact state knowledge in a same framework. For example, Petri nets have been used by McCarragher and Asada (1995a, 1995b, 1996) to monitor and control robotic assembly tasks using polygonal and polyhedral parts. Neural nets have been used in the context of robot learning by Asada (1990) and Skubic and Volz (2000). In Asada, for example, neural nets are used to represent and learn compliances from force and velocity teaching data.

HMM is a very popular technique in data segmentation. This stochastic technique, originally developed for speech recognition problem (Rabiner 1989), has been success-fully adapted to monitor contact states in assembly tasks. In this framework, the relation-

ship between the observations and the states is usually represented using mixture of Gaussian signals, and the task information is encoded inside a state network defined by the likelihood of transitions among states. One of the advantages of this technique is that both the Gaussian probability density function and the probabilities of transitions can be obtained from unsupervised training, e.g., Baum-Welch algorithm (Baum and Petrie 1966). One early example is found in Hannaford and Lee (1991), in which an HMM is used to extract four contact events from force/torque measurements. In Hovland and McCarragher (1998), a multiple HMM approach is used to monitor the 11 contact events describing the robotic insertion of a 2D L-shape part. The task is modeled as a discrete event dynamic system in which each event is represented by a HMM. A recognition rate of 97% is achieved in 0.5-0.6 s.

Eberman (1997) presents an alternate approach to HMM by building a contact state observer using stochastic parameter estimation and change detection theory. Each contact state is represented by a linear parameterized model. A prior distribution for the parameters is obtained from training data. A maximum likelihood estimator is then used to estimate the parameters given force and velocity measurements. The estimator outputs the log-likelihood between the model and the measurements and also the residuals of the process. The residuals are fed to a change detector that computed the log-likelihood of transitions among states. These statistics are then sent to a single detection procedure that uses a beam search strategy over a given task network to determine the most likely path corresponding to the measurements.

2.2 Thesis Objectives

The prior work presented in this chapter can be used to summarize the needs for contact state estimation in poorly known environments:

- There is no complete framework in the literature that discusses the problem of contact state estimation in poorly known environments.

- The estimation of the contact parameters is usually limited to small uncertainties.

- Contact state estimation has been mainly addressed as an implementation problem in the literature. As a result, very few tools have been developed to investigate the a priori feasibility of contact estimation. In particular, no testing strategy has been developed to test systematically the distinguishability, identifiability, observability, and excitability of contact states.

Based on these limitations, the objective of this thesis is defined as follows: given a geometrical description of a task, a contact topology, and a set of sensors, the goal of this research is to provide design tools that can help generate contact state models and contact state networks that will permit the feasibility of contact state estimation in poorly known environments. Given this objective, a design framework is provided for the implementation of contact state estimators in poorly known environments. Its main contributions are:

- The identifiability and distinguishability of parameterized contact models are analyzed using a unifying algebraic testing method based on Taylor series expansion.

The testing method is applicable to any contact state model regardless of the chosen sensing modality.

- Task feasibility in poorly known environments is reduced to a contact state observability problem. The concept of forward projection on the parameter history is introduced as a solution to the observability problem.

- The effect of the sensor signals on the parameters is analyzed analytically by deriving closed-form expressions for the contact parameters.

- Task knowledge, encoded as a probability transition matrix, is derived from a direct mapping between the contact state graph representing the task in a structured environment and a distinguishable state graph representing the task in a poorly known environment.

In addition to the progress made in the design phase of the estimator, the following contributions to the implementation phase of the estimator are presented:

- Large uncertainties (i.e., unknown parameters) are considered in the implementation phase of the estimator by using a nonlinear least squares algorithm.

- An HMM is implemented as a contact state detector. This approach provides a unifying probabilistic framework to combine the results from the estimation step with the a priori knowledge of the task.

Chapter 3

Topology and Modeling of Contact States

Manipulation tasks are readily described as a succession of contact states that describe how the manipulated object is in contact with objects in the environment. The nature of a contact state is characterized by the geometric features that are used to model the contacting objects (e.g., vertex, edge, face). As an example, Fig. 3.1 shows a planar manipulating robot placing a block in a corner. A sequence of three contact states is used to complete the task: a vertex-edge contact, a double vertex-edge contact, and a double edge-edge contact.
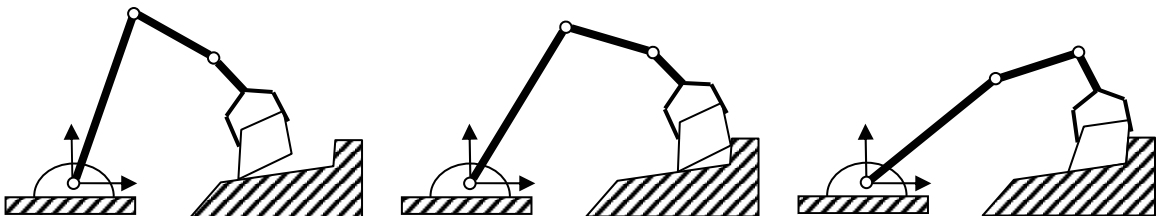
Figure 3.1: Sequence of three contact states used to place a block in a corner.

Contact states are naturally described geometrically; nevertheless, in order to be detected, they also need to be described with respect to the available sensing information (i.e., robot sensing). The objective of this chapter is to provide the background on contact topology and contact state modeling necessary to understand the next chapters of this thesis. The first part of this chapter reviews the contact topology associated with polygonal and polyhedral objects. Additional material on this topic can be found in a list of papers published by Xiao and her colleagues (Xiao 1993, Xiao and Zhang 1997, Xiao and Ji 2001). The Second part of the chapter discusses the modeling of contact states using pose, velocity and force sensing. As a result of this modeling, contact states are represented as homogeneous nonlinear algebraic equations parameterized by time-dependent sensor data and time-independent parameters representing the unknown locations and positions of the objects in contact. The velocity and force representations of contact states are discussed using wrench bases, twist bases, and screw transformations. Additional background on this material can be found in Bruyninckx (1995) and Murray et al. (1994).

3.1 Contact State Topology

As shown in Fig. 3.1, each contact state is characterized by a geometrical description of the two objects in contact in terms of a finite number of contacting elements. For polygons and polyhedra these elements are vertex and edge and vertex, edge and face, respectively.

3.1.1 Single Contact State

Contact states describe the contact between a manipulated object and fixed objects in the environment. As a result, the number of single contacts between the two objects is n_e^2 where n_e represents the number of geometric elements (i.e., $n = 2$ in 2D, and $n = 3$ in 3D), as summarized in Table 3.1 and 3.2.

Notations for Table 3.1 and Table 3.2

$a^m - b^f$: Contact between the element a belonging to the manipulated object (a^m) and the element b belonging to the shaded fixed object (b^f).

$(a,b) \in \{V, E, F\}$

   V: Vertex

   E: Edge

   F: Face

Table 3.1: Planar single contacts between a manipulated object and a fixed object.
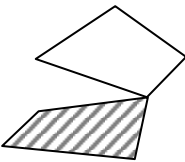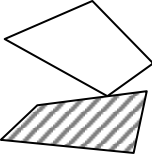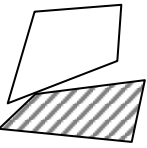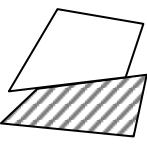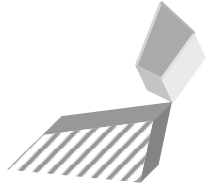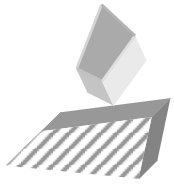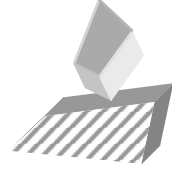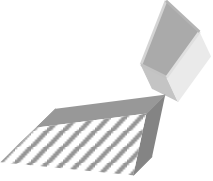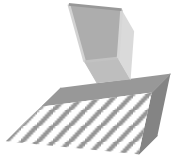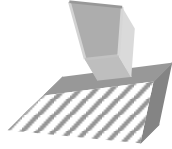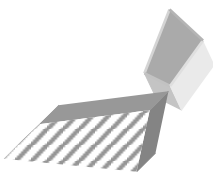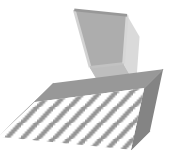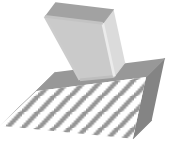
$V^m - V^f$	$V^m - E^f$
$E^m - V^f$	$E^m - E^f$

Table 3.2: Spatial single contacts between a manipulated objects and a fixed object.

$V^m - V^f$	$V^m - E^f$	$V^m - F^f$
$E^m - V^f$	$E^m - E^f$	$E^m - F^f$
$F^m - V^f$	$F^m - E^f$	$F^m - F^f$

As discussed in Xiao (1993), several of these single contacts are limiting cases of other ones, and as such should be ignored. In 2D for example, $\left\{ V^m - V^f \right\}$ can be considered as a part of $\left\{ V^m - E^f \right\}$, $\left\{ E^m - V^f \right\}$, or $\left\{ E^m - E^f \right\}$, and as such should be discarded to avoid any ambiguity. Table 3.3 summarizes all the possible degenerate contact states.

Table 3.3: Degenerate contact states.

2D	$V^m - V^f$	
3D	$V^m - V^f$	$V^m - E^f$
	$E^m - V^f$	$E^m - E^f$

Note that these degenerate cases are also of limited interest due to implementation difficulty (e.g., a vertex-on-vertex contact is difficult to realize in practice). One exception to these degenerate cases is the $\{E^m - E^f\}$ contact. This contact can be considered non-degenerate if the two edge elements are crossing.

3.1.2 Multiple Contact States

Situations involving multiple contact states can occur when concave objects are in contact or when the manipulated object contacts multiple fixed objects in the environment. The possible number of combinations involving single contacts is given by the equation (3.1), where n represents the number of single contacts and k is the number of contact possibilities.

$$m = C_k^n + n \tag{3.1}$$

As an example, Table 3.4 enumerates all the possible pairs of contacts that constitute a double contact for 2D polygons ($n = 4$, $k = 2$, $m = 10$). Only the upper triangular part of the table is considered since the lower part describes the same pairs of contacts (e.g., $\{E^m - E^f, V^m - E^f\}$ is equivalent to $\{V^m - E^f, E^m - E^f\}$).

Table 3.4: Double contacts for polygons.

	$V^m - V^f$	$V^m - E^f$	$E^m - V^f$	$E^m - E^f$
$V^m - V^f$	X	X	X	X
$V^m - E^f$		X	X	X
$E^m - V^f$			X	X
$E^m - E^f$				X

It can be shown (Xiao and Zhang 1997) that many of the combinations given by (3.1) are in fact topologically equivalent to lower combinations of single contacts. As an example, Fig. 3.2 shows that the double contact $\{E^m - E^f, E^m - E^f\}$ where the edges are parallel is equivalent to a single contact $\{E^m - E^f\}$. Moreover, Xiao and Zhang (1997) proved that multiple contacts composed of three or more single contacts are always equivalent to either a single contact or a limited combination of two or three single contacts.
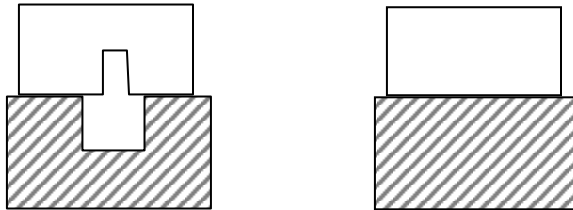
Figure 3.2: An edge-edge contact and its topologically equivalent single contact.

This notion of contact equivalence is essential when building a contact state estimator since it can directly reveal the distinguishability of two contact states (i.e., two topologically equivalent contact states are indistinguishable). This concept of distinguishability will be investigated in details in Chapter 4.

3.2 Contact State Modeling

The implementation of a contact state estimator based on contact geometry requires knowing the dimensions and locations of the contact elements. In the context of poorly known environments, this information needs to be estimated, and as a consequence, higher level representations of the contact states, based on available sensor measurements, are needed. Several sensing modalities are commonly available with manipulating robots; examples include position, orientation, force and torque sensing. Contact state modeling involves finding a map between the geometric constraints that characterize the contact states in the Cartesian space and the available sensors. As a first step, coordinate frames and transformation matrices describing the unknown relative positions and orientations of the two objects in contact are developed. Then, contact states are modeled by algebraic constraint equations parameterized by sensor data and time-independent location uncertainties.

3.2.1 Contact State Parameterization

Contact states are characterized by the locations (i.e., positions and orientations) of the contacting elements (e.g., vertex, edge, face, etc). Therefore, local coordinate frames

must be defined to represent the locations of each contact. Additionally, global frames must be defined to represent the location of the manipulating robot and its gripper. These frames are independent of the contact geometry. Four frames are defined as follows:

- $\mathfrak{R}^w$ is the world coordinate frame associated with the manipulating robot. Fixed objects in the environment are located with respect to this frame. The position and orientation of the robot gripper are expressed with respect to this frame.

- $\mathfrak{R}^g$ is the coordinate frame associated with the robot gripper. The fixed location and orientation of the manipulated object is defined with respect to this frame. Force and torque are expressed with respect to this frame.

- $\mathfrak{R}^m$ is the local coordinate frame associated with the contact element on the manipulated object. If the contact involves more than one contact element, multiple local frames must be defined (i.e., one for each contact element).

- $\mathfrak{R}^f$ is the local coordinate frame associated with the contact element on the fixed environment object. If the contact involves more than one contact element, then multiple local frames must be defined.

The positions and orientations of the local coordinate frames $\mathfrak{R}^m$ and $\mathfrak{R}^f$ depend on the nature of the contacting element. The following rules are developed to assign the local frames uniformly:

- Vertex: the coordinate frame associated with a vertex is positioned at the vertex origin and has the orientation of the global frame associated with the object to which the vertex belongs.

- Edge: the coordinate frame associated with an edge is positioned at one the two vertices bounding the edge such that the edge is oriented along the positive x-axis. The y-axis is oriented in the direction of the outward normal of the edge and it is perpendicular to the normal of the face from which the edge belongs to. The remaining z-axis follows the right hand rule.

- Face: the coordinate frame associated with a face is positioned at one of the vertices bounding the face such that its z-axis points in the direction of the outward normal of the face. The y-axis is oriented perpendicularly to the z-axis, toward the inside of the face. The remaining x-axis follows the right hand rule.

Figure 3.3 illustrates how global and local frames are assigned for three different contact states. In each case, the global frames, $\Re^w$ and $\Re^g$ are assigned arbitrarily whereas the local frames are assigned following the methodology presented above. Note that in practice, the global frames depend on the geometry of the manipulating robot and can be assigned using the Denavit-Hartenberg convention (Denavit and Hartenberg 1955).

a) $\left\{ V^m - E^f \right\}$

b) $\left\{ V_1^m - E_1^f, V_2^f - E_2^m \right\}$

c) $\left\{ V^m - F^f \right\}$
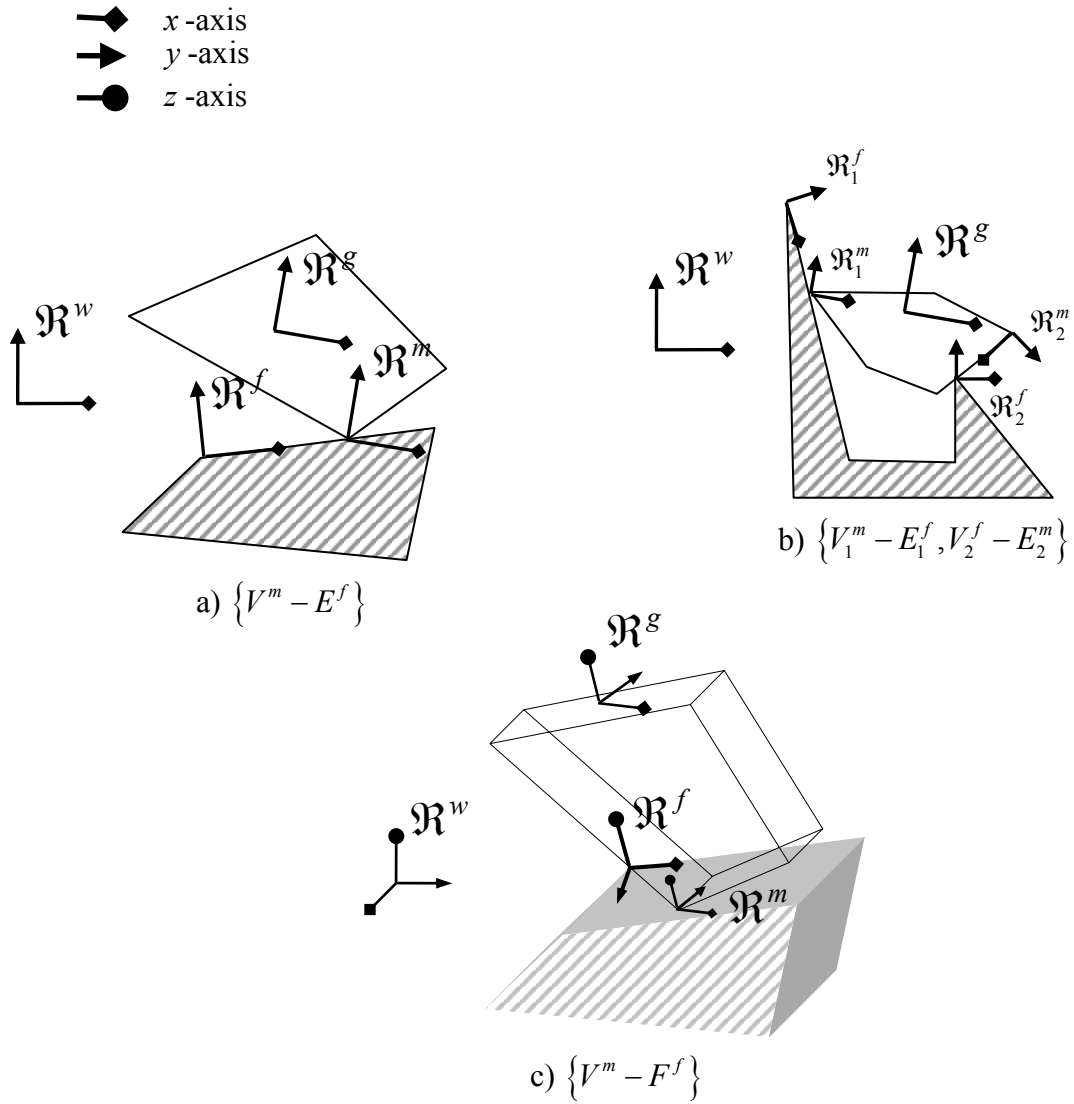
Figure 3.3: Example of frames assignments for four different types of contacts.

Transformation matrices

To express the location of a frame $\Re^a$ with respect to a frame $\Re^b$, the concept of a homogeneous transformation matrix is utilized. A change of coordinate frames is given

by the transformation matrix T_a^b in equation (3.2); where $R_a^b \in \mathbb{R}^{k \times k}$ represents a rotation

matrix and $P_a^b \in \mathbb{R}^k$ represents a position vector.

$$T_a^b = \begin{pmatrix} R_a^b & P_a^b \\ 0_{1*k} & 1 \end{pmatrix}, \qquad \begin{array}{l} k = 2 \text{ in 2D} \\ k = 3 \text{ in 3D} \end{array} \qquad (3.2)$$

The yaw-pitch-roll convention is used to express the orientation matrix R_a^b in equa-

tion (3.3). The yaw, pitch, and roll correspond to a θ_y rotation around the x_a-axis, a θ_p

rotation around the y_a-axis, and a θ_r rotation around the z_a-axis, respectively.

$$R_a^b = \begin{pmatrix} \cos\theta_r & -\sin\theta_r & 0 \\ \sin\theta_r & \cos\theta_r & 0 \\ 0 & 0 & 1 \end{pmatrix} \begin{pmatrix} \cos\theta_p & 0 & \sin\theta_p \\ 0 & 1 & 0 \\ -\sin\theta_p & 0 & \cos\theta_p \end{pmatrix} \begin{pmatrix} 1 & 0 & 0 \\ 0 & \cos\theta_y & -\sin\theta_y \\ 0 & \sin\theta_y & \cos\theta_y \end{pmatrix} \qquad (3.3)$$

Using this nomenclature, three homogeneous transformations, $T_w^g(t)$, $T_g^m(t)$, and

$T_w^f(t)$ are defined. $T_w^g(t)$ is a homogeneous transform matrix which relates the gripper

frame to the world frame based on the geometry of the remote manipulator. Similarly,

$T_g^m(t)$ relates the manipulated object to the gripper frame, and $T_w^f(t)$ relates the

environment object to the world frame.

These three matrices have the generic form given by equation (3.4) in 2D and equa-

tion (3.5) in 3D, where $\{a,b\} \in \{w, g, m, f\}$

$$T_a^b(t) = \begin{pmatrix} \cos\theta^a(t) & -\sin\theta^a(t) & x_b(t) \\ \sin\theta^a(t) & \cos\theta^a(t) & y_b(t) \\ 0 & 0 & 1 \end{pmatrix} \qquad (3.4)$$

$$T_a^b(t) = \left(\begin{pmatrix} \cos\theta_r^a(t) & -\sin\theta_r^a(t) & 0 \\ \sin\theta_r^a(t) & \cos\theta_r^a(t) & 0 \\ 0 & 0 & 1 \end{pmatrix} \begin{pmatrix} \cos\theta_p^a(t) & 0 & \sin\theta_p^a(t) \\ 0 & 1 & 0 \\ -\sin\theta_p^a(t) & 0 & \cos\theta_p^a(t) \end{pmatrix} \begin{pmatrix} 1 & 0 & 0 \\ 0 & \cos\theta_y^a(t) & -\sin\theta_y^a(t) \\ 0 & \sin\theta_y^a(t) & \cos\theta_y^a(t) \end{pmatrix} \begin{matrix} x_b(t) \\ y_b(t) \\ z_b(t) \end{matrix} \right) \qquad (3.5)$$

It is assumed that the location of the manipulated object and the location of the environment object are unknown with respect to the gripper frame and world frame respectively. Moreover, it is also assumed that the manipulated object does not slip in the gripper, and that the environment object is static. As a result, T_g^m and T_w^f are unknown time-independent matrices. In contrast, the matrix $T_w^g(t)$ is a known time-dependent matrix since the location of the gripper with respect to the world frame is assumed to be perfectly known.

3.2.2 Pose Representation

Contact states represent geometric constraints between the manipulated object and the fixed objects in the environment. These constraints proscribe some of the poses (i.e., position, orientation) between the manipulated object and the environment object. As a result, some components of the homogeneous transformation matrix between the frame

associated with the manipulated object and the frame associated with the fixed environment object must be zero (i.e., some components of T_f^m or T_m^f must be zero). As an example, Fig. 3.4 shows a planar $\{V^m - E^f\}$ contact. Due to the contact geometry, no translation normal to the environment object's edge is allowable, and therefore $T_f^m(2,3)$ must be zero in (3.4).
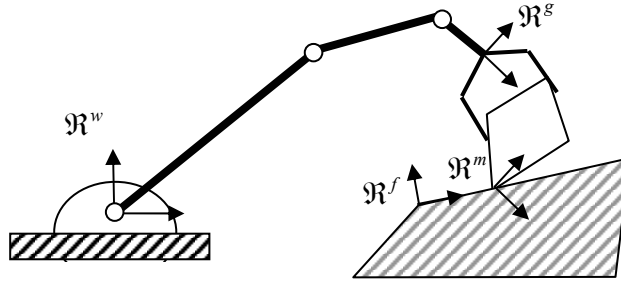
Figure 3.4: Constraint configuration of a robot due to a planar vertex-edge contact.

The number of components of the matrix T_f^m and T_m^f that can be zero depends on the nature of the contact state. This number is limited to six in the 2D case, and twelve in the 3D case, as shown in (3.6) and (3.7).

$$
\text{2D case:} \begin{cases}
\textit{No translation along } x_f & \Rightarrow \quad T_f^m(1,3) = 0 \\
\textit{No translation along } y_f & \Rightarrow \quad T_f^m(2,3) = 0 \\
\textit{No rotation around } z_f & \Rightarrow \quad T_f^m(1,2) = 0 \\
\textit{No translation along } x_m & \Rightarrow \quad T_m^f(1,3) = 0 \\
\textit{No translation along } y_m & \Rightarrow \quad T_m^f(2,3) = 0 \\
\textit{No rotation around } z_m & \Rightarrow \quad T_m^f(1,2) = 0
\end{cases}
\tag{3.6}
$$

$$3D \text{ case:} \begin{cases} \text{No translation along } x_f & \Rightarrow & T_f^m(1,4) = 0 \\ \text{No translation along } y_f & \Rightarrow & T_f^m(2,4) = 0 \\ \text{No translation along } z_f & \Rightarrow & T_f^m(3,4) = 0 \\ \text{No rotation around } x_f & \Rightarrow & T_f^m(3,2) = 0 \\ \text{No rotation around } y_f & \Rightarrow & T_f^m(3,1) = 0 \\ \text{No rotation around } z_f & \Rightarrow & T_f^m(2,1) = 0 \\ \text{No translation along } x_m & \Rightarrow & T_m^f(1,4) = 0 \\ \text{No translation along } y_m & \Rightarrow & T_m^f(2,4) = 0 \\ \text{No translation along } z_m & \Rightarrow & T_m^f(3,4) = 0 \\ \text{No rotation around } x_m & \Rightarrow & T_m^f(3,2) = 0 \\ \text{No rotation around } y_m & \Rightarrow & T_m^f(3,1) = 0 \\ \text{No rotation around } z_m & \Rightarrow & T_m^f(2,1) = 0 \end{cases} \tag{3.7}$$

In both the 2D and 3D cases in (3.6) and (3.7), the constraints on the rotations can be found by analyzing the form of the transformation matrices T_f^m or T_m^f. In the 3D case, for example, the homogeneous transformation matrix T_f^m has the form given by (3.5). If the constraint prevents any rotation around the x_f-axis (i.e., the yaw angle is zero), then the rotation matrix of T_f^m can be written as in (3.8). As a result, the absence of rotation around the x_f-axis implies that $R_f^m(3,2)$ is zero resulting in $T_f^m(3,2)$ being zero.

$$\begin{aligned}
R_f^m &= \begin{pmatrix} \cos\varphi_r & -\sin\varphi_r & 0 \\ \sin\varphi_r & \cos\varphi_r & 0 \\ 0 & 0 & 1 \end{pmatrix} \begin{pmatrix} \cos\varphi_p & 0 & \sin\varphi_p \\ 0 & 1 & 0 \\ -\sin\varphi_p & 0 & \cos\varphi_p \end{pmatrix} \begin{pmatrix} 1 & 0 & 0 \\ 0 & 1 & 0 \\ 0 & 0 & 1 \end{pmatrix} \\
&= \begin{pmatrix} \cos\varphi_r \cos\varphi_p & -\sin\varphi_r & \cos\varphi_r \sin\varphi_p \\ \sin\varphi_r \cos\varphi_p & \cos\varphi_r & \sin\varphi_r \sin\varphi_p \\ -\sin\varphi_p & 0 & \cos\varphi_p \end{pmatrix}
\end{aligned} \tag{3.8}$$

58

Since the homogeneous transformation between the manipulated object and the environment object is not directly known, T_f^m or T_m^f must be computed in an indirect way using the available information of the problem (i.e., sensor data, time-dependent location unknowns). In that effect, the kinematic closure equation (3.9) can be used to close the loop between the manipulated object and the environment object, as illustrated in Fig. 3.5. As a result, the transformation matrices T_f^m and T_m^f can be expressed using the kinematic measurements (i.e., $T_w^g(t)$) and the parameterized location unknowns associated with the manipulated object and the environment object (i.e., T_g^m and T_f^w) as shown in equation (3.10).

$$T_w^g(t)T_g^mT_m^fT_f^w = I \tag{3.9}$$

$$\begin{cases} T_f^m = T_f^wT_w^g(t)T_g^m \\ T_m^f = T_m^gT_g^w(t)T_w^f \end{cases} \tag{3.10}$$
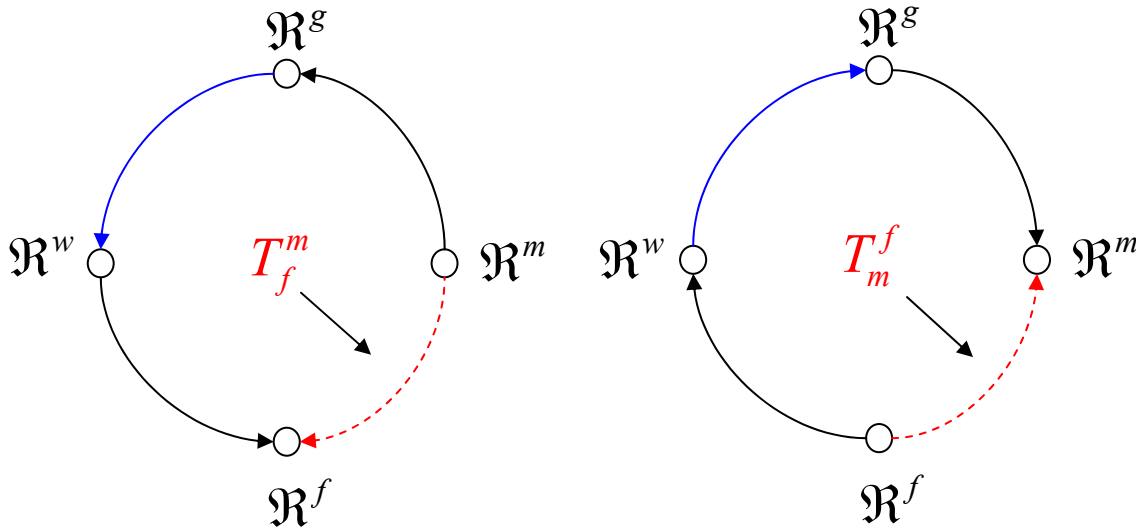
Figure 3.5: Kinematic closure equation.

As a final step, pose equations are created by expressing the constraints (3.6), (3.7), using the kinematic closure equations (3.10). To make these equations algebraic, the unknown trigonometric nonlinearities inside the transformation matrices T_g^m and T_w^f are eliminated using the change of variables $m_i = \cos\theta_i$, $m_{i+1} = \sin\theta_i$ ($i = 1$ in 2D, and $i = 1, 3, 5$ in 3D). This change of variables reduces (3.4) to (3.11), and (3.5) to (3.12). Similar equations are obtained for T_w^f by replacing the variable m by the variable f in (3.11) and (3.12).

$$T_g^m = \begin{pmatrix} m_1 & -m_2 & m_3 \\ m_2 & m_1 & m_4 \\ 0 & 0 & 1 \end{pmatrix} \qquad \text{where} \quad m_1^2 + m_2^2 = 1 \qquad (3.11)$$

$$T_g^m = \begin{pmatrix} m_1 m_3 & -m_2 m_5 + m_1 m_4 m_6 & m_1 m_4 m_5 + m_2 m_6 & m_7 \\ m_2 m_3 & m_1 m_5 + m_2 m_4 m_6 & m_2 m_4 m_5 - m_1 m_6 & m_8 \\ -m_4 & m_3 m_6 & m_3 m_5 & m_9 \\ 0 & 0 & 0 & 1 \end{pmatrix} \qquad \text{where} \quad \begin{cases} m_1^2 + m_2^2 = 1 \\ m_3^2 + m_4^2 = 1 \\ m_5^2 + m_6^2 = 1 \end{cases} \quad (3.12)$$

The final expressions of T_f^m and T_m^f are obtained in 2D by substituting (3.11) and (3.4) in (3.10), and in 3D by substituting (3.12) and (3.5) in (3.10). The detailed expressions of the matrices used to compute (3.6) and (3.7) are presented in Appendix A. An example detailing the derivation of a pose equation for a vertex-to-edge contact is pre-

sented in section 3.3. The general form of the pose equation is given by the constraint equation (3.13) where p represents the unknown geometric parameters characterizing the contact (e.g., m_i, f_i) and $s(t)$ represents the known kinematic configurations of the manipulating robot.

$$h(p, s(t)) = 0 \qquad (3.13)$$

3.2.3 Wrench and Twist Representations

Contact states can also be described using force and moment constraints resulting from the physics of the contact. For example, in order to maintain a $\{V^m - E^f\}$ contact, the vertex of the manipulated object must exert a force normal to the edge of the fixed object at the contact point (assuming a frictionless contact). Similarly, the same force and a moment preventing any rotation of the manipulated object must be exerted when maintaining a $\{E^m - E^f\}$ contact. Therefore, enumerating all the possible forces and moments necessary to maintain a contact is another way of characterizing contact states.

Alternately, linear and angular velocities can also be used to represent contact states. In this context, contacts can be characterized by enumerating all the linear and angular velocities allowable by the contact. For example, in order to maintain a 2D $\{V^m - E^f\}$ contact, the vertex of the manipulated object is allowed to slide along the fixed edge and rotate around the contact point. Contrasting to the force representation and the kinematic representation of section 3.2.2., velocity representations use motion freedoms as opposed to motion constraints to describe a contact.

A large body of literature has been devoted to force and velocity representations of contacts as described in section 2.1.2. As a general approach, wrench bases, twist bases, and screw transformation matrices are commonly used to express the effect of forces and velocities in a given coordinate frame (Bruyninckx 1995). The wrench and twist definitions and properties presented below can be found in several robotics textbooks, e.g., Murray et al. (1994).

Wrench: A wrench $F^i \in \mathbb{R}^n$ is a vector consisting of a force/moment pair $F^i = [f, m]^T$ expressed in the frame $\mathfrak{R}^i$ where $f \in \mathbb{R}^k$, $m \in \mathbb{R}^{n-k}$, $\{n = 3, k = 2\}$ in 2D, and $\{n = 6, k = 3\}$ in 3D.

Twist: A twist $V^i \in \mathbb{R}^n$ is a vector consisting of a linear/angular velocity pair $V^i = [v, \omega]^T$ expressed in the frame $\mathfrak{R}^i$ where $v \in \mathbb{R}^k$, $\omega \in \mathbb{R}^{n-k}$.

Wrench basis: A wrench basis $G^i \in \mathbb{R}^{n \times p}$ is a matrix whose columns represent the independent directions of the force/moment which produce no motion of the manipulated rigid body in the frame $\mathfrak{R}^i$. For multiple contacts, the total wrench basis is the union of the wrench basis of its individual contacts expressed in the same coordinate frame.

Twist basis: A twist basis $J^i \in \mathbb{R}^{n \times q}$ is a matrix whose columns represent the independent directions of the linear/angular velocity allowed by the contact in the frame $\mathfrak{R}^i$. For multiple contacts, the total twist basis is the intersection of the twist bases of its individual contacts expressed in the same coordinate frame.

Wrenches and twists are often referred to as wrench of constraint and twist of freedom in the contact literature (Duffy 1990). Wrench and twist bases can be obtained by inspection when expressed with respect to a coordinate frame $\Re^c$ located at the contact. This frame is positioned at the contact patch centroid and has the same orientation as the highest order contact element involved in the contact (e.g., an edge for a vertex-edge contact, a face for an edge-face contact). For two contacting elements of the same type, the orientation of $\Re^c$ is chosen arbitrarily to be the same as the element associated with the fixed object.

Wrench consistency-based equation: $\qquad F^i = G^i \phi$ $\hfill$ (3.14)

where $\phi \in \mathbb{R}^p$ represents the intensity of the wrench.

Twist consistency-based equation: $\qquad V^i = J^i \lambda$ $\hfill$ (3.15)

where $\lambda \in \mathbb{R}^q$ represents the intensity of the twist.

Wrench screw transformation matrix: A screw transformation matrix ${}^F S_a^b$ is used to transform a wrench or a wrench basis from the frame $\Re^b$ to the frame $\Re^a$.

$$\text{In 2D: } {}^F S_a^b = \begin{bmatrix} R_a^b & 0_{2\times1} \\ \begin{bmatrix} -P_a^b(2) & P_a^b(1) \end{bmatrix} R_a^b & 1 \end{bmatrix} \tag{3.16}$$

$$\text{In 3D: } {}^F S_a^b = \begin{bmatrix} R_a^b & 0_{3\times3} \\ \begin{bmatrix} P_a^b \times \end{bmatrix} R_a^b & R_a^b \end{bmatrix} \tag{3.17}$$

where $P_a^b \times$ is the skew-symmetric matrix represented by $P_a^b \times = \begin{bmatrix} 0 & -P_a^b(3) & P_a^b(2) \\ P_a^b(3) & 0 & -P_a^b(1) \\ -P_a^b(2) & P_a^b(1) & 0 \end{bmatrix}$

The rotation matrix R_a^b and the position vector P_a^b were defined in 3.2.2.

Twist screw transformation matrix: A screw transformation matrix $^V S_a^b$ is used to trans-

form a twist or a twist basis from the frame $\mathfrak{R}^b$ to the frame $\mathfrak{R}^a$.

$$\text{In 2D: } {}^V S_a^b = \begin{bmatrix} R_a^b & \begin{bmatrix} P_a^b(2) \\ -P_a^b(1) \end{bmatrix} \\ 0_{1\times2} & 1 \end{bmatrix} \tag{3.18}$$

$$\text{In 3D: } {}^V S_a^b = \begin{bmatrix} R_a^b & \begin{bmatrix} P_a^b \times \end{bmatrix} R_a^b \\ 0_{3*3} & R_a^b \end{bmatrix} \tag{3.19}$$

As mentioned in Murray et al. (1994, p.63), wrench transformation matrices can be used to represent a wrench with respect to a coordinate frame which is not inside the rigid body. The obtained wrench represents the equivalent force/moment pair applied as if a lever arm were physically present between the coordinate frame and the rigid body. Therefore, care must be taken when applying a wrench transformation matrix to avoid creating artificial force/moment pairs. A similar comment applies to twist computation.

Assuming a frictionless contact between rigid objects implies that no instantaneous power is dissipated when moving a rigid body through an applied force. In this situation,

64

the wrench is said to be reciprocal to the twist and the inner product between the wrench and the twist is zero (Ball 1900):

$$F^i \cdot V^i = 0 \qquad (3.20)$$

The reciprocity condition (3.20) can then be used with the wrench and twist consistency equations (3.14) and (3.15) to show reciprocity between the wrench and twist bases:

$$\left(G^i\right)^T J^i = 0 \qquad (3.21)$$

In addition, equation (3.20) can be combined with the consistency equations (3.14) and (3.15) to produce reciprocity equations for the wrench (3.22) and twist (3.23) respectively.

$$\left(J^i\right)^T F^i = 0 \qquad (3.22)$$

$$\left(G^i\right)^T V^i = 0 \qquad (3.23)$$

It is assumed that forces and moments are measured by a force sensor located at the gripper coordinate frame, and that velocity is computed with respect to the world frame. As a result, a wrench transformation matrix must be used to transform a wrench basis from the contact frame to the world frame and a twist transformation matrix must be defined to transform a twist basis from the contact frame to the gripper frame. The

reciprocity equations for the measured wrench and measured twist are expressed as follows:

$$\left(^{V}S_{g}^{c}J^{c}\right)^{T}F^{g}=0 \tag{3.24}$$

$$\left(^{F}S_{w}^{c}G^{c}\right)^{T}V^{w}=0 \tag{3.25}$$

The screw transformation matrices used in (3.24) and (3.25) are not directly known; however, they can be computed indirectly by applying the closure chain described in Fig. 3.4 to screw transformations, as shown in (3.26).

$$S_{w}^{g}(t)S_{g}^{m}S_{m}^{f}S_{f}^{w}=I \tag{3.26}$$

As illustrated in Fig. 3.5, there exist two possible paths to go from one frame to another in a closed kinematic chain. As a result, there are two ways of expressing the reciprocity equation for the measured wrench and measured twist, as shown in (3.27) and (3.28), respectively. In practice, the path that most simplifies $^{V}S_{g}^{c}$ or $^{F}S_{w}^{c}$ is chosen.

$$\begin{cases}\left(^{V}S_{g}^{m}{}^{V}S_{m}^{c}J^{c}\right)^{T}F^{g}=0\\\left(^{V}S_{g}^{w}(t)^{V}S_{w}^{f}{}^{V}S_{f}^{c}J^{c}\right)^{T}F^{g}=0\end{cases} \tag{3.27}$$

$$\begin{cases}\left(^{F}S_{w}^{f}{}^{F}S_{f}^{c}G^{c}\right)^{T}V^{w}=0\\\left(^{F}S_{w}^{g}(t)^{F}S_{g}^{m}{}^{F}S_{m}^{c}G^{c}\right)^{T}V^{w}=0\end{cases} \tag{3.28}$$

The final expressions of the reciprocity equations for the measured wrench and measured twist are obtained in 2D by substituting (3.18) in (3.27) and (3.16) in (3.28) respectively, and in 3D, by substituting (3.19) in (3.27) and (3.17) in (3.28). As for the pose equation, these equations are made algebraic by replacing the trigonometric nonlinearities by polynomial expressions. An example illustrating the concepts of the reciprocity equation for the measured wrench and measured twist is given in section 3.3.

Equations (3.27) and (3.28) only hold when no power is dissipated during the motion. As a consequence, these equations generally do not apply during transitions between contact states since transitions almost always create impact forces (Eberman 1995).

3.2.4   Relationship Between the Pose and Twist Equations

The pose equations derived in section 3.2.2 represent constraints on the configurations of the manipulator robot (e.g., $\{x(t), y(t), \theta(t)\}$ in 2D) imposed by the geometric nature of the contact states. Given a geometric description of the manipulated object and the fixed object, the configurations that satisfy the pose equations associated with a contact state can be computed using (3.6) or (3.7). The result is a set of configuration points that describe a surface in the configuration space (C-surface in Mason 1981). This concept is illustrated in Fig. 3.6. The pose equation derived in (3.33) is utilized to extract the $\{x(t), y(t), \theta(t)\}$ configurations associated with the given geometry of a vertex-edge contact. Figure 3.6(a) shows one possible configuration in the Cartesian space; Fig. 3.6(b) shows multiple configurations in the Cartesian space, and Fig. 3.6(c) shows the C-surface associated with the contact.

67
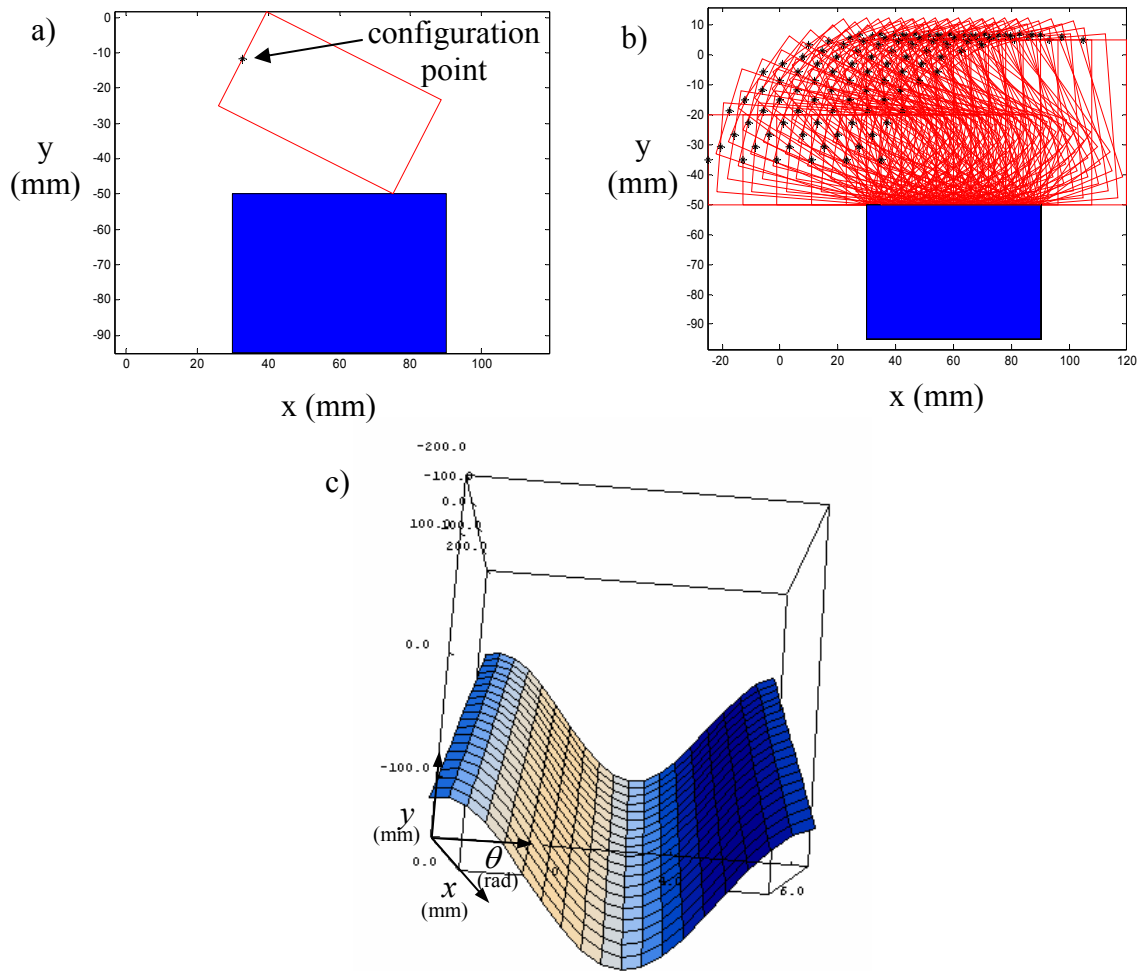
Figure 3.6: Representation of a vertex-edge contact. a) Representation of the contact in the Cartesian space for one configuration, b) Representation of the contact in the Cartesian space for multiple configurations, and c) Representation of the contact in the configuration space.

The geometric properties of the configuration space have been extensively studied in the literature, e.g., Arnold (1989). The relationship between the kinematic equation and the twist reciprocity equation can be derived from the cotangent space of the C-surface. The cotangent space N is the space of all the wrenches (Arnold 1989) as shown in (3.29).

From a geometrical point of view, the cotangent vector at a configuration s is given by the normal of the C-surface at that point, as expressed in (3.30).

$$N = G^w \qquad (3.29)$$

$$N = \nabla h(p, s(t)) = \left[\frac{\partial h}{\partial s_1} \quad \frac{\partial h}{\partial s_2} \quad \cdots \quad \frac{\partial h}{\partial s_n} \right]^T \qquad (3.30)$$

Using the chain rule, the time derivative of the pose equation is expressed in (3.31) as the product of the measured twist and the gradient of the pose equation. As a result, the reciprocity equation for the measured twist is equivalent to the time derivative of the pose equation as shown in (3.32).

$$\frac{dh(p, s(t))}{dt} = \sum_{i=1}^{n} \frac{\partial h}{\partial s_i} \dot{s}_i = \left[\nabla h \right]^T V^w \qquad (3.31)$$

$$\frac{dh(p, s(t))}{dt} = \left(G^w \right)^T V^w \qquad (3.32)$$

3.3 A Contact State Modeling Example

To illustrate the modeling techniques presented in this chapter, a vertex-to-edge contact between two polygons is considered in Fig. 3.7. The pose equation, the reciprocity equation for the twist and the reciprocity equation for the wrench corresponding to this contact are derived in this section.
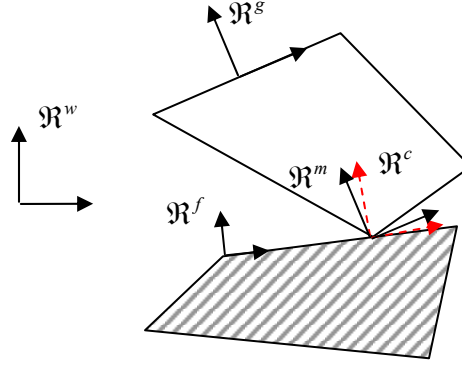
Figure 3.7: Single vertex-edge contact between two polygons.

3.3.1 Pose Equation

No translation normal to the environment object's edge is allowable. Therefore, $T_f^m(2,3)$ must be zero. Following Appendix A, the corresponding equation can be written as:

$$h_p : f_2 f_3 - f_1 f_4 - f_2 x + f_1 y + \left(-f_2 m_3 + f_1 m_4\right)\cos\theta + \left(f_1 m_3 + f_2 m_4\right)\sin\theta = 0 \quad (3.33)$$

3.3.2 Reciprocity Equation for the Measured Twist

As shown in Fig. 3.7, the frame $\Re^c$ associated with the contact is located at the contacting vertex and has the orientation of the frame associated with the fixed object (i.e., $\Re^f$). As a result, the transformation matrix between the contact frame and the manipulated object frame reduces to a rotation matrix.

$$T_m^c = \begin{pmatrix} R_m^f & 0_{2\times1} \\ 0_{1\times2} & 1 \end{pmatrix} \quad (3.34)$$

In this frame, the basis for the wrench can be written as follows:

$$G^c = \begin{pmatrix} 0 \\ 1 \\ 0 \end{pmatrix} \tag{3.35}$$

The wrench basis can then be expressed in the world frame using (3.28):

$$G^w = \tilde{R}_w^g(t)\,{}^F S_g^m\,{}^F S_m^c G^c \tag{3.36}$$

$$\text{where } \tilde{R}_w^g(t) = \begin{pmatrix} R_w^g(t) & 0_{2\times 1} \\ 0_{1\times 2} & 1 \end{pmatrix}$$

Note that for the sake of simplicity, the joints and links of the manipulated robot are not modeled in this example. As a consequence, there is no physical link between the gripper frame and the world frame. Thus, the last screw transformation matrix in (3.28) is replaced by a rotation matrix $\tilde{R}_w^g$. Using (3.16), the wrench basis can be expanded as follows:

$$G^w = \begin{pmatrix} -f_2 \\ f_1 \\ f_2\left(\sin\theta\, m_3 + \cos\theta\, m_4\right) + f_1\left(\cos\theta\, m_3 - \sin\theta\, m_4\right) \end{pmatrix} \tag{3.37}$$

71

As a final step, the reciprocity equation for the measured twist is expressed in (3.38) using (3.28). One can easily verify that this equation corresponds to the derivative with respect to time of the pose equation presented in (3.33).

$$h_t : -f_2 v_x + f_1 v_y + \left(\left(f_1 m_3 + f_2 m_4 \right) \cos \theta + \left(f_2 m_3 - f_1 m_4 \right) \sin \theta \right) \omega = 0 \quad (3.38)$$

3.3.3 Reciprocity Equation for the Measured Wrench

The basis for the twist can be written in the contact frame $\Re^c$ by inspection, as shown in (3.39). This basis corresponds to the motions allowable by the contact.

$$J^c = \begin{pmatrix} 1 & 0 \\ 0 & 0 \\ 0 & 1 \end{pmatrix} \quad (3.39)$$

The twist basis can then be expressed in the gripper frame using (3.27):

$$J^g = {}^V S_g^m \, {}^V S_m^c J^c \quad (3.40)$$

Using (3.18), the twist basis can be expanded as follows:

$$J^g = \begin{pmatrix} f_1 \cos \theta + f_2 \sin \theta & m_4 \\ f_2 \cos \theta - f_1 \sin \theta & -m_3 \\ 0 & 1 \end{pmatrix} \quad (3.41)$$

As a final step, the reciprocity equation for the measured wrench is expressed in (3.42) using (3.27).

$$h_w : \begin{cases} F_y \left(f_2 \cos\theta - f_1 \sin\theta \right) + F_x \left(f_1 \cos\theta + f_2 \sin\theta \right) = 0 \\ \tau - F_y m_3 + F_x m_4 = 0 \end{cases} \qquad (3.42)$$

3.4 Summary

This chapter discussed the representation of contact states. In the first part of the chapter, the representation of contact states in Cartesian space was reviewed. It was shown that rigid polygonal and polyhedral objects could be described using a limited number of geometric elements (i.e., vertex, edge, and face) which could then be combined to form contact states. This approach was utilized to derive lists of possible single and double contact states for tasks involving polygonal and polyhedral objects.

In the second part of the chapter, the representation of contact states in the sensor space was presented. Three sensor modalities were considered (i.e., pose, twist, and wrench) and techniques based on kinematic constraints and twist and wrench reciprocity were described to obtain the contact models. As a result, contact states were modeled as homogeneous nonlinear algebraic equations parameterized by time-dependent sensor data and time-independent parameters representing the unknown locations and positions of the objects in contact.

As shown in Fig. 1.4, the two sub-problems of contact topology and contact state modeling treated in this chapter affect all of the remaining design problems associated with the construction of a contact state estimator. The next chapter discusses the distinguishability and identifiability of the contact models developed in this chapter. These two properties are needed to ensure the feasibility of contact state estimation as well as

the feasibility of parameter estimation. As discussed, the contact topology can be chosen to ensure contact state distinguishability in the Cartesian space (i.e., no degenerate contact states in Table 3.3). Nevertheless, tools need to be created to investigate the distinguishability of contact states in the sensor space. The next chapter presents a solution to this problem. In addition, the identifiability of the parameters associated with each contact model is also investigated.

Chapter 4

Identifiability and Distinguishability Testing

This chapter addresses two fundamental questions that must be answered when formulating mathematical descriptions of contact states: are the contact states distinguishable from each other? Can the unknown or imprecisely known parameters in these descriptions be identified? An analytical method is presented for evaluating the distinguishability and identifiability of a set of contact state models described by nonlinear algebraic equations. In contrast to the analytical techniques proposed in the literature that focus either on distinguishability or identifiability, the proposed approach, based on Taylor series expansion of the contact equations, presents a unified technique for the testing of both properties. Moreover, it can be applied to any contact model that

can be written as homogeneous equations, regardless of the sensing modality (e.g., pose, wrench, twist) and dimensionality (e.g., planar, spatial) chosen to represent the model.

This chapter starts by defining the concepts of identifiability and distinguishability in the context of contact state estimation. In particular, it is shown that identifiability reduces to a uniqueness problem whereas distinguishability reduces to an existence problem. Both problems require contact models to be compared and analyzed. A method based on Taylor series expansion of contact models is utilized to test the capability of candidate models to estimate both the parameters and the states. The technique is illustrated for several planar and spatial examples. A complexity analysis of the method applied to pose equations is discussed at the end of the chapter..

4.1 Contact State Distinguishability and Identifiability Definitions

Given nonlinear algebraic models of contact states, parameterized by sensor variables, $s(t)$, and time-independent configuration parameters, p (e.g., any of the contact state models derived in 3.3), distinguishability and identifiability can be defined in the manner of Walter and Pronzato (1996) as follows:

Definition 4.1. *Two contact state models A and B, parameterized by a sensor path $s(t)$ and by configuration parameters (p for A and q for B) are <u>distinguishable</u> if, for almost any sensor path $s(t)$ of sufficient length, there is no solution for the parameter set $\{p, q\}$ such that the contact models are satisfied simultaneously.*

Definition 4.2. *A contact state model A is <u>globally identifiable</u> if, given almost any sensor path $s(t)$ of sufficient length, there exists a unique solution for p that satisfies model A. If there are a finite number of solutions then contact model A is <u>locally identifiable</u>.*

In these definitions, the sensor path must be at least of the minimum length corresponding to the number of unknown parameters associated with the models. The phrase "almost any sensor path" is meant to rule out unexciting paths. In definition 4.2, local identifiability is equivalent to the model being minimal (i.e., a model in which unidentifiable parameters are eliminated or grouped into terms which are identifiable, Gautier and Khalil 1990). Note that a model being minimal guarantees the existence of a solution but not its uniqueness.

The following section develops a systematic method for evaluating these definitions for contact states modeled as homogeneous nonlinear algebraic equations.

4.2 Taylor Series Testing of Distinguishability and Identifiability

Distinguishability and identifiability testing is based on finding practical ways to analyze and compare equations. In that regard, Taylor series expansion can be effective since it allows a nonlinear model to be written as a unique set of algebraic equations in which each equation corresponds to a coefficient of the series. Thus, Taylor series reduce the distinguishability and identifiability testing to a comparison of the different coefficients of the series. While there are an infinite number of coefficients, a decision

on distinguishability and identifiability can often be made based on comparing a modest number of coefficients. As a result, no approximation is being made when using the series. This technique was successfully applied to testing the identifiability and distinguishability of zero-input state-space models (e.g., Pohjanpalo 1978, Walter and Pronzato 1996). In this approach, the Taylor series of the output vector is written as a succession of time derivatives evaluated at time $t = 0^+$. These coefficients form a set of algebraic equations that must be solved for all the possible sets of parameters. Although the sets of equations can be difficult to solve by hand, tools from commutative algebra can be used to simplify the equations (Raksanyi et al. 1985).

In developing a Taylor series approach for contact models, the model M is permitted to be nonlinear in the parameters p as well as the sensor variables $s(t)$,

$$M : \begin{cases} F(p, s(t)) = 0 \\ H(p) = 0 \end{cases} \tag{4.1}$$

$F(\cdot)$ includes all the sensor-dependent equality constraints while $H(\cdot)$ models any additional equality constraint on the parameters. Assuming that the function $F(p, s)$ is analytic, a Taylor series expansion of order k with respect to the sensor variables can be written as:

$$\begin{cases} F(p,s) = \sum_{i=0}^{k} a_i(p,s_0) \dfrac{(s-s_0)^i}{k!} \\[2ex] a_i(p,s_0) = \dfrac{d^i F(p,s)}{ds^i}\bigg|_{s=s_0} \end{cases} \qquad (4.2)$$

Note that each coefficient of the Taylor series (i.e., $a_i(p,s_0)$) is a function of the unknown constant parameters and the known sensor values. If more than one sensor variable appears in the model, then partial derivatives with respect to all the sensor variables can be computed. Equation (4.3) shows a second order expansion of a function of three variables $\{s_1, s_2, s_3\}$. This expansion could be applied, for example, to planar contact states described using pose equations by substituting $\{s_1, s_2, s_3\}$ by $\{x, y, \theta\}$.

$$\begin{cases} F(p,\{x,y,\theta\}) = F(p,s)\big|_{s=s_0} + \sum_{i=1}^{3} \dfrac{\partial F(p,s)}{\partial s_i}\bigg|_{s=s_0} (s_i - s_{i0}) + \sum_{i=1}^{3}\sum_{j=1}^{3} \dfrac{\partial^2 F(p,s)}{\partial s_i \partial s_j}\bigg|_{s=s_0} \dfrac{(s_i - s_{i0})(s_j - s_{j0})}{2!} + \cdots \\[2ex] s = \{s_1, s_2, s_3\} \\[1ex] s_0 = \{s_{10}, s_{20}, s_{30}\} \end{cases} \qquad (4.3)$$

Since the function $F(p,s)$ is assumed to be infinitely differentiable with respect to its sensor variables, its mixed derivatives are equal. With m as the number of sensor variables and k as the order of the expansion, the number of coefficients n_c of the series is given by:

$$n_c = \frac{(k+m)!}{k!\,m!} \qquad (4.4)$$

4.2.1 Distinguishability Testing

Based on the uniqueness of the Taylor series expansion, two contact state models are equivalent if and only if all the coefficients of their expansions are equal, as given below:

$$A(p,s) = B(q,s) \Leftrightarrow \begin{cases} a_0(p,s_0) = b_0(q,s_0) \\ a_1(p,s_0) = b_1(q,s_0) \\ \quad\vdots \\ a_n(p,s_0) = b_n(q,s_0) \\ H_1(p) = H_2(q) \end{cases} \tag{4.5}$$

This equality leads to the following test for distinguishability.

Definition 4.3. *Two contact state models A and B in the form of (4.1) are distinguishable if and only if for any s_0, (i) given any choice of p, there is no solution to (4.5) for q, and (ii) given any choice of q, there is no solution to (4.5) for p.*

To demonstrate that two models A and B are distinguishable, their Taylor coefficients (i.e., $a(p,s_0)$ and $b(q,s_0)$) must differ in at least one equation of (4.5) for all choices of parameters.

4.2.2 Identifiability Testing

The identifiability of a contact model can be tested by considering how many sets of parameters yield the same Taylor series coefficients in (4.2). This test can be performed by counting the number of solutions for p, given $\hat{p}$, in the equation below:

$$A(p,s) = A(\hat{p},s) \Leftrightarrow \begin{cases} a_0(p,s_0) = a_0(\hat{p},s_0) \\ a_1(p,s_0) = a_1(\hat{p},s_0) \\ \quad\vdots \\ a_n(p,s_0) = a_n(\hat{p},s_0) \\ H_1(p) = H_1(\hat{p}) \end{cases} \qquad (4.6)$$

This test can be stated formally as follows.

Definition 4.4. *A contact state mode A is <u>identifiable</u> if and only if, for all s_0 , given any*

$\hat{p}$, there is a unique solution to (4.6), which is $p = \hat{p}$. If a finite number of solutions for

p exist then A is <u>locally identifiable</u>. A is <u>unidentifiable</u> if an infinite number of

solutions exist.

Since the Taylor series is developed around nominal sensor values, the approach

appears to be local in the space of sensor variables. It is important to note, however, that

the solutions for the parameters are obtained without substituting numerical values for the

sensor values s_0 and so the results are truly global in the sensor space.   Testing

identifiability involves solving for the number of solutions for p in (4.6). Note that the

solution $p = \hat{p}$ always exists.

4.3 Examples

Four examples are presented to illustrate the Taylor series technique of testing the distinguishability and identifiability of contact models for polygonal and polyhedral objects. The first two test the distinguishability and identifiability of a pair of polygonal contact models while the last two focus on the identifiability and distinguishability testing of a pair of polyhedral contact models.

4.3.1   Example 1 – Distinguishability of Polygonal Vertex–Edge Contacts

As a first example, the distinguishability of the models developed for the contact states of Fig. 4.1 is tested. The pose equations for the contacts $\left\{V^m - E^f\right\}$ and $\left\{E^m - V^f\right\}$ (i.e., contact A and contact B respectively) are obtained using the technique described in section 3.2.2. The corresponding equations are shown in (4.7) and (4.8).
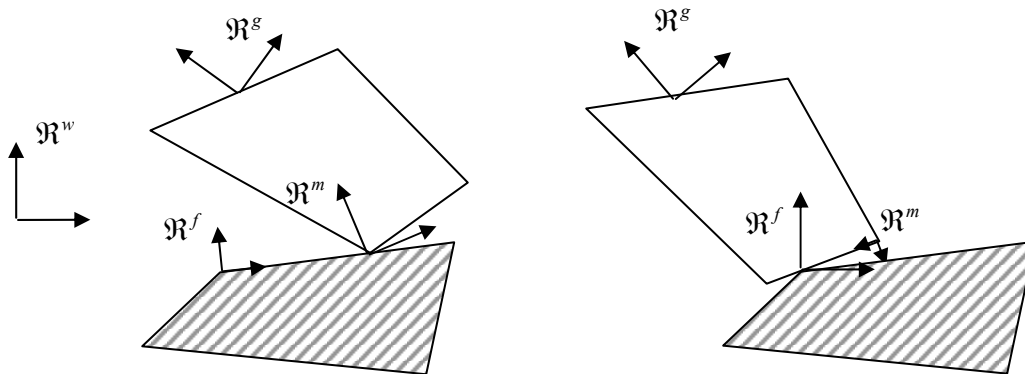
Figure 4.1: Contact between two polygons. a) Contact between a vertex of the manipulated object and an edge of the fixed object, and b) Contact between a vertex of the fixed object and an edge of the manipulated object.

$$A: \begin{cases} F^a(p,s) = p_5 + (p_2 p_3 - p_1 p_4)\cos\theta(t) - (p_1 p_3 + p_2 p_4)\sin\theta(t) + p_2 x(t) - p_1 y(t) = 0 \\ H^a(p) = p_1^2 + p_2^2 - 1 = 0 \end{cases} \quad (4.7)$$

$$B: \begin{cases} F^b(q,s) = q_5 + (q_1 q_4 - q_2 q_3 + q_2 x(t) - q_1 y(t))\cos\theta(t) - (q_1 q_3 + q_2 q_4 - q_1 x(t) - q_2 y(t))\sin\theta(t) = 0 \\ H^b(q) = q_1^2 + q_2^2 - 1 = 0 \end{cases}$$

$$(4.8)$$

Series coefficients are given in (4.9) for contact A and in (4.10) for contact B. Due to the cyclic nature of the derivatives of sine and cosine, derivative terms beyond second order do not generate independent equations.

$$\begin{cases} a_0 = F^a(p,s_0) = p_5 + (p_2 p_3 - p_1 p_4)\cos\theta_0 - (p_1 p_3 + p_2 p_4)\sin\theta_0 + p_2 x_0 - p_1 y_0 = 0 \\ a_1 = F^a_\theta(p,s_0) = -(p_1 p_3 + p_2 p_4)\cos\theta_0 - (p_2 p_3 - p_1 p_4)\sin\theta_0 \\ a_2 = F^a_x(p,s_0) = p_2 \\ a_3 = F^a_y(p,s_0) = -p_1 \\ a_4 = F^a_{\theta\theta}(p,s_0) = -(p_2 p_3 - p_1 p_4)\cos\theta_0 + (p_1 p_3 + p_2 p_4)\sin\theta_0 \\ a_5 = F^a_{\theta x}(p,s_0) = 0 \\ a_6 = F^a_{\theta y}(p,s_0) = 0 \\ a_7 = F^a_{xx}(p,s_0) = 0 \\ a_8 = F^a_{xy}(p,s_0) = 0 \\ a_9 = F^a_{yy}(p,s_0) = 0 \end{cases} \quad (4.9)$$

$$\begin{cases} b_0 = F^b(q,s_0) = q_5 + (q_1q_4 - q_2q_3 + q_2x_0 - q_1y_0)\cos\theta_0 - (q_1q_3 + q_2q_4 - q_1x_0 - q_2y_0)\sin\theta_0 = 0 \\ b_1 = F_\theta^b(q,s_0) = -(q_1q_3 + q_2q_4 - q_1x_0 - q_2y_0)\cos\theta_0 - (q_1q_4 - q_2q_3 + q_2x_0 - q_1y_0)\sin\theta_0 \\ b_2 = F_x^b(q,s_0) = q_2\cos\theta_0 + q_1\sin\theta_0 \\ b_3 = F_y^b(q,s_0) = -q_1\cos\theta_0 + q_2\sin\theta_0 \\ b_4 = F_{\theta\theta}^b(q,s_0) = -(q_1q_4 - q_2q_3 + q_2x_0 - q_1y_0)\cos\theta_0 + (q_1q_3 + q_2q_4 - q_1x_0 - q_2y_0)\sin\theta_0 \\ b_5 = F_{\theta x}^b(q,s_0) = -q_2\sin\theta_0 + q_1\cos\theta_0 \\ b_6 = F_{\theta y}^b(q,s_0) = q_1\sin\theta_0 + q_2\cos\theta_0 \\ b_7 = F_{xx}^b(q,s_0) = 0 \\ b_8 = F_{xy}^b(q,s_0) = 0 \\ b_9 = F_{yy}^b(q,s_0) = 0 \end{cases} \qquad (4.10)$$

Applying Definition 3 to test the distinguishability of models (4.7) and (4.8) involves combining (4.9)-(4.10) in the form of (4.5). It can be directly observed that the pair of equations below cannot be satisfied since they contradict $q_1^2 + q_2^2 = 1$ in (4.8).

$$\begin{cases} a_5 = b_5 \\ a_6 = b_6 \end{cases} \Leftrightarrow \begin{cases} 0 = -q_2\sin\theta_0 + q_1\cos\theta_0 \\ 0 = q_1\sin\theta_0 + q_2\cos\theta_0 \end{cases} \Rightarrow q_1^2 + q_2^2 = 0 \qquad (4.11)$$

Since the equations have no solution regardless of whether p or q is given, the two contact state models are distinguishable.

4.3.2   Example 2 – Identifiability of a Polygonal Vertex–Edge Contact

The identifiability of the contact model representing the contact state of Fig. 4.1(a) is tested here. To apply Definition 4, at least five independent equations are needed to

solve for the five parameters $p_1 - p_5$. The Taylor series coefficients expressed in (4.9)

provide five equations which can be combined with the last equation of (4.7) to obtain a

set of six equations in the form of (4.6).

$$
\left\{
\begin{array}{c}
p_5 + (p_2 p_3 - p_1 p_4)\cos\theta_0 - (p_1 p_3 + p_2 p_4)\sin\theta_0 + p_2 x_0 - p_1 y_0 \\
= \hat{p}_5 + (\hat{p}_2 \hat{p}_3 - \hat{p}_1 \hat{p}_4)\cos\theta_0 - (\hat{p}_1 \hat{p}_3 + \hat{p}_2 \hat{p}_4)\sin\theta_0 + \hat{p}_2 x_0 - \hat{p}_1 y_0 = 0 \\
-(p_1 p_3 + p_2 p_4)\cos\theta_0 - (p_2 p_3 - p_1 p_4)\sin\theta_0 = -(\hat{p}_1 \hat{p}_3 + \hat{p}_2 \hat{p}_4)\cos\theta_0 - (\hat{p}_2 \hat{p}_3 - \hat{p}_1 \hat{p}_4)\sin\theta_0 \\
p_2 = \hat{p}_2 \\
-p_1 = -\hat{p}_1 \\
-(p_2 p_3 - p_1 p_4)\cos\theta_0 + (p_1 p_3 + p_2 p_4)\sin\theta_0 = -(\hat{p}_2 \hat{p}_3 - \hat{p}_1 \hat{p}_4)\cos\theta_0 + (\hat{p}_1 \hat{p}_3 + \hat{p}_2 \hat{p}_4)\sin\theta_0 \\
p_1^2 + p_2^2 = \hat{p}_1^2 + \hat{p}_2^2 = 1
\end{array}
\right.
\tag{4.12}
$$

To obtain all possible solutions for p given $\hat{p}$, it can be seen that the third and fourth

equations define uniquely p_1 and p_2 and that this solution also satisfies the sixth

equation. Given p_1 and p_2, the remaining parameters appear linearly in the three

remaining equations. Consequently, equation (4.12) admits only one solution, given

below.

$$
\begin{aligned}
p_1 &= \hat{p}_1 \\
p_2 &= \hat{p}_2 \\
p_3 &= \hat{p}_3 \\
p_4 &= \hat{p}_4 \\
p_5 &= \hat{p}_5
\end{aligned}
\tag{4.13}
$$

By Definition 4, contact state A is globally identifiable.

4.3.3 Example 3 – Identifiability of a Polyhedral Vertex–Face Contact

To demonstrate the applicability of the approach to polyhedral models, this example considers the identifiability of the contact $\{V^m - F^f\}$ shown in Fig. 4.2.
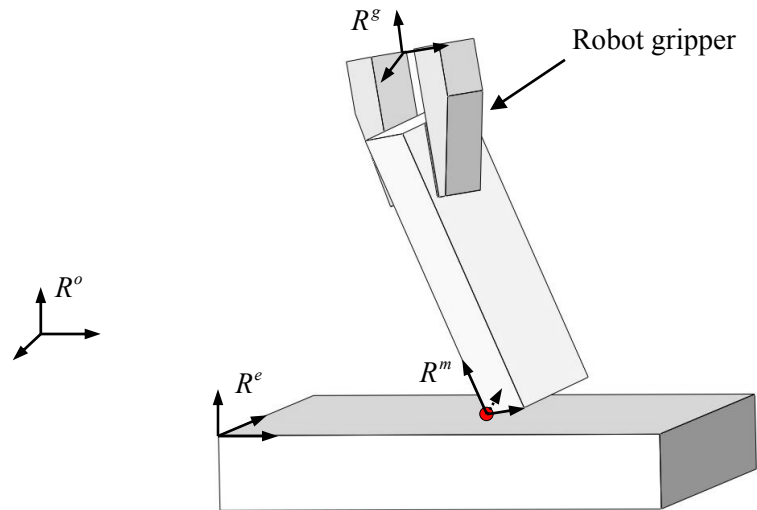
Figure 4.2: Vertex – Face contact state.

Using the techniques described in section 3.2.2, the contact model can be written as follows:

$$C: \begin{cases} F^c(p,s) = p_{10} + K_1 x(t) + K_2 y(t) + K_3 z(t) \\ \quad + p_7 \left[K_1 \cos\beta(t)\cos\alpha(t) + K_2 \cos\beta(t)\sin\alpha(t) - K_3 \sin\beta(t) \right] \\ \quad + p_8 \left[\begin{array}{l} K_1\left(\cos\alpha(t)\sin\gamma(t)\sin\beta(t) - \cos\gamma(t)\sin\alpha(t)\right) \\ + K_2\left(\cos\gamma(t)\cos\alpha(t) + \sin\gamma(t)\sin\beta(t)\sin\alpha(t)\right) + K_3 \cos\beta(t)\sin\gamma(t) \end{array} \right] \\ \quad + p_9 \left[\begin{array}{l} K_1\left(\cos\gamma(t)\cos\alpha(t)\sin\beta(t) + \sin\gamma(t)\sin\alpha(t)\right) \\ + K_2\left(-\cos\alpha(t)\sin\gamma(t) + \cos\gamma(t)\sin\beta(t)\sin\alpha(t)\right) + K_3 \cos\gamma(t)\cos\beta(t) \end{array} \right] = 0 \\[6pt] K_1 = p_1 p_4 p_5 + p_2 p_6 \\ K_2 = p_2 p_4 p_5 - p_1 p_6 \\ K_3 = p_3 p_5 \\[6pt] p_1^2 + p_2^2 = 1 \\ p_3^2 + p_4^2 = 1 \\ p_5^2 + p_6^2 = 1 \end{cases} \qquad (4.14)$$

Here, $[p_1, p_2, p_3, p_4, p_5, p_6]$ are used to parameterize the three unknown rotations used in T_o^e and $[p_7, p_8, p_9]$ represent the unknown translations used in T_g^m. The parameter p_{10} represents the magnitude of the position vector between the world and environment object frames projected on the normal of the contact's face. The sensor variables $\{x, y, z, \alpha, \beta, \gamma\}$ represent the position and orientation of the robot gripper.

At least ten equations are needed to solve for the ten parameters. Since six sensor variables are available, seven Taylor coefficients are provided through first order expansion. These equations can be combined with the last three equations of (4.14) to obtain the desired number of equations. Since $p_1 - p_6$ are the only coefficients multiplying $\{x(t), y(t), z(t)\}$, the first order coefficients with respect to these sensing

variables can be combined with the last three constraint equations of (4.14) to produce the algebraic system of six equations:

$$\begin{cases} a_1 = F_x^c\left(p, s_0\right) = K_1 = p_1 p_4 p_5 + p_2 p_6 \\ a_2 = F_y^c\left(p, s_0\right) = K_2 = p_2 p_4 p_5 - p_1 p_6 \\ a_3 = F_z^c\left(p, s_0\right) = K_3 = p_3 p_5 \\ p_1^2 + p_2^2 = 1 \\ p_3^2 + p_4^2 = 1 \\ p_5^2 + p_6^2 = 1 \end{cases} \qquad (4.15)$$

This system admits an infinite number of solutions given in (4.16) with p_5 and p_6 as free parameters. Note that the choice of the free parameters is arbitrary; any pair $\{p_1, p_2\}$, $\{p_3, p_4\}$ or $\{p_5, p_6\}$ can be chosen to solve for the remaining parameters. By Definition 4, the contact state is unidentifiable.

$$\begin{cases} p_1 = \dfrac{-2\hat{p}_2 \hat{p}_4 p_5 p_6 + \hat{p}_1\left(p_6^2 + \hat{p}_4^2 p_5^2\right)}{p_6^2 + \hat{p}_4^2 p_5^2} \\ p_2 = \dfrac{2\hat{p}_1 \hat{p}_4 p_5 p_6 + \hat{p}_2\left(\hat{p}_4^2 p_5^2 + p_5^2 - 1\right)}{p_6^2 + \hat{p}_4^2 p_5^2} \\ p_3 = \hat{p}_3 \\ p_4 = \hat{p}_4 \end{cases} \qquad (4.16)$$

Equation (4.16) shows that two out of the three angles specifying the orientation of the environment object can be uniquely identified. This can be explained geometrically by noticing that the contact state is invariant under rotations of the environment object about the face's normal. This suggests that the contact should be re-parameterized using

only two angles to model the orientation uncertainty of the environment object. In this case, p_5 and p_6 can be selected arbitrarily giving a unique solution to (4.16). Note that over-parameterization is often a result of applying general modeling techniques, such as the techniques presented in section 3.2. To obtain a minimal representation, the unidentifiable parameters must be grouped to form identifiable parameters or eliminated (Gautier and Khalil 1990). This reduction task can be difficult to implement analytically for arbitrary models. The proposed identifiability test is a general tool for detecting the presence of unidentifiable parameters.

Given that p_1 - p_4 are identifiable, the identifiability of the remaining parameters can be investigated by looking at the four remaining first order Taylor coefficients of (4.14), as shown in (4.17).

$$
\begin{cases}
a_0 = F^c(p,s_0) = p_{10} + K_1 x_0 + K_2 y_0 + K_3 z_0 + p_7 U + p_8 V + p_9 W \\
a_4 = F^c_\alpha(p,s_0) = p_7 U_\alpha + p_8 V_\alpha + p_9 W_\alpha \\
a_5 = F^c_\beta(p,s_0) = p_7 U_\beta + p_8 V_\beta + p_9 W_\beta \\
a_6 = F^c_\gamma(p,s_0) = p_7 U_\gamma + p_8 V_\gamma + p_9 W_\gamma
\end{cases}
\tag{4.17}
$$

In these equations, the variables U, V, W and their derivatives are nonlinear functions of the known variables $\alpha, \beta, \gamma, K_1, K_2,$ and K_3. Moreover, it can be shown that these four equations are linearly independent. As a consequence, $p_7 \ldots p_{10}$ can be uniquely identified given that K_1, K_2 and K_3 are known. Therefore, the vertex-face contact model is said to be globally identifiable, as long as the orientation uncertainty of the environment object is parameterized by two angles.

4.3.4 Example 4 – Distinguishability of Polyhedral Vertex–Face Contacts

This example examines the distinguishability of two contacts having the same topological form. The two contact models consist of a single vertex of the manipulated object in contact with either of two orthogonal faces of the environment object, as shown in Fig 4.3. The equations characterizing the contacts $\{V^m - F_1^f\}$ and $\{V^m - F_2^f\}$ are presented in (4.18) and (4.19) respectively. Note that (4.18) and (4.19) are minimal parameterizations obtained by selecting $p_5 = q_5 = 1$ and $p_6 = q_6 = 0$.
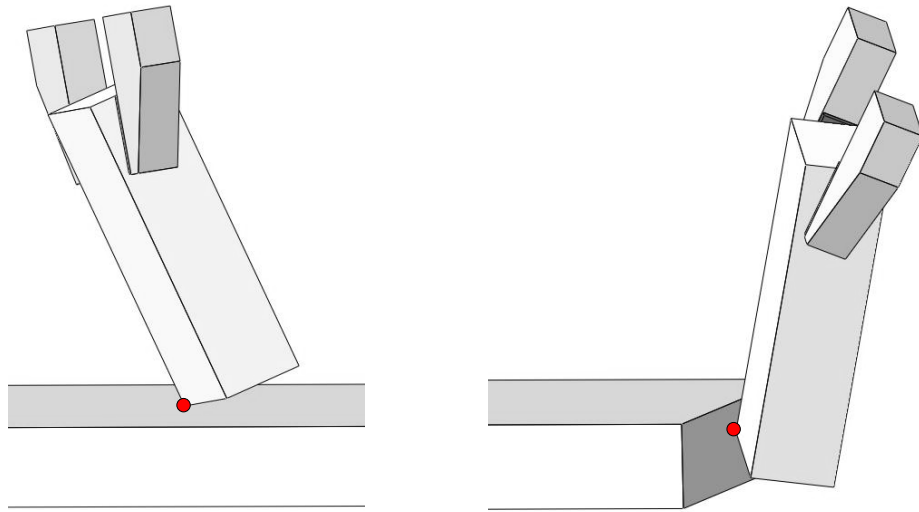
Figure 4.3: Two vertex–face contact states in which the location of the contact point is the same on the manipulated object but on two orthogonal faces of the environment object.

$$C' : \begin{cases} F^{c'}(p,s) = p_{10} + p_1 p_4 x(t) + p_2 p_4 y(t) + p_3 z(t) \\ + p_7 \left[p_1 p_4 \cos\beta(t)\cos\alpha(t) + p_2 p_4 \cos\beta(t)\sin\alpha(t) - p_3 \sin\beta(t) \right] \\ + p_8 \begin{bmatrix} p_1 p_4 \left(\cos\alpha(t)\sin\gamma(t)\sin\beta(t) - \cos\gamma(t)\sin\alpha(t) \right) \\ + p_2 p_4 \left(\cos\gamma(t)\cos\alpha(t) + \sin\gamma(t)\sin\beta(t)\sin\alpha(t) \right) + p_3 \cos\beta(t)\sin\gamma(t) \end{bmatrix} \\ + p_9 \begin{bmatrix} p_1 p_4 \left(\cos\gamma(t)\cos\alpha(t)\sin\beta(t) + \sin\gamma(t)\sin\alpha(t) \right) \\ + p_2 p_4 \left(-\cos\alpha(t)\sin\gamma(t) + \cos\gamma(t)\sin\beta(t)\sin\alpha(t) \right) + p_3 \cos\gamma(t)\cos\beta(t) \end{bmatrix} = 0 \quad (4.18) \\ \\ p_1^2 + p_2^2 = 1 \\ p_3^2 + p_4^2 = 1 \end{cases}$$

$$D : \begin{cases} F^{d}(q,s) = q_{10} + q_1 q_3 x(t) + q_2 q_3 y(t) - q_4 z(t) \\ + q_7 \left[q_1 q_3 \cos\beta(t)\cos\alpha(t) + q_2 q_3 \cos\beta(t)\sin\alpha(t) + q_4 \sin\beta(t) \right] \\ + q_8 \begin{bmatrix} q_1 q_3 \left(\cos\alpha(t)\sin\gamma(t)\sin\beta(t) - \cos\gamma(t)\sin\alpha(t) \right) + \\ q_2 q_3 \left(\cos\gamma(t)\cos\alpha(t) + \sin\gamma(t)\sin\beta(t)\sin\alpha(t) \right) - q_4 \cos\beta(t)\sin\gamma(t) \end{bmatrix} \\ + q_9 \begin{bmatrix} q_1 q_3 \left(\cos\gamma(t)\cos\alpha(t)\sin\beta(t) + \sin\gamma(t)\sin\alpha(t) \right) \\ + q_2 q_3 \left(-\cos\alpha(t)\sin\gamma(t) + \cos\gamma(t)\sin\beta(t)\sin\alpha(t) \right) - q_4 \cos\gamma(t)\cos\beta(t) \end{bmatrix} = 0 \quad (4.19) \\ \\ q_1^2 + q_2^2 = 1 \\ q_3^2 + q_4^2 = 1 \end{cases}$$

Since the orientation of the contacting face is the only difference between the two contacts, distinguishability is analyzed by looking at the parameters defining the unknown orientation of the two faces, i.e., $p_1 \ldots p_4$ for contact C' and $q_1 \ldots q_4$ for contact D. As a consequence, the distinguishability problem reduces to the comparison of the first order Taylor coefficients with respect to the position sensing variables. Definition 3 is applied to the equations formed by combining the three first order coefficients of

(4.18) and (4.19) together with the final equations of (4.18) and (4.19) in the form of (4.5).

$$
\begin{cases}
a_1 = b_1 \\
a_2 = b_2 \\
a_3 = b_3 \\
p_1^2 + p_2^2 = q_1^2 + q_2^2 = 1 \\
p_3^2 + p_4^2 = q_3^2 + q_4^2 = 1
\end{cases}
\Leftrightarrow
\begin{cases}
F_x^{c'}(p,s_0) = F_x^d(q,s_0) \\
F_y^{c'}(p,s_0) = F_y^d(q,s_0) \\
F_z^{c'}(p,s_0) = F_z^d(q,s_0) \\
p_1^2 + p_2^2 = q_1^2 + q_2^2 = 1 \\
p_3^2 + p_4^2 = q_3^2 + q_4^2 = 1
\end{cases}
\Leftrightarrow
\begin{cases}
p_1 p_4 = q_1 q_3 \\
p_2 p_4 = q_2 q_3 \\
p_3 = -q_4 \\
p_1^2 + p_2^2 = q_1^2 + q_2^2 = 1 \\
p_3^2 + p_4^2 = q_3^2 + q_4^2 = 1
\end{cases}
\qquad (4.20)
$$

The two solutions of (4.20) for p given q appear in (4.21). The same solutions arise when the system is solved for q given p. These two solutions define the same orientation and thus constitute a single solution.

$$
\begin{cases}
p_1 = q_1 \\
p_2 = q_2 \\
p_3 = -q_4 \\
p_4 = q_3
\end{cases}
,
\begin{cases}
p_1 = -q_1 \\
p_2 = -q_2 \\
p_3 = -q_4 \\
p_4 = -q_3
\end{cases}
\qquad (4.21)
$$

The final solution for (4.5) is given by (4.22).

$$
\begin{cases}
p_1 = q_1 \\
p_2 = q_2 \\
p_3 = -q_4 \\
p_4 = q_3 \\
p_7 = q_7 \\
p_8 = q_8 \\
p_9 = q_9 \\
p_{10} = q_{10}
\end{cases}
\qquad (4.22)
$$

This solution yields the anticipated result indicating the orthogonality of the two contact faces. By Definition 3, since a solution exists, the two contact states are indistinguishable. If, however, the orientation angle θ of the environment object with respect to the normal of its front face is known then:

$$
\begin{aligned}
p_3 &= q_3 = \cos\theta \\
p_4 &= q_4 = \sin\theta
\end{aligned}
$$
(4.23)

Equation (4.23) contradicts (4.22); consequently the contact states are distinguishable. This result can be explained geometrically by noticing that a 90 degree rotation around the environment object's front face of the contact depicted in Fig 4.3(a) leads to the contact pictured in Fig 4.3(b), making the two contacts indistinguishable. On the other hand, if the rotation angle is known, then the two contacts are distinguishable since no transformation than can change Fig 4.3(a) to Fig. 4.3(b) exists.

Recall that in Example 3, the vertex-face contact model used here was made identifiable by eliminating the parameter corresponding to rotation about the face's normal. Example 4 reveals that distinguishability can further restrict the choice of parameterization (i.e., free parameters) beyond what is needed for identifiability.

4.4 Computational Complexity Analysis

The distinguishability and identifiability tests presented in this thesis reduce to solving the sets of algebraic equations in (4.5) and (4.6). Determining the actual number of solutions to sets of nonlinear algebraic equations constitutes a challenge whose

difficulty increases with the number of equations, v, in the set. In this section, upper and lower bounds, $v_{\min}$ and $v_{\max}$, are derived on the number of equations in the sets described by (4.5) and (4.6) for pose equations.

4.4.1 Identifiability Testing

The complexity of the proposed approach depends on the size of the system of equations in (4.6) used to test identifiability. The goal of identifiability is to show that there is a unique set of parameters satisfying the system of nonlinear equations in (4.6). By construction, the system admits at least one solution. Since exactly determined systems of nonlinear equations usually admit multiple solutions, additional equations may be needed to show uniqueness. As a consequence, a lower bound on the number of independent algebraic equations needed to solve for the unknowns is given by n, the number of unknown parameters associated with the given contact equation.

$$v_{\min} = n \tag{4.24}$$

If $H(\cdot)$ in (4.6) provides β equations, then the number of Taylor series coefficient equations, n_c, needed to achieve this lower bound is given by:

$$n_c \geq v_{\min} - \beta \tag{4.25}$$

This is a lower bound on n_c since there is no guarantee that the algebraic equations from the Taylor series are independent. This bound on the number of coefficients can be related to the minimum order of the series, k_{min}, needed to produce them by substituting the minimum value of n_c from (4.25) into (4.4).

$$k_{min} = \min_{k=1,2,3,\ldots} \left[\left(\frac{(k+m)!}{k!m!} - v_{min} + \beta \right) \right] > 0 \qquad (4.26)$$

An upper bound on the series order can be derived by noting that pose equations involve only cyclic and polynomial functions of the sensor variables. As a consequence, the terms in the Taylor coefficients start repeating or go to zero after a finite number of differentiations. The number of differentiations required for a variable to repeat or go to zero is defined here as the degree of cyclicity of the variable and is denoted $C(\cdot)$.

The degree of cyclicity associated with the angular sensor variables s_a (e.g., $s_a = \{\alpha(t), \beta(t), \gamma(t)\}$ in 3D) equals four since, in every term (see e.g., (4.14)), the angular variables appear as linear trigonometric functions, e.g., sine or cosine. The degree of cyclicity for the positional sensor variables s_p (e.g., $s_p = \{x(t), y(t), z(t)\}$ in 3D) equals one since they appear linearly in the kinematic pose equations. See (4.14) as an example.

Since identifiability testing involves comparing sets of equations having identical structures, the signs of the repeating functions cancel, which reduces the cyclicity of the angular variables for identifiability testing from four to two:

$$C(s_a) = 2 \qquad C(s_p) = 1 \qquad (4.27)$$

For example, when testing (4.10) for identifiability, it can be seen that b_3 and b_5 yield the same equations when written in the form of (4.6). As a consequence, the upper bound k_{max} on the series order is given by:

$$k_{max} = \dim(s_a) \cdot C(s_a) \tag{4.28}$$

in which $\dim(s_a) = 1$ in 2D and $\dim(s_a) = 3$ in 3D. Therefore, the maximum number of equations available to test for identifiability is

$$v_{max} = \frac{(k_{max} + m)!}{k_{max}! m!} + \beta \tag{4.29}$$

While v_{max} can be large, many of these equations are either zero or redundant. The subset $v_{max}^* \leq v_{max}$ of nonzero independent equations can be obtained using a computer algebra package. The number of equations used to solve for identifiability is bounded as $v_{min} \leq v \leq v_{max}^* \leq v_{max}$. This bound can related to n_c, the number of Taylor coefficients, as:

$$v_{min} \leq \beta + n_c \leq v_{max}^* \tag{4.30}$$

96

Table 4.1 presents the lower and upper bounds as well as the actual number of equations, v_{act}, needed to test for identifiability in Examples 2 and 3, corresponding to equations (4.7) and (4.14). In both cases, the actual number of coefficients needed corresponds to the lower bound.

Table 4.1: Bounds on the number of equations needed for identifiability testing.

$v = n_c + \beta$	β	v_{min}	v^*_{max}	v_{max}	v_{act}
Example 2: $\{V^m - E^f\}$	1	5	6	11	5
Example 3: $\{V^m - F^f\}$	3	10	33	927	10

4.4.2 Distinguishability Testing

The goal of distinguishability testing is to show that there is no set of parameters satisfying the system of nonlinear equations in (4.5). To do so, at least one contradiction, valid for all choices of parameters, must be found in these equations. Assuming that a contradiction is not present in $H_1(p) = H_2(q)$, at least one Taylor coefficient is needed to establish distinguishability, resulting in the following lower bound:

$$n_c \geq 1 \Rightarrow v_{min} \geq \beta + 1 \qquad (4.31)$$

In contrast to identifiability testing, the lack of structural similarities between the left and right sides of (4.5) prevent the simplifications presented for identifiability (i.e., elimination of the redundant and nonzero parameters). Therefore, an upper bound on the number of coefficients for distinguishability testing is not easily established. In practice, the Taylor coefficients are computed one by one until a contradiction is found. If no contradiction is found after a large number of coefficients (i.e., $k = 10$ in (4.4)), then one gives up without drawing a conclusion on the distinguishability of the contact states.

Note that when a contradiction can be found, the actual number of equations computed for distinguishability testing depends on the order in which the Taylor coefficients are computed. In Example 1, the second order mixed derivatives $F_{\theta x}$ and $F_{\theta y}$ are needed to prove distinguishability. These derivatives correspond to the sixth and seventh coefficients, respectively, of (4.9) and (4.10). This choice in the order of the coefficients is arbitrary (e.g., $F_{\theta x}$ could be computed before $F_{\theta \theta}$); however, it impacts the number of equations computed for distinguishability. The worst possible ordering results in the computation of all the Taylor coefficients associated with the order of the expansion that yields a contradiction in (4.5). This expansion's order is labeled k^* and the number of equations corresponding to the worst ordering is given as follows:

$$v_{\max} = \frac{\left(k^* + m\right)!}{k^*!\, m!} + \beta \tag{4.32}$$

Table 4.2 gives the bounds as well as the actual number of equations, v_{act}, needed to test for the distinguishability of Examples 1 and 4. A second order expansion and first order expansion were needed for Examples 1 and 4, respectively.

Table 4.2: Bounds on the number of equations needed for distinguishability testing.

$v = n_c + \beta$	β	v_{min}	v_{max}	v_{act}
Example 1 $\left\{V^m - E^f\right\}$ vs. $\left\{E^m - V^f\right\}$	1	2	11	8
Example 4 $\left\{V^m - F_1^f\right\}$ vs. $\left\{V^m - F_2^f\right\}$	2	3	9	5

4.5 Summary

This chapter presented a method for determining the distinguishability and identifiability of smooth nonlinear algebraic models describing contact states. The Taylor series method provides a unified approach to testing the capability of candidate models to estimate both the parameters and the states. The analytical nature of the approach is well suited for poorly known environments since no numerical value for the contact parameters is necessary for the testing. The complexity of the method depends on the number of Taylor coefficients that needs to be computed. For pose equations, it can be shown that this number is bounded above and below for identifiability testing and lower bounded for distinguishability testing. For the examples considered, a modest number of

terms were needed for testing. As a result, no approximation is being made when using the series for testing contact distinguishability and identifiability.

In the context of contact state estimation, the proposed identifiability and distinguishability tools offer the following advantages. First, the identifiability tool provides a useful method to redesign contact models by detecting and removing the unidentifiable parameters, as discussed in example 4. Second, the distinguishability tool provides a practical way of analyzing the partitioning of the sensor space corresponding to the contact states. As illustrated in examples 1 and 4, pose information is sufficient to distinguish between the two polygonal contacts $\{V^m - E^f\}$ and $\{V^f - E^m\}$, whereas it is not sufficient to distinguish between the two polyhedral contacts $\{V^m - F_1^f\}$ and $\{V^m - F_2^f\}$. As a result, the contacts $\{V^m - E^f\}$ and $\{V^f - E^m\}$ form two separate regions in the sensor space, whereas contacts $\{V^m - F_1^f\}$ and $\{V^m - F_2^f\}$ are lumped into the same region in the sensor space.

While the examples presented here involved only elemental contacts based on pose equations, the methodology is equally applicable to more complex contacts using additional sensor modalities. Additional work is needed to test the identifiability and distinguishability of all of the contacts associated with the polygonal and polyhedral objects presented in Table 3.1-3.4. Moreover, the relationship among distinguishability in different sensor spaces remains to be investigated.

In this chapter, the distinguishability of contacts is based on the structure of the contact models and sensor information. The next chapter discusses how additional information, such as parameter history, can be used to augment the distinguishability of contact states. This augmented distinguishability is then used to investigate the observability of contact states in poorly known environments.

Chapter 5

Contact State Observability and Task Encoding

Given a geometric description of the objects composing a task and a contact state topology, a contact state graph representing all possible contact sequences that can lead to task completion can be generated. This contact state graph can then be used for task planning, assuming that each state of the graph can be determined using sensor data. The objective of this chapter is to investigate whether it is possible to distinguish each contact state from the others inside a contact state graph, given that the environment is poorly known. This property, known as observability, is essential when testing the feasibility of a task.

The first section of the chapter discusses task representation, and an example illustrating the construction of a contact state graph for a block placing task is provided.

The second section of the chapter analyzes the observability of the exemplified contact state graph in the context of poorly known environments. To this end, the contact state graph obtained from task decomposition is reduced to account for the distinguishably constraints associated with poorly know environments. Then, a forward projection from the observable reduced graph to the contact state graph using a finite history of the contact state parameters is presented as a solution to the observability problem in poorly known environments. Once a contact state graph is shown to be observable, then it can be encoded to be used inside a contact state estimator. The final section of this chapter addresses the problem of encoding a state graph in a form that is well suited for implementation purposes. The approach employed here uses a probability transition matrix to mathematically represent the task and the likelihood of transitions between contact states.

5.1 Task Representation

Manipulation tasks involving geometrical objects are naturally decomposed into contact states. Given a list of contact states (i.e., contact topology in Chapter3), several algorithms have been developed to automatically decompose a task into sequences of contact states (Xiao and Ji 2001). These sequences are then assembled into a contact state graph in which each node represents a contact state and each link represents a possible transition from a contact state to another. In this thesis, automatic decomposition of the task is not addressed; however, an example of manual decomposition of an assembly task requiring the placement of a block is considered.

5.1.1 Contact Topology

As illustrated in Fig. 5.1, the task is defined by two polygonal objects. The block is assumed to be rectangular, and the edges defining the corner are assumed to be infinite. As a consequence, the task involves two edges from the fixed corner (i.e., E_1^f, E_2^f), and four edges and four vertices from the manipulated object (i.e., $E_{1...4}^m, V_{1...4}^m$). The block is assumed to be grasped (i.e., crossed circle) by a planar manipulating robot.
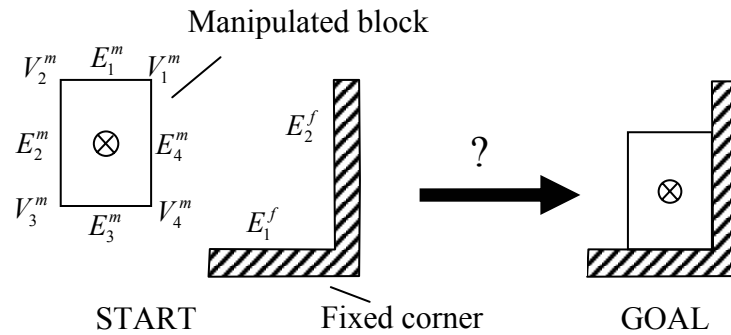
Figure 5.1: Block-in-corner assembly task.

By enumerating all the possible contacts, it can be seen that 25 contacts can occur between the edges and vertices composing the task. As shown in Fig. 5.2, the task comprises one no-contact, eight vertex-to-edge contacts, eight edge-to-edge contacts, four double vertex-to-edge contacts, and four double edge-to-edge contacts. The black wedge inside the crossed circle of the manipulated object indicates its orientation.
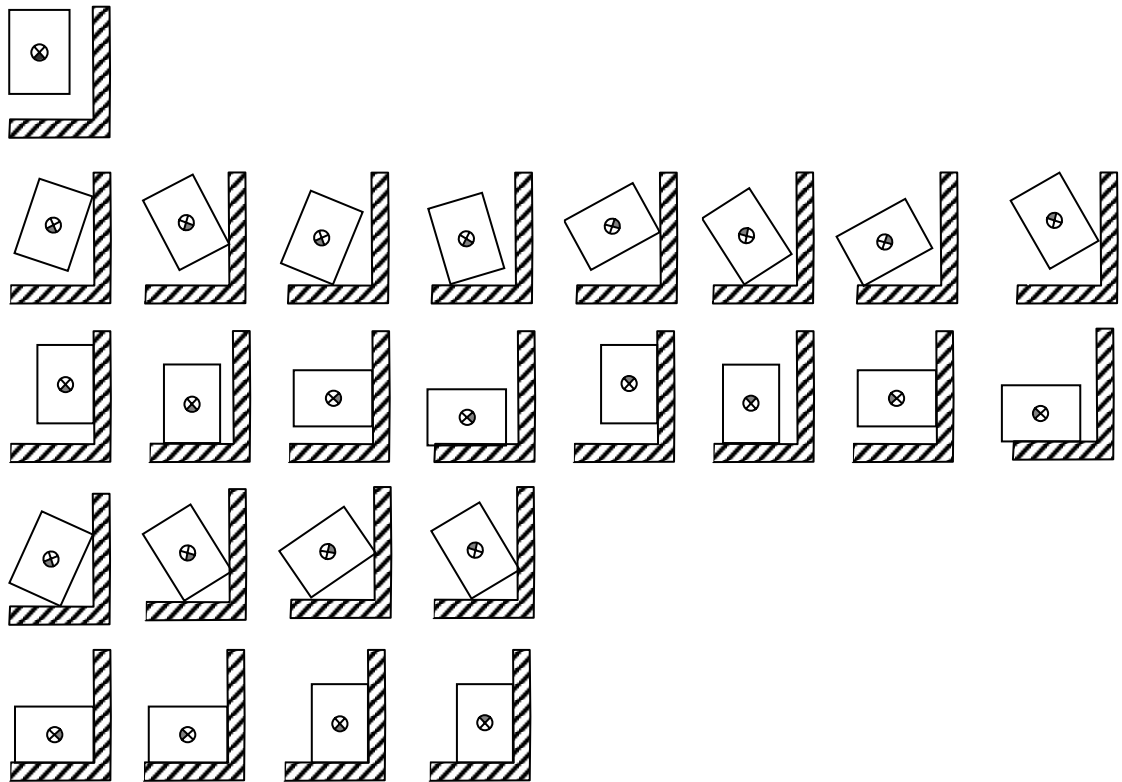
Figure 5.2: Contact state topology of a block-in-corner assembly task.

5.1.2 Task Decomposition

Using the contact topology presented in Fig. 5.2, the contact state graph associated with the block-in-corner task can be generated manually, as shown in Fig. 5.3. This graph comprises 128 possible transitions between states. The transitions between the no-contact and the double contacts are not modeled since they are very unlikely. The number of possible contact state sequences required to reach the corner position from the free motion position depends on the number of connections involved in the sequence. It should be clear that this number becomes large very quickly.
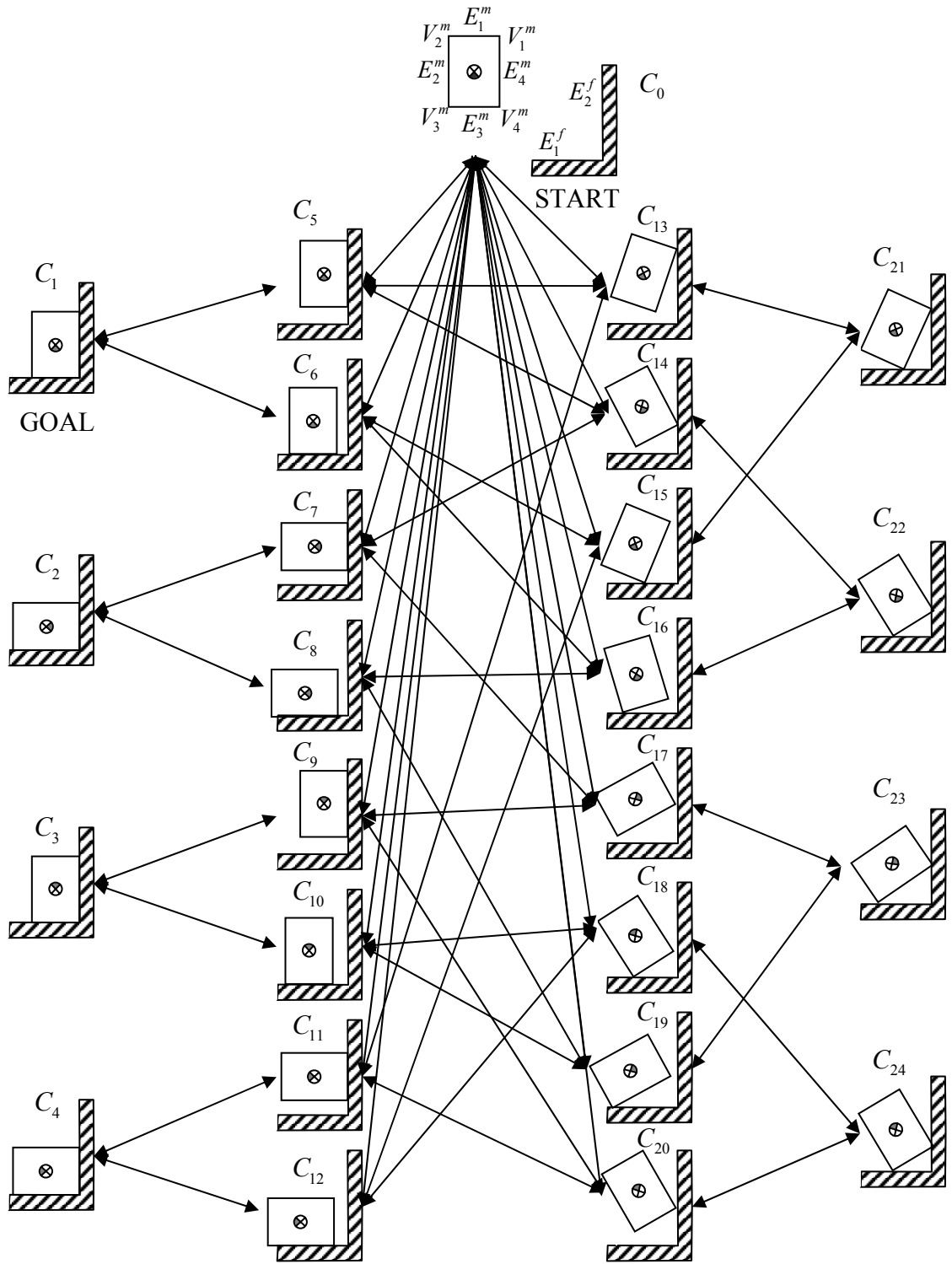
Figure 5.3: Contact state graph representing a block-in-corner assembly task.

5.2 Contact State Observability

For a task to be feasible, all the contact states composing a given contact state graph must be distinguishable. For example, the goal of the task illustrated in Fig. 5.3 is to place the manipulated block in contact with the environment corner. The task is completed when contact state C_1 is reached. Therefore, contact C_1 needs to be distinguished from all the other contacts composing the graph since reaching a goal without recognizing it does not result in task completion. The concept of distinguishability presented in section 4.1 tests the distinguishability of contact states based on current sensing information; however, this information may not be sufficient to recognize all the possible contacts composing the task. The distinguishability of every contact state inside a contact state graph is discussed in this section by introducing the concept of observability. By analogy with control theory, the concept of observability is defined as follows:

Definition 5.1. A contact state graph is said to be observable if, given a finite history of contact state transitions, the distinguishability of the contact models (as defined in Chapter 4) together with the task information are sufficient to determine the initial contact state.

This problem of observability can be related to the problem of recognizability introduced by Erdmann (1986) and Donald and Jennings (1991) (i.e., see section 2.1.6). In this context, the notion of task information represents the task based knowledge that

can be utilized to augment the distinguishability of the contact states obtained from the current sensing.

The objective of this section is to investigate contact state observability in poorly known environments. To this end, the observability of the contact state graph illustrated in Fig. 5.3 is discussed. First, it is shown that only groups of contact states can be distinguished inside the contact graph when assuming that the environment is poorly known. As a result, a reduced graph containing only groups of distinguishable contact states is extracted using distinguishability testing. Second, task information, represented as a finite history of the contact state parameters, is presented as a way of augmenting distinguishability. Finally, distinguishability testing and a forward projection of the parameter history are combined to show observability.

5.2.1 Distinguishable State Graph

As discussed in Chapter 4, every pair of contacts having the same topological form is indistinguishable without further information regarding the orientation of the edges or the location of the vertices. Analyzing the contact state graph of Fig. 5.3, it can be observed that only five different groups of topologically different contact states are utilized to construct the graph: no contact, vertex-to-edge, edge-to-edge, double vertex-to-edge, and double edge-to-edge. Using the distinguishability test presented in section 4.2.1, these groups of contacts can be shown to be distinguishable; however the individual contacts inside the groups are indistinguishable. (e.g., C_{13} and C_{14}, C_{10} and C_{12}).

Figure 5.4 shows how the 25 contact states of Fig. 5.3 can be reduced to a five-state graph in which each state comprises an indistinguishable subset of the original states. This reduced state graph is defined as a *distinguishable graph*; it corresponds to a minimum representation of the task imposed by the current sensing of the system. Each node in this reduced graph is distinguishable from the others.
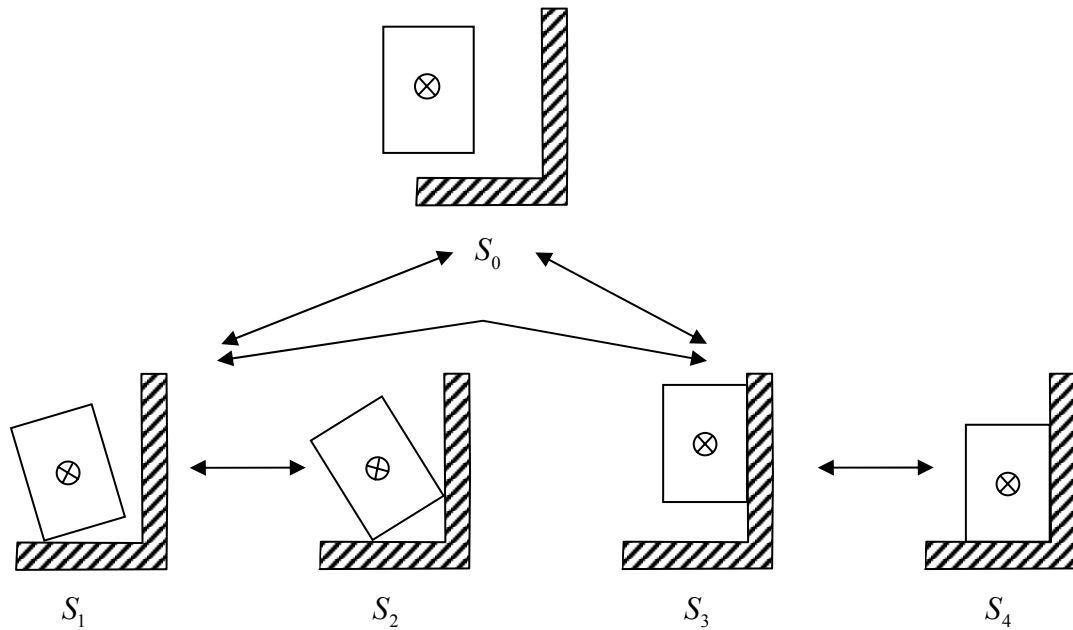
Figure 5.4: Distinguishable contact state graph.

5.2.2 Observability Conjecture

Planning in the distinguishable state graph shown in Fig. 5.4 does not have substantial value since each node represents a group of several contact states. To be practical, planning has to be done in the contact state graph of Fig. 5.3. This section investigates

how task information can be used to augment distinguishability and achieve contact state graph observability.

In the context of poorly known environments, the observability problem can be stated as follows: how many transitions are needed in a distinguishable graph to determine a contact state in its associated contact state graph? Based on current sensing information, the type but not the exact state can be determined; however, distinguishability can be augmented by using the information contained in the parameter estimates. In fact, it can be noticed that parameter values can be used to 'label' contact states. As an example, the topologically equivalent contact states C_{13} and C_{16} in Fig. 5.3 are considered. The vertex-edge contact equation derived in (3.33) is satisfied when either contact C_{13} or C_{16} is active. The position of the top right vertex V_1^m is estimated when C_{13} is active, whereas the position of the bottom left vertex V_3^m is estimated when C_{16} is active. As a result, storing the parameter history of the task can help to distinguish the contact states associated with the task. This reasoning leads to the following conjecture:

Observability Conjecture (2D): *Given the label, but not the location of the closest manipulated object vertex to the gripper frame, the contact state path to determine the contact state history is one that permits estimation of all manipulated and environment object model parameters.*

The idea of the conjecture is to extract all the object features (i.e., vertices and edges in 2D), with respect to a ground truth (i.e., the label of the closest manipulated object vertex to the gripper frame is known), that were used to build the contact state graph. Once this parameter information is known, then it can be combined with distinguishability testing to determine the contact states inside the state graph. For example, if a vertex-edge contact is detected and the estimated parameters correspond to the location of the vertex V_1^m and the orientation of the edge E_2^f, then it can be concluded that contact C_{13} has been reached.

To illustrate this conjecture, the parameter history associated with the sequence of states shown in Fig. 5.5 is analyzed. The unknown grasp location of the manipulated object is represented by a crossed circle. The vertex V_2^m is assumed to be the closest to the gripper. Starting from the vertex-edge contact C_{13}, the manipulated object is rotated clockwise four times then slid until it reaches the bottom edge of the fixed corner, resulting in the state sequence $C_{13} \rightarrow C_{11} \rightarrow C_{20} \rightarrow C_9 \rightarrow C_{17} \rightarrow C_{23}$.
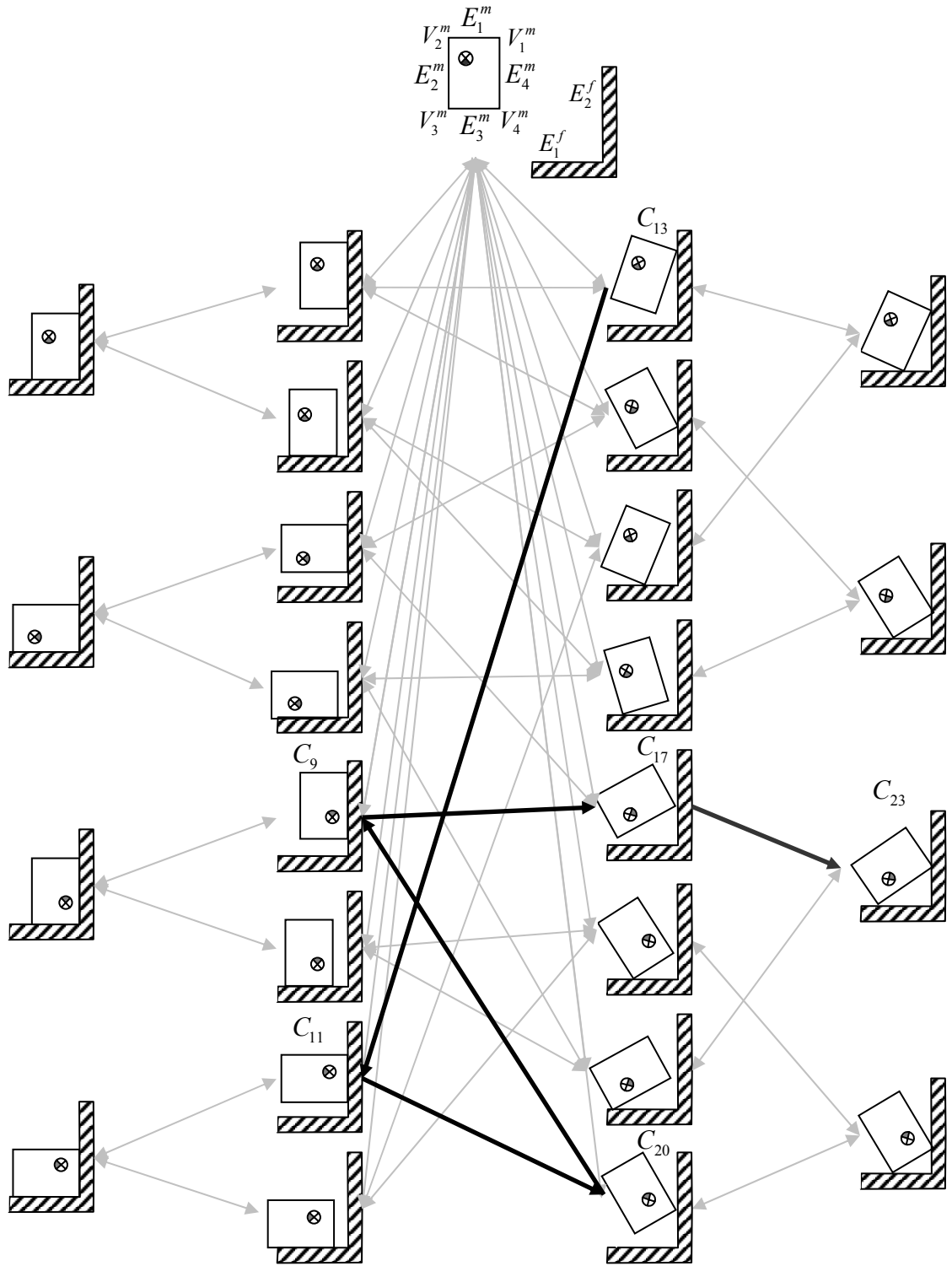
Figure 5.5: Example of a contact sequence that permits estimation of all manipulated and environment object model parameters.

Figure 5.6 shows the state sequence and the associated parameter history combined with the known geometry of the task. First, the location of the vertex V_1^m and the orientation of the edge E_2^f are estimated. Second, the orientation and part of the length of the edge E_1^m are estimated. Third, the vertex V_2^m is estimated resulting in the complete identification of the length of E_1^m. Fourth, the orientation and part of the length of the edge E_2^m are estimated. Fifth, the location of the vertex V_3^m is identified and combined with the parameter history and the a priori knowledge of the objects' shape to estimate the remaining parts of the rectangular manipulating object. Finally, the orientation of the edge E_1^f is estimated. At this point, the information obtained from the parameter values is sufficient to permit estimation of all manipulated and environment object parameters. As a result, contact state C_{23} is determined in the contact state graph shown in Fig. 5.3, and recursively, all the contact states leading to C_{23} are also determined. By definition 5.1, the contact state graph is said to be observable.
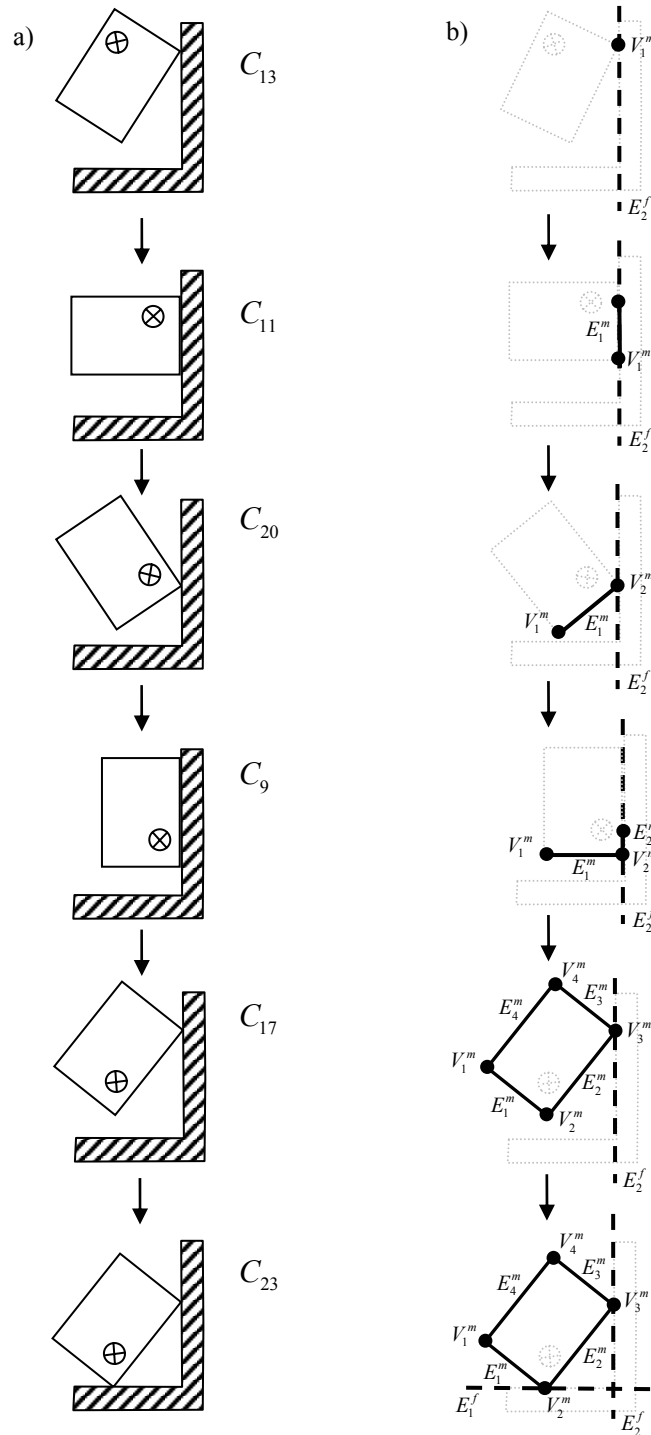
Figure 5.6. Forward projection on the parameter history. a) Contact state sequence in which the block is rotated clockwise and then slid toward the bottom edge of the fixed corner, and b) The parameter history is combined with the knowledge of the objects'shape resulting in a 2D model of the manipulated object and its environment.

Ultimately, the concept of observability is goal dependent. If the goal is to put the cube inside the corner regardless of its orientation, then the distinguishable state graph provides sufficient information. However, the more specific the goal is, the more critical the problem of observability becomes. Parameters were assumed to be perfectly estimated in this discussion. Nevertheless, noise or poor excitation can result in an erroneous estimation of the parameters that can degrade the observability of the graph.

The sequence of states presented in Fig. 5.6 results in a complete geometric construction of the objects used in the task; however, not every sequence of contact states results in a full model. The question of the necessary number of steps needed to construct arbitrary polygons or polyhedrons is not addressed in this thesis. A sufficient condition can be provided using forward projection on the parameter history. The sequence proposed in Fig. 5.5 is one possible projection; however other sequences also exist.

5.3 Task Encoding

If a contact state graph is shown to be observable, then it means that enough information (i.e., sensing information, parameter history, and task structure) is available to disambiguate every contact state inside the graph. As a next step, the observable contact state graph needs to be encoded in a mathematical form suitable for implementation in a contact state estimator. The approach employed here uses a probability transition matrix to represent the probability of specific contact state transitions embodied in a task contact state network.

5.3.1 Contact State Network

Probabilistic approaches can be used to encode the likelihood of transitions among the states of a contact state graph. In this context, the contact state graph is transformed into a network structure in which each node corresponds to a contact state, and each transition among states (including self-transition) is weighted by its probability of occurrence. As an example, the state network associated with the distinguishable state graph of Fig. 5.4 is presented in Fig. 5.7. Grey connectors represent transitions that were not modeled in the state graph (i.e., infeasible transitions or highly unlikely transitions), and the a_{ij}'s are used to label the possible transitions.

$$S_0 : \{0\} \qquad S_1 : \left\{ V^m - E^f \right\} \qquad S_2 : \left\{ \begin{matrix} V^m - E^f \\ V^m - E^f \end{matrix} \right\} \qquad S_3 : \left\{ E^m - E^f \right\} \qquad S_4 : \left\{ \begin{matrix} E^m - E^f \\ E^m - E^f \end{matrix} \right\}$$
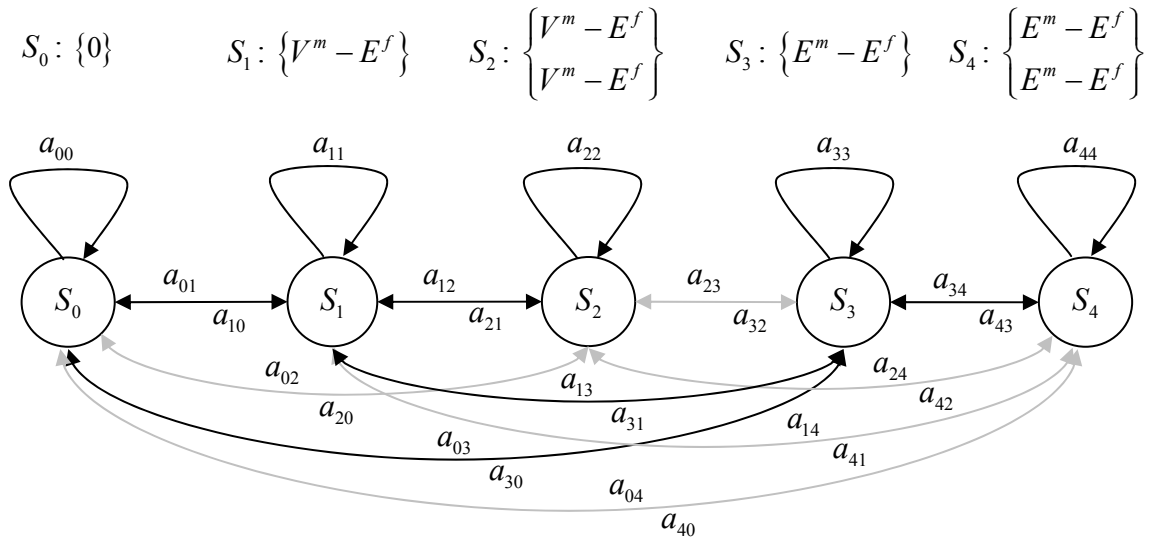
Figure 5.7: Distinguishable state network.

116

The state network can be represented in a compact way using an $n \times n$ probability transition matrix A, as described in (5.1). Each element of the matrix, a_{ij} in (5.2), corresponds to the probability of being in a state i given the previous state j. As an example, the probability transition matrix associated with the network described in Fig. 5.7 is shown in (5.3). In this example, the probabilities associated with infeasible or highly unlikely transitions are set to zero. The selection of the remaining probabilities is discussed in the next section.

$$A = \begin{bmatrix} a_{00} & a_{01} & \cdots & a_{0(n-1)} \\ a_{10} & a_{11} & & a_{1(n-1)} \\ \vdots & & \ddots & \vdots \\ a_{(n-1)0} & & & a_{(n-1)(n-1)} \end{bmatrix} \quad with \quad \begin{array}{c} \sum_{j=0}^{n-1} a_{ij} = 1 \\ a_{ij} \geq 0 \end{array} \tag{5.1}$$

$$a_{ij} = P\left(c_{t+1} = C_i \,/\, c_t = C_j\right) \tag{5.2}$$

$$A = \begin{bmatrix} a_{00} & a_{01} & 0 & a_{03} & 0 \\ a_{10} & a_{11} & a_{12} & a_{13} & 0 \\ 0 & a_{21} & a_{22} & 0 & 0 \\ a_{30} & a_{31} & 0 & a_{33} & a_{34} \\ 0 & 0 & 0 & a_{43} & a_{44} \end{bmatrix} \tag{5.3}$$

5.3.2 Selection of the Probability Transition Matrix

This section presents a two-step method to assign values to the transition probability matrix. As a first step, simple rules corresponding to the limited knowledge of the task

are used to assign the transition probabilities. As a second step, these probabilities are weighted by counting how often each transition is used in the state graph.

Step 1: Empirical Knowledge

    As a first step, a set of simple rules based on empirical knowledge of manipulation tasks is used to assign the transition probabilities. These rules are as follows:

- State transitions are short: $a_{ii} > a_{ij}$, $0 \leq i, j \leq n-1$

- The no-contact to contact transition is more likely to occur with single contacts than with multiple contacts (e.g., $a_{01} \gg a_{02}$ in (5.3))

- Once the manipulated block is in contact, it stays in contact: $a_{i0} = 0$, $1 \leq i \leq n-1$

- Unconstrained transitions are set uniformly following the row constraint of (5.1)

The third rule is controller dependent and can be relaxed depending on the application (e.g., teleoperated manipulation task). These rules are applied to the state network of Fig. 5.7 resulting in the symbolic transition matrix shown in (5.4). Numerical values can be assigned by setting the self-transition probabilities. The self-transitions are set to 0.8 in this example (i.e., $a_{ii} > a_{ij}$) and the remaining probabilities are set uniformly following the row constraint of (5.1), as shown in (5.5).

$$A = \begin{bmatrix} a_{00} & a_{01} & 0 & a_{03} & 0 \\ 0 & a_{11} & a_{12} & a_{13} & 0 \\ 0 & a_{21} & a_{22} & 0 & 0 \\ 0 & a_{31} & 0 & a_{33} & a_{34} \\ 0 & 0 & 0 & a_{43} & a_{44} \end{bmatrix} \qquad (5.4)$$

$$A = \begin{bmatrix} .8 & .1 & 0 & .1 & 0 \\ 0 & .8 & .1 & .1 & 0 \\ 0 & .2 & .8 & 0 & 0 \\ 0 & .1 & 0 & .8 & .1 \\ 0 & 0 & 0 & .2 & .8 \end{bmatrix} \qquad (5.5)$$

Step 2: Adjacency Matrix Analysis

As a second step, the probabilities of the non-zero off-diagonal terms are weighted by counting how often each transition is used in the state graph. This computation can be done using the adjacency matrix associated with the state graph. The adjacency matrix is simply a transition matrix in which each feasible transition is set to one and others (including self transitions) are set to zero (Wilson 1985). One interesting property of this matrix is that its kth power gives the number of paths of length k between two states. For example, the element $(1,2)$ of the third power 25×25 adjacency matrix associated with the contact state graph of Fig. 5.3 corresponds to the number of paths having three connections between the contacts C_0 and C_1. In this example, there exists four paths with three transitions as shown in (5.6).

119

$$C_0 \rightarrow C_{13} \rightarrow C_5 \rightarrow C_1$$
$$C_0 \rightarrow C_{15} \rightarrow C_6 \rightarrow C_1$$
$$C_0 \rightarrow C_{16} \rightarrow C_6 \rightarrow C_1 \qquad (5.6)$$
$$C_0 \rightarrow C_{14} \rightarrow C_5 \rightarrow C_1$$

Therefore, the adjacency matrix can be used to count all the transition occurrences in the contact state graph by computing all the possible sequences of lengths k (i.e., $k = 1, 2, 3 \ldots$) between the initial and final contact states (i.e., the 'start' state and 'goal' state in Fig. 5.3). For each k, the transition occurrences are sorted into a $n \times n$ state transition matrix D_k with zero diagonal elements. Summing the matrix D_k over a large range of k (e.g., $k_{max} = 10$) indicates how often each transition occurs in the state graph. This number is then normalized to obtain the likelihood of transitions (excluding self-transitions) associated with the state graph as shown in the matrix A^* in (5.7).

$$A^*(i, j) = \frac{\sum_{k=1}^{k_{max}} D_k(i, j)}{\sum_{l=1}^{n} \sum_{k=1}^{k_{max}} D_k(i, l)} \qquad where \; i \neq j \qquad (5.7)$$

As a final step, the transition probability matrix is obtained by setting the self-transitions probabilities and using equation (5.8) for the off-diagonal terms.

$$A(i, j) = A^*(i, j)\big(1 - A(i, i)\big) \qquad where \; i \neq j \qquad (5.8)$$

This technique can also be used to assign the transition probabilities associated with the distinguishable state graph of Fig. 5.4. To this end, the transitions of the contact state graph needs to be sorted according to the possible transitions of the distinguishable state graph. For example, the twelve transitions (i.e., four sequences with $k = 3$ transitions) of (5.6) correspond to four a_{01} transitions, four a_{13} transitions, and four a_{34} transitions in (5.4). This result is written in a compact form in the matrix H_k in (5.9). The computational complexity associated with the H_k matrix depends on the length of the sequence k and the size of the adjacency matrix.

$$H_3 = \begin{bmatrix} 0 & 4 & 0 & 0 & 0 \\ 0 & 0 & 0 & 4 & 0 \\ 0 & 0 & 0 & 0 & 0 \\ 0 & 0 & 0 & 0 & 4 \\ 0 & 0 & 0 & 0 & 0 \end{bmatrix} \tag{5.9}$$

For the block-in-corner example presented in Fig. 5.3, sequences staring at C_0 and ending at C_1 were computed for up to 10 transitions (i.e., $k_{max} = 10$) resulting in more than 70,000 transitions in the contact state graph. These transitions were then sorted with respect to the distinguishable state graph and normalized according to (5.7), as shown in (5.10).

121

$$A^* = \begin{bmatrix} 0 & .7 & 0 & .3 & 0 \\ 0 & 0 & .2 & .8 & 0 \\ 0 & 1 & 0 & 0 & 0 \\ 0 & .5 & 0 & 0 & .5 \\ 0 & 0 & 0 & 1 & 0 \end{bmatrix} \qquad (5.10)$$

As a final step, self-transitions are set to 0.8 and equation (5.8) is utilized to obtain the probability transition matrix associated with the distinguishable state network of Fig. 5.7.

$$A = \begin{bmatrix} .8 & .14 & 0 & .06 & 0 \\ 0 & .8 & .04 & .16 & 0 \\ 0 & .2 & .8 & 0 & 0 \\ 0 & .1 & 0 & .8 & .1 \\ 0 & 0 & 0 & .2 & .8 \end{bmatrix} \qquad (5.11)$$

5.4 Summary

The concept of observability is important in the design of contact state estimators since a task might not be feasible if the contact state graph is unobservable. In the context of poorly known environments, observability was solved using a map between the distinguishable graph representing the task in the poorly known environment and the contact state graph representing the task in the structured environment. This mapping was defined as a forward projection on the parameter history associated with the execution of the task.

The next two chapters focus on the implementation of a contact state estimator. In particular, it is shown how the probability transition matrix presented in this chapter can be used inside a decision test to represent the task knowledge necessary to the segmentation of the contact states.

Chapter 6

Parameter Estimation and Data Excitation

Contact state estimation is a dual estimation problem involving the identification of contact state parameters as well as the estimation of the contact states corresponding to the sensor information. As shown in Fig. 6.1, the first part in the implementation of a contact state estimator is the realization of a multiple model estimation algorithm. This algorithm estimates the parameters and residuals associated with each contact model, given sensor data and a list of contact state models. The second part of the contact estimator uses these results as inputs to a decision test that determines which one of the contact models is the most likely to correspond to the sensor data. This chapter addresses the implementation of the estimation algorithm utilized during multiple model estimation. The next chapter will discuss the implementation of the decision test.
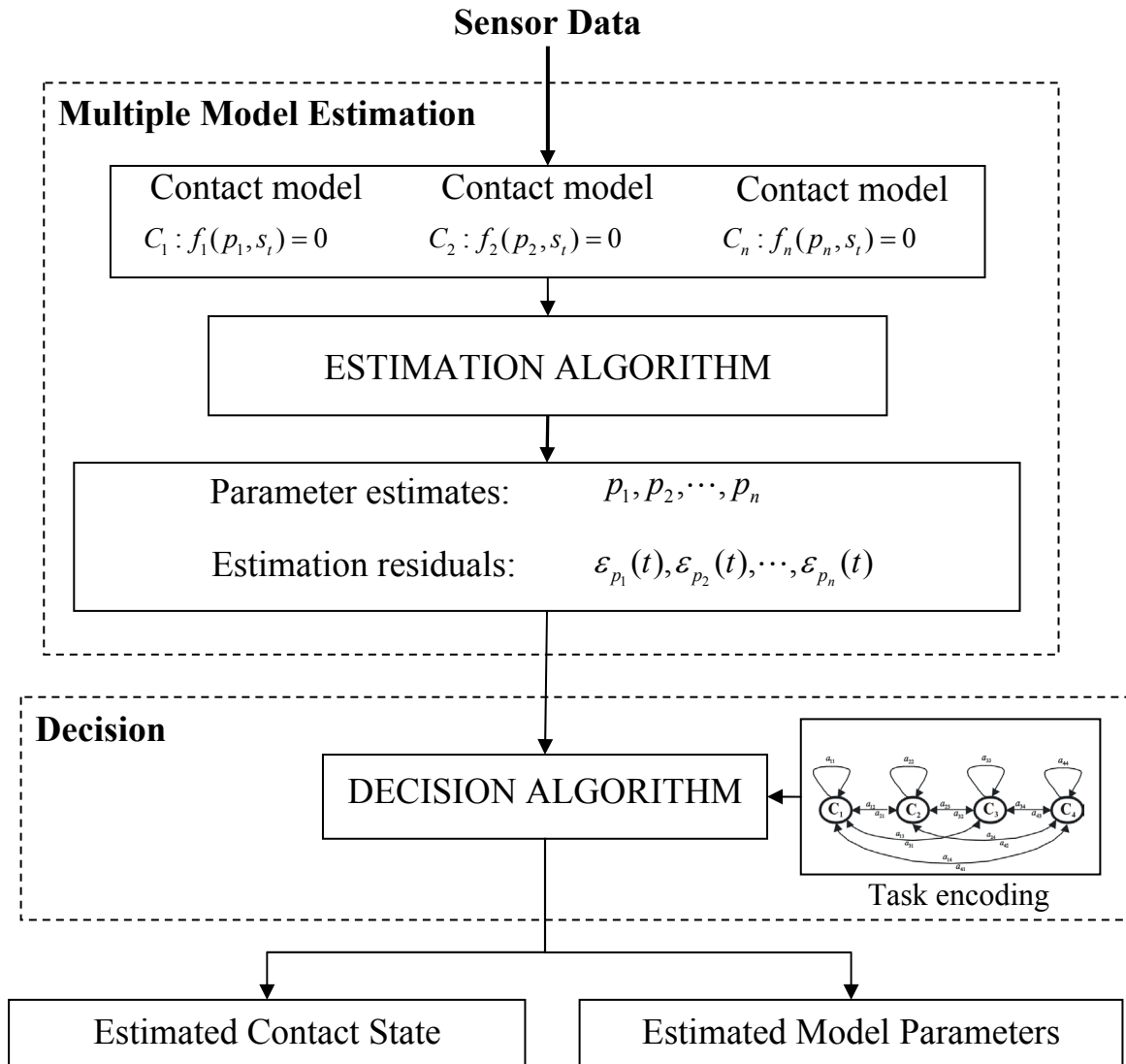
Figure 6.1: The two parts of the implementation of a contact state estimator: multiple model estimation and contact state estimation.

The estimation algorithm of Fig. 6.1 needs to satisfy two important criteria when used for contact state estimation in poorly known environments: 1) the algorithm must be fast, and 2) the algorithm must be robust to a poor choice of initial estimates. These two criteria are highly dependent on the excitation of the sensor path since a poor choice of excitation can result in slow convergence or erroneous estimates. As an example,

consider a probe of unknown length L, moving on an edge of unknown slope β, as depicted in Fig. 6.2. The position and orientation of the probe $\{x_i, y_i, \theta_i\}$ are sufficient information to identify L and β. A bad choice of sensor excitation, however, can result in erroneous parameter estimates as illustrated in Fig. 6.2(a) and Fig. 6.2(b). In the first case, the probe is pivoting around the contact point resulting only in the identification of the probe's length L. In the second case, the probe is sliding with a constant orientation resulting only in the identification of the edge's slope. Intuitively, a good excitation requires all but one sensor signal to be independently excited as depicted in Fig. 6.2(c). Finding an exciting path can be challenging since the contact constraint limits the possible configurations and reduces the possible sensor paths. As a result, excitation conditions that can guarantee the estimation of all the parameters associated with the contact models are needed when implementing the estimation algorithm of a contact state estimator.
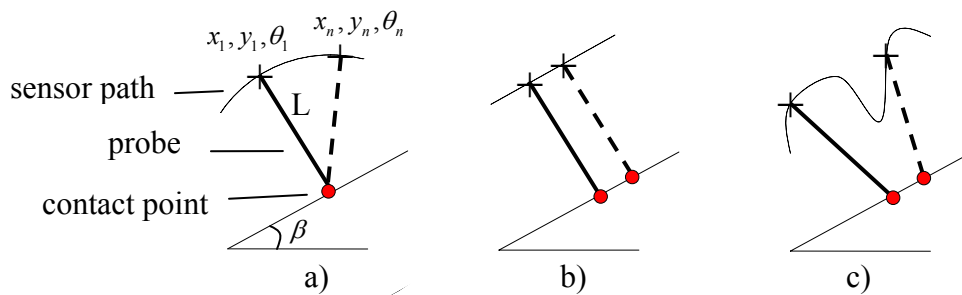
Figure 6.2: Probe moving on an inclined line. a) The probe is pivoting around the contact point resulting in a poor exciting path. b) The probe is sliding with a constant orientation resulting in a poor exciting path. c) The probe is sliding and rotating resulting in an exciting path.

This chapter addresses the two problems of parameter estimation and sensor excitation. Two estimations algorithms are presented: an implicit method and an explicit method. The implicit method is used in the implementation of the contact state estimator, whereas the explicit method is utilized in the design of sensor paths. The implicit method uses the Levenberg-Marquardt algorithm, a nonlinear least squares technique, to estimate the parameters. This method is well suited for poorly known environments since no accurate nominal parameter values are needed to initialize the algorithm. The explicit method uses multiple differentiations of the sensor signals to provide closed-form solutions for the parameters associated with the contact models. Even though this method is far too sensitive to sensor noise to be used in practice, it provides an interesting basis to analyze the effect of sensor excitation on parameter estimation.

6.1 Estimation Algorithm: Implicit Solution

Parameter estimates and sensor excitation conditions can be explicitly characterized when a closed-form solution to the estimation problem is available. Obtaining such a solution is relatively easy for linear algebraic systems (i.e., Gaussian elimination); however, it still remains a difficult challenge for nonlinear systems. As a consequence, implicit solutions based on numerical optimization techniques are commonly used (e.g., Gill et al. 1981, Ljung 1987). The objective of these algorithms is to find a solution that can minimize a given cost function. For contact state estimation in a poorly known environment, the estimator needs to be robust to poor initial conditions and needs good convergence properties. The Levenberg-Marquardt method, a least squares minimization

technique corresponding to these criteria, is reviewed in the next section (Gill et al. 1981).

6.1.1 The Levenberg-Marquardt Algorithm

As shown in Chatper 3, contact states can be modeled as nonlinear homegeneous equations parametrized by sensor variables $s(t)$ and unknown constant parameters p:

$$f(p, s(t)) = 0 \tag{6.1}$$

The sum of squares function defined in (6.2) is used as a cost function to minimize (6.1) with respect to p. This function is commonly chosen for its simplicity and algebraic properties (Gill et al. 1981).

$$F(p) = \frac{1}{2} \sum_{i=1}^{m} f^T(p, s(t_i)) f(p, s(t_i)) \equiv \frac{1}{2} \|f(p)\|^2 \equiv \frac{1}{2} f(p)^T f(p) \tag{6.2}$$

where $f(p) = \begin{bmatrix} f(p, s(t_1)) & f(p, s(t_2)) & \cdots & f(p, s(t_n)) \end{bmatrix}^T$

The goal of the minimization process is to find a search direction d, in the parameter space, that can result in a large reduction of $F(p)$. The direction is then used to update the estimate as shown in (6.3).

$$p_{k+1} = p_k + d_k \qquad (6.3)$$

If $F(p)$ is linearly approximated, then a simple way of minimizing this cost function is to follow the direction of the negative gradient. This direction is known as the steepest descent and is defined as follows:

$$d_k = -g_k \qquad (6.4)$$

Steepest descent methods are easy to implement since they only require the computation of the gradient; however, they are not very efficient (i.e., slow convergence). A more efficient solution is to approximate the cost function by a quadratic:

$$F(p_k + d) \approx F_k + g_k^T d + \frac{1}{2} d^T G_k d \qquad (6.5)$$

where g is the gradient and G is the Hessian.

The minimum is achieved when the gradient vanishes, yielding the search direction that solves equation (6.6). This direction is known as the Newton direction (Gill et al. 1981).

$$G_k d_k = -g_k \qquad (6.6)$$

The nature of the least squares cost function allows for easy computations of the gradient and the Hessian matrix:

$$g(p) = J(p)^T f(p) \qquad (6.7)$$

$$G(p) = J(p)^T J(p) + Q(p) \qquad (6.8)$$

Least squares methods usually assume that the first order term of the Hessian dominates the second-order terms (i.e., $Q(p)$). This assumption is valid only if the problem has a small residual at the solution. Since homogeneous equations are used to model contact equations, the assumption is satisfied for the contact state corresponding to the observed sensor data. As a result, both the Hessian and the gradient can be computed using only $J(p)$, the Jacobian matrix of $f(p)$. Assuming that $Q(p)$ can be neglected, the Newton direction (6.6) becomes:

$$d_k = -\left(J_k^T J_k \right)^{-1} J_k^T f_k \qquad (6.9)$$

If the quadratic form is a bad approximation, the best thing to do is to utilize the steepest descent direction defined in (6.4) with the gradient equation (6.7).

$$d_k = -J_k^T f_k \qquad (6.10)$$

The Levenberg-Marquardt (L.M.) provides a method to switch between Newton's method and the steepest descent method. The idea is to use the steepest descent when far from the minimum and then switch to the Newton's method when close to the minimum. The L.M. direction is given by (6.11), where λ_k is non-negative scalar. If λ_k is zero then

the L.M. direction reduces to the Newton direction, and if λ_k tends to infinity then the

L.M. direction reduces to the steepest descent direction.

$$d_k = -\left(J_k^T J_k + \lambda_k I\right)^{-1} J_k^T f_k \qquad (6.11)$$

Several approaches can be implemented to compute λ_k (Numerical Recipes, p.684, 1988). The idea is to increase or decrease λ_k when the cost function at the current iteration is greater or smaller than the cost function at the previous iteration.

The L.M. method is an unconstrained least squares technique. As a consequence, the contact equations must be taken in their unconstrained forms. As an example, the algebraic equation corresponding to a $\{V^m - E^f\}$ contact is considered in (6.12). This equation can be utilized with a least squares estimator if p_1 and p_2 are replaced by their trigonometric counterparts, as shown in (6.13).

$$\begin{cases} p_5 + (p_2 p_3 - p_1 p_4)\cos\theta(t) - (p_1 p_3 + p_2 p_4)\sin\theta(t) + p_2 x(t) - p_1 y(t) = 0 \\ p_1^2 + p_2^2 = 1 \end{cases} \qquad (6.12)$$

$$\begin{aligned} p_1 &= -\sin p_0 \\ p_2 &= \cos p_0 \end{aligned} \qquad (6.13)$$

6.1.2   Estimator implementation

As shown in (6.3), nonlinear optimization methods are iterative. Therefore, the rate of convergence is an important factor when deciding on an optimization algorithm. The Levenberg-Marquardt algorithm has been shown to have linear convergence during its steepest descent mode and quadratic convergence during its Newton mode (Gill et al. 1981). As a consequence, the rate of convergence of the algorithm depends on the choice of initial conditions. A poor choice of initial conditions will mostly yield linear convergence while a good one will mostly result in quadratic convergence.

The estimator can be implemented in a batch mode or in a recursive mode. Traditionally, batch techniques are used for estimating time-invariant parameters while recursive techniques are used for estimating time-varying parameters. In the context of multiple model estimation, the parameters associated with all of the contact states must be estimated simultaneously, as shown in Fig. 6.2. In this situation, parameters can be seen as 'quasi time-invariant' or 'quasi time-varying' since they are constant for the model associated with the active contact and 'varying' for the other contact models. As a result, both recursive and batch techniques can be used with some modifications to estimate the parameters. A recursive technique can be used with an added forgetting factor to limit the corruption of the good estimates when transitioning from one contact state to another. Similarly, a batch technique could be used in a sliding window of fixed length as shown in Fig. 6.3. In this research, the latter estimation technique is used since batch nonlinear least squares shows faster convergence and better robustness to noise than its recursive counterpart. The selection of the moving data window length δ is

determined by two considerations. Its lower bound is provided by *n*, the number of parameters to be estimated in (6.1). This is the minimum number of time steps needed to solve the over-determined set of equations representing the contact states. Its upper bound corresponds to the minimum time interval a contact state is expected to be active. For a minimum time interval T_m and sampling frequency F_s, the window length is bounded by:

$$n < \delta < F_s \cdot T_m \tag{6.14}$$
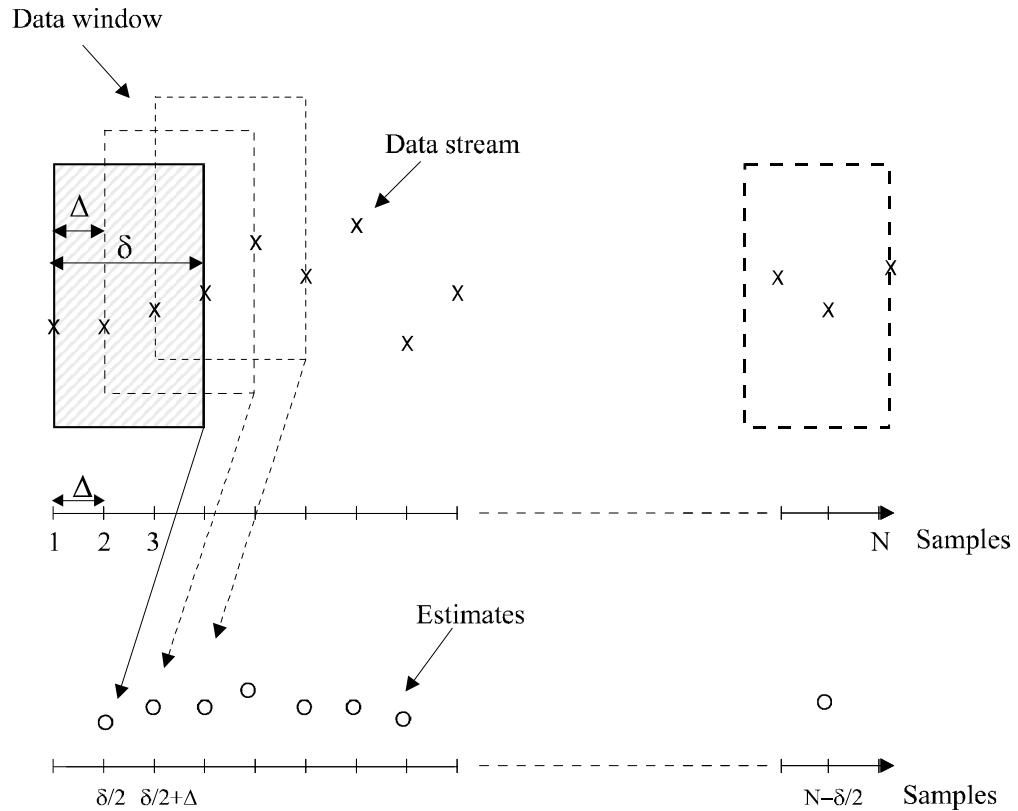
Figure 6.3: Estimation using a sliding window estimation scheme.

In practice, sliding nonlinear least squares can be computationally intensive, especially when poor initial conditions are chosen. One easy solution is to set the speed of the manipulator robot such that it allows enough computational time. A second and more elegant solution is to use the estimates associated with a detected active contact state to initialize all the contact models that share the same parameters. This type of re-initialization can be done after a contact transition has been detected. Implementation of this technique will be discussed in section 7.2.3.

6.1.3 Excitation Condition

Ideally, contact states have the form presented in (6.1). Realistically, however, small errors due to sensor noise and unmodeled disturbances result in a nonzero residual ε in (6.15). We make the assumption that these errors can be modeled as normally distributed random variables with zero mean and covariance σ^2. As a result, the residual's probability distribution (pdf), defined as p_ε for a given contact state C_i, is as follows:

$$
\begin{aligned}
f(p,s) &= \varepsilon \\
p_\varepsilon &= P\big(\varepsilon / C_i\big)
\end{aligned}
\tag{6.15}
$$

Due to the nonlinear structure of $f(\cdot)$, the pdf of (6.15) is hard to characterize analytically; however, it can be estimated off-line using Monte-Carlo simulations. As an an example, Fig 6.4 shows the result of a Monte-Carlo simulation corresponding to a vertex-to-edge contact. First, given the dimensions of the polygons and the location of

the static object (i.e., filled rectangle), the configuration space corresponding to the contact state is computed (C-surface in Mason 1981). The space is discretized, and 2,500 configurations (i.e., x, y, θ) are computed. Fig. 6.4(a) shows one possible configuration. The configurations are then corrupted by adding a normally distributed noise of zero mean and variance σ^2 ($\sigma_x^2 = \sigma_x^2 = \sigma_\theta^2 = 0.5$ for this simulation). The residual is computed for each configuration and the residuals' pdf is built by normalizing the residuals' histogram. The process is repeated for rectangles of variable sizes and locations. The dimensions of both rectangles and the configuration of the fixed rectangle are chosen randomly inside a uniform distribution. Fig. 6.4(c) shows the pdf resulting from one hundred different rectangles (i.e., 2500×100 residuals were computed to build the pdf). It is clear that the distribution can be well approximated using a unimodal Gaussian. To be complete, this simulation should be run for every possible contact state.
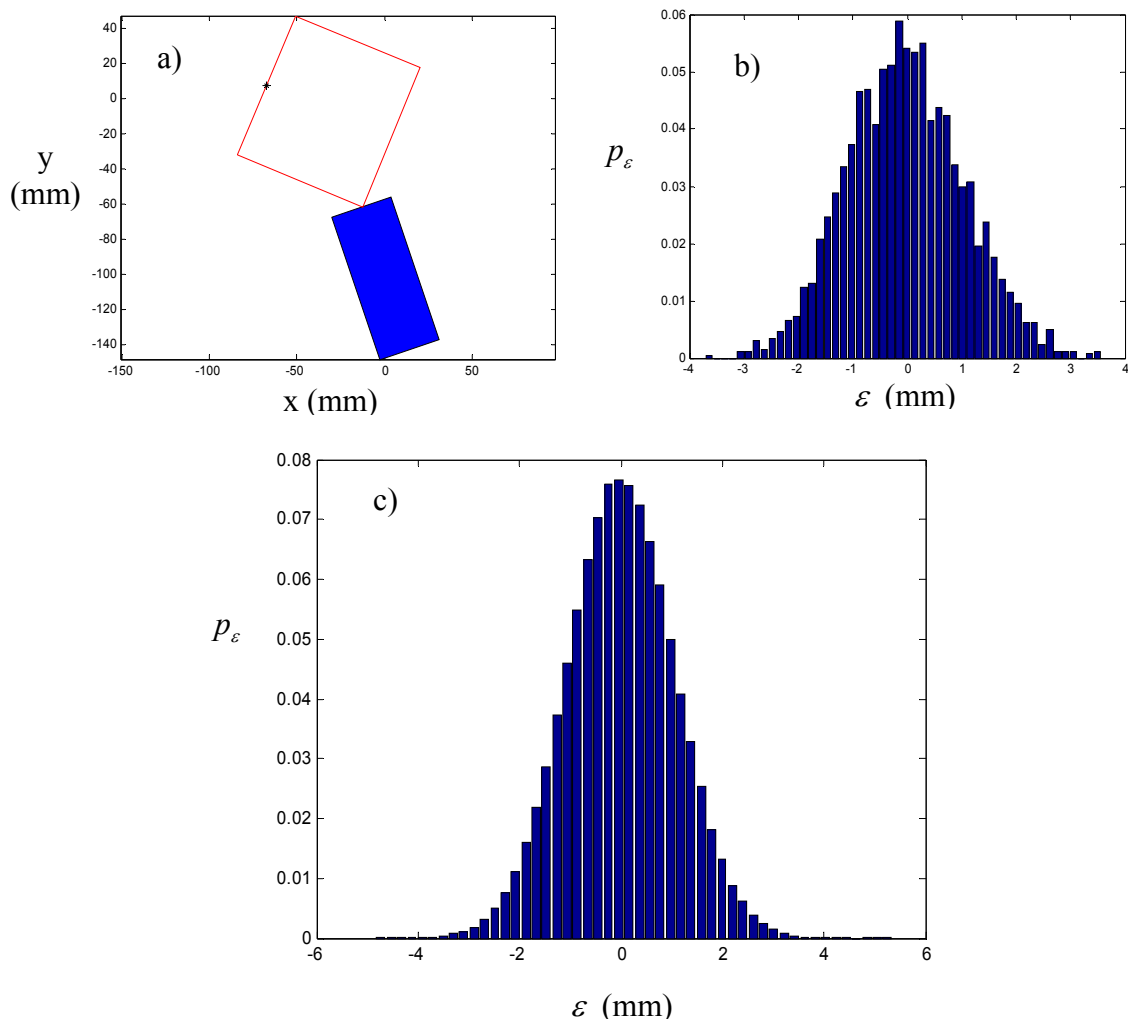
Figure 6.4: Contact's residual pdf by Monte Carlo simulation. a) A simulated configuration of a vertex-to-edge contact, b) Contact's residual pdf corresponding to objects of fixed sizes and locations, and c) Contact's residual pdf corresponding to objects of different sizes and locations.

Using a linear approximation, the covariance matrix of the parameters K can be expressed using the Hessian and the covariance of the error (Bates and Watts 1988):

$$\hat{\sigma}^2 = G(\hat{p})K \tag{6.16}$$

Least squares techniques assume that the second order term of the Hessian can be neglected (i.e., (6.8)), and as a result (6.16) can be simplified as follows:

$$K \approx \left(J(\hat{p})^T J(\hat{p}) \right)^{-1} \hat{\sigma}^2 \qquad (6.17)$$

The amount of uncertainty in the parameters is measured by the parameter covariance matrix K. This uncertainty can be used to derive a confidence interval on the estimates:

$$\hat{p}_i - t_\alpha \sqrt{\frac{K_{ii}}{m}} \le p_i \le \hat{p}_i + t_\alpha \sqrt{\frac{K_{ii}}{m}} \qquad (6.18)$$

where t_α is the upper $(1-\alpha)/2$ critical value for a student distribution with $m-1$ degrees of freedom. For a 95% confidence interval, $\alpha = 0.05$. Tables of t-values can be found in statistics books, e.g., Dougherty (1990).

Excitable paths should result in small intervals in (6.18). Since the paths (i.e., sensor data) only affect the covariance matrix, excitation is directly related to the magnitude of diagonal terms of the K matrix. It is clear from (6.17) that good excitation should ensure that the Hessian matrix $J(p)^T J(p)$ is invertible. The Hessian matrix is well-conditioned if the Jacobian is far from singularity and badly conditioned otherwise. The condition number κ is commonly used to test for matrix conditioning (Lawson and Hanson 1974). In the literature, matrices with a low condition number are generally considered well

conditioned (Schröer et al. 1992). Paths yielding a condition number $\kappa\left(J(p)\right) \leq 100$ are typically considered as exciting paths. Note that the Levenberg-Marquardt method already improves the conditioning of the Hessian inversion by adding a constant to the main diagonal of the matrix to be inverted.

6.2 Estimation Algorithm: Explicit Solution

Explicit methods provide closed-form solutions for the parameters associated with the contact models that depend only on the sensor variables. Closed-form solutions are interesting since they are computationally efficient and provide insights on the type of sensor paths that need to be used to estimate the parameters (i.e., excitation conditions).

This section presents an explicit estimation technique for the parameters associated with the pose equation of (6.12). Exploiting the structure of the kinematic equations, multiple differentiations of the contact equations are used to decouple the nonlinear estimation problem into two sub-problems. First, the nonlinear mapping between the Taylor coefficients characterizing the contact model and the parameters is defined. Then, the nonlinear relationship between the Taylor coefficients and the sensor variables is expressed using multiple differentiations of the contact model. These two nonlinear maps are then combined to provide a closed-form solution for the parameters that depends only on the sensor measurements and their derivatives.

6.2.1 Estimation Through Differentiation

As discussed in section 4.4, pose equations can be characterized exactly by a finite number of Taylor coefficients. In that context, the goal of identifiability testing is to show that there exists a unique inverse mapping between the Taylor coefficients representing the contact equations and the parameters, as shown in (6.19). In this equation, f_s is the finite vector of Taylor coefficients associated with the algebraic contact state model shown in (6.1).

$$p = g^{-1}\left(f_s, s(t)\right) \tag{6.19}$$

If the inverse of g is unique, then the model is said to be globally identifiable. The model is locally identifiable if a finite number of inverse mappings exist. The feasibility of the inversion as well as its computation was the focus of the identifiability test presented in section 4.2. This inversion can be difficult to solve by hand; however, tools from commutative algebra can often be used to obtain a solution (e.g., Gröbner bases).

As an example, the inversion of the equations used to characterize the pose equations of the globally identifiable contact $\left\{V^m - E^f\right\}$ described in (6.12) is presented in (6.20). Note that for this example the inversion is easily done by hand.

$$
\begin{cases}
f(p,s) = p_5 - (p_1 p_3 + p_2 p_4)\cos\theta(t) - (p_2 p_3 - p_1 p_4)\sin\theta(t) - p_1 x(t) - p_2 y(t) = 0 \\
f_\theta(p,s) = -(p_1 p_3 + p_2 p_4)\cos\theta(t) - (p_2 p_3 - p_1 p_4)\sin\theta(t) \\
f_x(p,s) = p_2 \\
f_y(p,s) = -p_1 \\
f_{\theta\theta}(p,s) = -(p_2 p_3 - p_1 p_4)\cos\theta(t) + (p_1 p_3 + p_2 p_4)\sin\theta(t)
\end{cases}
$$

$$\Downarrow \tag{6.20}$$

$$
\begin{cases}
p_1 = -f_x \\
p_2 = -f_y \\
p_3 = (f_\theta f_y - f_x f_{\theta\theta})\cos\theta(t) - (f_\theta f_x + f_y f_{\theta\theta})\sin\theta(t) \\
p_4 = -(f_\theta f_x + f_y f_{\theta\theta})\cos\theta(t) - (f_\theta f_y - f_x f_{\theta\theta})\sin\theta(t) \\
p_5 = f_{\theta\theta} - f_x x(t) - f_y y(t)
\end{cases}
$$

To obtain an explicit solution for the parameters, the Taylor coefficients of (6.19) are expressed using the known sensor variables $s(t)$. The chain rule is used to express the exact differentials of the analytic function $f(p, s(t))$ as a function of Taylor coefficients and exact differentials of the sensor variables. Equation (6.21) shows the differentiation for three sensor variables $\{\theta, x, y\}$.

$$
\begin{cases}
0 = f(x, y, \theta) \\
0 = df = f_\theta d\theta + f_x dx + f_y dy \\
0 = d^2 f = f_\theta d^2\theta + f_x d^2 x + f_y d^2 y + f_{\theta\theta}(d\theta)^2 + f_{xx}(dx)^2 \\
\qquad + f_{yy}(dy)^2 + 2 f_{\theta x} d\theta dx + 2 f_{\theta y} d\theta dy + 2 f_{xy} dx dy \\
\vdots \\
0 = d^n f = \ldots
\end{cases}
\tag{6.21}
$$

The homogeneous system of equations represented by (6.21) can be written in a compact form as the product between the Taylor coefficient vector f_s and a matrix M which is function of the differentials of the sensor variables, as expressed in (6.22). Moreover, the special structure of the kinematic equations, expressed through the finite number of Taylor coefficients, can be used to reduce the matrix M to a $n_c \times n_c$ square matrix, where n_c represents the number of nonzero and linearly independent Taylor coefficients. Equation (6.23) provides an iterative scheme to obtain the excitability matrix M.

$$0 = d^n f = M\left(d^n s\right) f_s \tag{6.22}$$

$$\begin{cases} M_{1,j} = \begin{cases} ds_j & 1 \le j \le \dim(s) \\ 0 & \dim(s) < j \le n_c \end{cases} \\ M_{i,j} = dM_{i-1,j} + \sum_{k=1}^{n_c} M_{i-1,k} T_{k,j} & 2 \le i \le n_c, 1 \le j \le n_c \\ T_{n_c \times n_c} : df_s \to f_s \end{cases} \tag{6.23}$$

As an example, (6.24)-(6.25) show the different steps that lead to the M matrix for the example presented in (6.20). As shown in Table 4.1, the pose equation associated with this contact possesses four independent Taylor coefficients, excluding the zero-order

coefficient. These four coefficients are used to obtain the T matrix of (6.23) by computing the total differentials of each Taylor coefficient:

$$
\begin{pmatrix} df_\theta \\ df_x \\ df_y \\ df_{\theta\theta} \end{pmatrix} = \underbrace{\begin{pmatrix} 0 & 0 & 0 & d\theta \\ 0 & 0 & 0 & 0 \\ 0 & 0 & 0 & 0 \\ -d\theta & 0 & 0 & 0 \end{pmatrix}}_{T} \begin{pmatrix} f_\theta \\ f_x \\ f_y \\ f_{\theta\theta} \end{pmatrix}
\tag{6.24}
$$

As a final step, the iterative scheme of (6.23) is used to obtain the M matrix shown in (6.25).

$$
\begin{pmatrix} 0 \\ 0 \\ 0 \\ 0 \end{pmatrix} = \underbrace{\begin{pmatrix} d\theta & dx & dy & 0 \\ d^2\theta & d^2x & d^2y & d\theta^2 \\ d^3\theta - d\theta^3 & d^3x & d^3y & 3d^2\theta d\theta \\ d^4\theta - 6d^2\theta d\theta^2 & d^4x & d^4y & 4d^3\theta d\theta + 3d^2\theta^2 - d\theta^4 \end{pmatrix}}_{M} \begin{pmatrix} f_\theta \\ f_x \\ f_y \\ f_{\theta\theta} \end{pmatrix}
\tag{6.25}
$$

The effects of the sensor signals on the Taylor coefficients can be analyzed by investigating the nullspace of M. It is important to notice that when a sensor path corresponds to an active contact state then the determinant of M goes to zero since the Taylor coefficients cannot be all equal to zero. Therefore, ψ, the dimension of the nullspace associated with M, must be greater than or equal to one. As a result, $n_c - \psi$ of the Taylor coefficients can be estimated as a function of the remaining coefficients (i.e., free parameters of the nullspace). A unique solution for the Taylor coefficients can be computed if there exists ψ remaining independent constraints on the Taylor coefficients

(i.e., equations that were not used to construct g in (6.19) or M in (6.22)). Note that this number of remaining equations, defined as v_r, is fixed and depends only on the structure of the pose equation, whereas the dimensionality of the nullspace, ψ, depends on the value of the sensor measurements. The relationship between v_r and ψ will be investigated in the next section when addressing the problem of data excitation. Assuming that there exist ψ remaining independent constraints on the Taylor coefficients (i.e., $v_r = \psi$), then a nonlinear mapping Φ between the nullspace of M and f_s can be found:

$$f_s = \Phi\left(\ker(M)\right) \tag{6.26}$$

The nullspace can be computed analytically using the echelon form of the matrix M. As a result, each component of the nullspace can be written as a nonlinear function of the sensor variables and their differentials:

$$\ker(M) = \Gamma(d^n s) \tag{6.27}$$

As an example, the one-dimensional nullspace of (6.25) is combined with the remaining equation of (6.12) (i.e., $p_1^2 + p_2^2 = 1$) to obtain all the Taylor coefficients of (6.20) in (6.28). The choice of the free variable $f_{\theta\theta}$ is arbitrary but does not change the end result.

$$
\begin{cases}
ker(M) = N \\[2mm]
\begin{pmatrix} f_\theta \\ f_x \\ f_y \end{pmatrix} = \begin{pmatrix} N_1 \\ N_2 \\ N_3 \end{pmatrix} f_{\theta\theta} \\[4mm]
p_1^2 + p_2^2 = 1 \Rightarrow f_x^2 + f_y^2 = 1 \Rightarrow f_{\theta\theta} = \pm\left(N_1^2 + N_3^2\right)^{-\frac{1}{2}}
\end{cases}
\tag{6.28}
$$

As a final step, the contact state parameters of (6.20) are written in terms of the nullspace components of M as shown in (6.29). The nullspace components are computed analytically using the row echelon form of M, as shown in (6.30). Each m_{ij} represents the 3×3 minors that corresponds to the $(i,j)^{th}$ element of M, as shown in (6.31). Combining equations (6.29)-(6.31) result in the closed-form solution of the contact state parameters.

$$
\begin{aligned}
p_1 &= -\frac{N_2}{\left(N_1^2 + N_3^2\right)^{-\frac{1}{2}}} \\[4mm]
p_2 &= -\frac{N_3}{\left(N_1^2 + N_3^2\right)^{-\frac{1}{2}}} \\[4mm]
p_3 &= \frac{\left(N_1 N_3 - N_2\right)\cos\theta - \left(N_1 N_2 + N_3\right)\sin\theta}{\left(N_1^2 + N_3^2\right)} \\[4mm]
p_4 &= -\frac{\left(N_1 N_2 + N_3\right)\cos\theta + \left(N_1 N_3 - N_2\right)\sin\theta}{\left(N_1^2 + N_3^2\right)} \\[4mm]
p_5 &= \frac{\left(1 - N_2 x - N_3 y\right)}{\left(N_1^2 + N_3^2\right)^{-\frac{1}{2}}}
\end{aligned}
\tag{6.29}
$$

$$M^{echelon} = \begin{pmatrix} 1 & 0 & 0 & \dfrac{m_{41}}{m_{44}} \\ 0 & 1 & 0 & -\dfrac{m_{42}}{m_{44}} \\ 0 & 0 & 1 & \dfrac{m_{43}}{m_{44}} \\ 0 & 0 & 0 & \underbrace{\det(M)}_{0} \end{pmatrix} \Rightarrow \begin{pmatrix} N_1 \\ N_2 \\ N_3 \end{pmatrix} = \begin{pmatrix} -\dfrac{m_{41}}{m_{44}} \\ \dfrac{m_{42}}{m_{44}} \\ -\dfrac{m_{43}}{m_{44}} \end{pmatrix} \tag{6.30}$$

$$\begin{cases} m_{41} = 3d^2\theta d\theta \left(dxd^2y - d^2xdy \right) - d\theta^2 \left(dxd^3y - d^3xdy \right) \\ m_{42} = 3d^2yd^2\theta d\theta^2 - d\theta^3 d^3y - 3d^2\theta^2 dyd\theta + dyd\theta^2 d^3\theta - dyd\theta^5 \\ m_{43} = 3d^2xd^2\theta d\theta^2 - d\theta^3 d^3x - 3d^2\theta^2 dxd\theta + dxd\theta^2 d^3\theta - dxd\theta^5 \\ m_{44} = d\theta \left(d^2xd^3y - d^3xd^2y \right) - d^2\theta \left(dxd^3y - d^3xdy \right) + \left(d^3\theta - d\theta^3 \right) \left(dxd^2y - d^2xdy \right) \end{cases} \tag{6.31}$$

Equation (6.32) summarizes the four steps that are needed to characterize explicitly the parameters associated with a contact equation. First, the model must be identifiable, and the inverse map g^{-1} between the parameters and the Taylor coefficients needs to be characterized. Second, multiple differentiations are used to obtain a linear map M between the Taylor coefficients and the derivatives of the contact equation. As a third step, the Taylor coefficients are expressed using the nullspace of M. Finally, the nullspace is computed using the minors of M which are nonlinear functions of the differentials of the sensor variables.

$$\begin{cases} p = g^{-1}\left(f_s, s(t)\right) \\ M\left(d^n s\right) f_s = d^n f = 0 \\ f_s = \Phi\left(\ker(M)\right) \\ \ker(M) = \Gamma(d^n s) \end{cases} \qquad (6.32)$$

6.2.2 Estimator Implementation

As a result of (6.32), the parameters are an explicit function of the sensor signals and their differentials. The number of sensor samples needed for the estimation depends on the maximum number of sensor signal differentiations and the numerical scheme used to compute these differentials. For example, the computation of the third order sensor differentials in (6.31) (e.g., $d^3\theta, d^3 x, d^3 y$) require five samples when using a second-order central difference scheme. Note that more samples are required if higher order central difference schemes are used.

Theoretically, this method is interesting since it allows for fast computations without the need for initial conditions. Unfortunately, this technique cannot be used in practice since it involves differentiation of potentially noisy sensor signals. To illustrate this point, an implicit estimation and an explicit estimation are conducted for a simulated path noise-free path corresponding to a vertex-to-edge contact state modeled in (6.12), as shown in Fig. 6.5. The implicit estimation is performed over a sliding window of length 10 using the initial conditions described in (6.34). The explicit solution is computed using (6.29)-(6.31). Both estimations converge to the true values (6.33), as shown in Fig. 6.6. The implicit estimation was computed in 24 seconds whereas the explicit estimation

was computed in less than 0.3 seconds on a Pentium III running at 800 MHz. Figure 6.7 shows the estimations result when the simulated path of Fig.6.4 is corrupted by a normally distributed noise of mean and covariance described in (6.35). It can be seen that the explicit estimation is extremely sensitive to the noise, whereas the implicit estimation still converges to the true values.

$$\begin{bmatrix} p_1 & p_2 & p_3 & p_4 & p_5 \end{bmatrix}^T = \begin{bmatrix} -0.64 & 0.77 & -15 & -55 & 47.42 \end{bmatrix}^T \tag{6.33}$$

$$\begin{bmatrix} p_1^{ini} & p_2^{ini} & p_3^{ini} & p_4^{ini} & p_5^{ini} \end{bmatrix}^T = \begin{bmatrix} -0.85 & 0.52 & -37.11 & -96.41 & -18.92 \end{bmatrix}^T \tag{6.34}$$

$$X \sim N(x, 0.5) \qquad Y \sim N(y, 0.5) \qquad \Theta \sim N(\theta, 0.5) \tag{6.35}$$
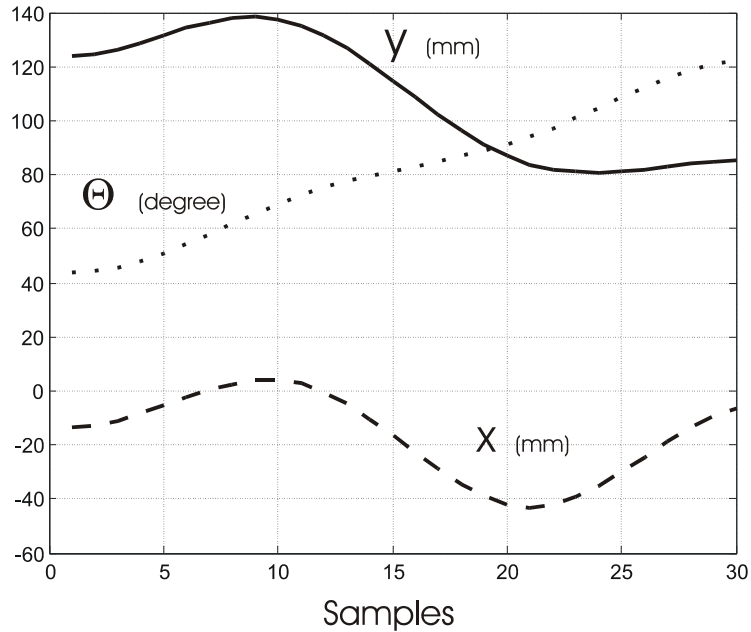
Figure 6.5: Sensor path associated with a vertex-edge contact.
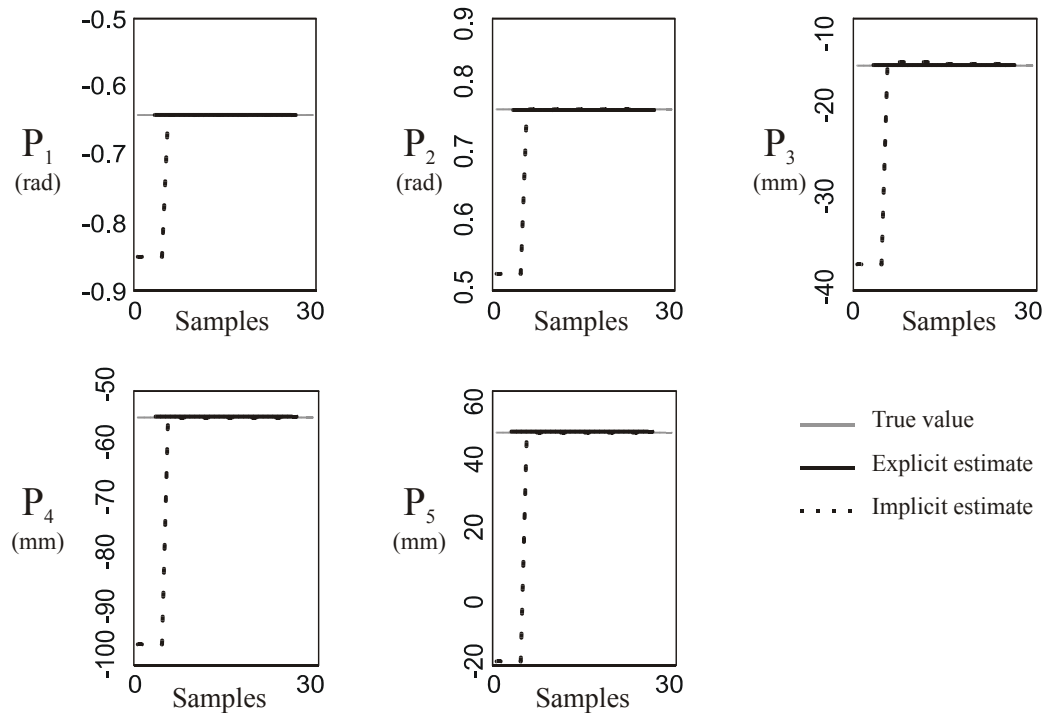
Figure 6.6: Noise-free explicit and implicit parameter estimations.
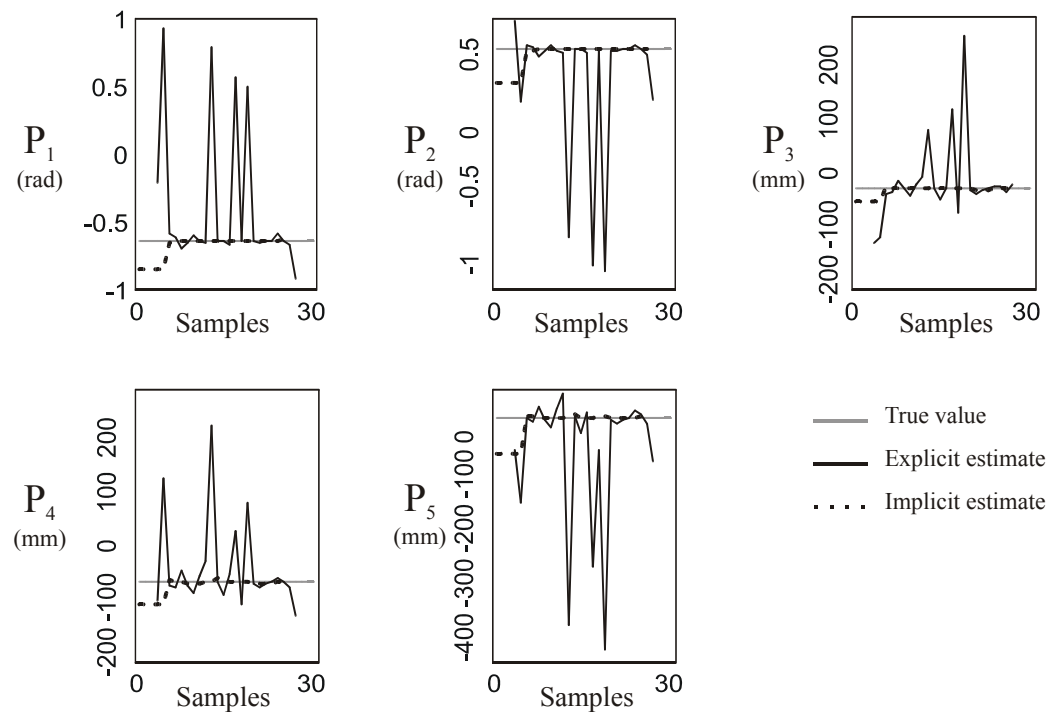
Figure 6.7: Noisy explicit and implicit parameter estimations.

148

Even though the explicit estimation scheme is not practical, the closed-form solution can give useful insights on the type of exciting paths that can be used for estimating the contact state parameters.

6.2.3 Excitation Condition

Assuming that a model is identifiable, a closed-form solution for the parameters can be found if the Taylor coefficients can be written as functions of the nullspace of M, as expressed in (6.26). As mention is section 6.2.1, this is possible if the number β^* of constraints on the Taylor coefficients satisfies the following inequality:

$$\beta^* \geq \dim\left(Ker\left(M\right)\right) \tag{6.36}$$

The quantity β^* represents the number of constraints on the parameters (e.g., $p_1^2 + p_2^2 = 1$ in (6.12)) that were not already utilized to test for identifiability (i.e., equations not used to construct g in (6.19)).

The dimension of the nullspace depends only on the sensor path, whereas β^* is a fixed quantity which depends only on the structure of the contact model. In addition, the dimension of the nullspace must be greater that one when the contact is satisfied since the Taylor coefficients cannot all be equal to zero. As a result, an excitation condition requires sensor paths that can satisfy:

$$1 \leq \dim\left(Ker\left(M\right)\right) \leq \beta^* \tag{6.37}$$

Many sensor paths can solve this problem; a practical solution is to choose a path that is simple to implement (e.g., low order derivative path). As an example, the vertex-edge contact illustrated in Fig. 6.4(a) and modeled in (6.12) is considered. The inequality (6.37) is satisfied if the nullspace of M is less or equal to one since β^* is equal to one for this contact (i.e., $\beta^* = \beta$ from Table 4.1). As a consequence, the sensor path must ensure that the nullspace is of dimension one. Analyzing the matrix M in (6.25), it can be seen that several paths can satisfy this criteria (e.g., paths such that $d^2\theta$, dx, and dy are nonzero in (6.25)).

It is also important to notice that even when (6.37) is satisfied, zero nullspace components can result in non-estimable parameters in the final closed-form solution. For example, if a path is chosen such that N_2 is zero but N_1 and N_3 are nonzero in (6.29), then the parameter p_1 cannot be estimated even though (6.37) is satisfied. As a consequence, an additional condition to obtain the full estimation of the parameters is to choose a path that produces non-zero nullspace components.

The two excitations conditions associated with a full explicit estimation can be summarized as follows:

- Sensor paths must be chosen such that (6.37) is satisfied.
- Sensor paths must be chosen such that all the components of the nullspace of M are nonzero.

These conditions can then be used as a design tool to create an input sensor path that will produce an explicit solution for all the parameters. A partial solution can be found, however, if either one of these two conditions is not satisfied. For example, it can be shown that a pure rotation (e.g., Fig. 6.1(b)) for the vertex-to-edge contact state modeled in (6.12) results in a nullspace of dimension two that does not satisfy (6.37); nevertheless, the parameters p_3 and p_4 can still be explicitly estimated in (6.12). The proof is provided in Appendix B.

The explicit method provides an interesting basis to analyze the effect of sensor excitation on parameter estimations; however, additional work is needed 1) to show that the sensor paths designed for the explicit method are also valid for the implicit method, 2) to show the sufficient and/or necessary nature of the two excitation conditions presented in this section and 3) to extend the technique to more complex contact states (e.g., spatial contact states).

6.3 Summary

This chapter investigated the implementation of an estimation algorithm for the multiple model estimation step of the contact state estimator. As a result, a sliding nonlinear least squares method using the Levenberg-Marquardt algorithm was chosen due to its robustness to poorly known nominal parameters. An explicit method was also proposed for pose equations. This method, based on multiple differentiations of the contact model, was shown to be fast but too sensitive to noise to be practically implemented. The analytical nature of the solution, however, provided a good foundation

to investigate the effect of sensor excitation on parameter estimation. In particular, two excitation conditions were derived and used as design tools to create sensor inputs that could ensure the estimation of all the parameters associated with a given contact model.

The next chapter discusses the entire implementation of a contact state estimator. First, t the implementation of a decision test that combines the residuals of the multiple model estimation algorithm developed in this chapter with the task encoding discussed in Chapter 5 (i.e., probability transition matrix) is presented. Then, the estimator is implemented and tested for a 3D peg-in-hole insertion task.

Chapter 7

Contact State Estimation Using a Hidden Markov Model

A final and essential aspect of contact state estimation is the implementation of a decision algorithm to resolve which contact state is active and which set of property estimates is valid. The goal of this chapter is to provide a decision test based on the estimation information coming from the multiple estimation algorithm described in Chapter 6 and the prior information coming from the task knowledge described in Chapter 5, as illustrated in Fig. 6.1. The approach employed here uses a Hidden Markov Model (HMM) to combine the residuals, representing how well the contact models fit the sensor data, with the probability of specific contact state transitions embodied in a task contact state network. The HMM presents a convenient statistical framework in which all the information regarding the task is converted into probabilities. Using this framework, a

Viterbi search algorithm is used to estimate the most likely path inside the task network corresponding to the given measurements.

The first part of this chapter reviews the HMM framework, and the second part presents an application in which two HMMs are successfully utilized to segment the four contact states used to describe a peg-in-hole insertion task.

7.1 The Hidden Markov Model Framework

An HMM can be described as a probabilistic observer by which a stochastic hidden process can be observed using the probabilistic structure of the task state network and a probabilistic relationship between the states and one or several observable stochastic signals. This section reviews the principal components that constitute an HMM and describes how they can be used to estimate contact states.

7.1.1 HMM Structure

The contact state network of an HMM is described by n, the number of states, ρ, the n-vector of initial state probabilities in (7.1), and A, the $n \times n$ state transition probability matrix defined in (5.1) and (5.2).

$$
\begin{aligned}
\rho &= \begin{bmatrix} \rho_1 & \rho_2 & \cdots & \rho_n \end{bmatrix}^T \; with \; \sum_{i=1}^{n} \rho_i = 1 \\
\rho_i &= P\big(c_1 = C_i\big) \qquad\qquad 1 \le i \le n
\end{aligned}
\tag{7.1}
$$

The probabilistic relationship between an observable signal sequence O, of length T,

and the different states that comprise the task network is given by the probability density function $B_i(O_t)$ defined as follows:

$$B_i(O_t) = P(O_t / c_t = C_i)$$
(7.2)

As a result, all the information relevant to the task is contained in the three probability measures: A, B, and ρ. Using Rabiner's notation (Rabiner 1989), HMM's are expressed in a compact form as:

$$\lambda = (A, B, \rho)$$
(7.3)

In order for an HMM to be mathematically practical, the following assumptions are made:

- Markov assumption: the current state only depends on the previous state.
- Stationarity assumption: the state transition probabilities are independent of the time at which the transitions occur.
- Statistical independence of the observations: the current observation is statistically independent of the previous observation.

7.1.2 HMM Based Segmentation

The HMM representation is appropriate to solve segmentation problems (e.g., speech recognition). In the HMM context, the segmentation problem can be posed as a decoding problem (i.e., uncovering the hidden states of the model). The objective is to find the

155

best sequence of states that maximizes the probability $P(Q/O,\lambda)$ (i.e., the probability of having the state sequence Q given the observations O and the model λ). The probability of maximizing $P(Q/O,\lambda)$ with respect to Q is equivalent to maximizing $P(Q,O/\lambda)$ with respect to Q as shown in (7.4).

$$P(Q/O,\lambda) = \frac{P(Q,O/\lambda)}{P(O/\lambda)} \tag{7.4}$$

The joint conditional probability $P(Q,O/\lambda)$ can be expressed as in Rabiner (1989):

$$P(Q,O/\lambda) = P(O/Q,\lambda)P(Q/\lambda) = \rho_{c_1} B_{c_1}(O_1) a_{c_1 c_2} B_{c_2}(O_2) a_{c_2 c_3} \dots a_{c_{T-1} c_T} B_{c_T}(O_T) \tag{7.5}$$

where the c's symbolize the states at time t_i (i.e., $Q = c_1 c_2 c_3 \cdots c_T$)

Maximizing (7.5) with respect to Q requires the computation of (7.5) for all the possible state sequences. This number is exponential in the number of observations. For example, a problem with only three observation samples and two states has a maximum of eight state sequences (i.e., 111 - 222 - 112 - 221 - 211 - 122 - 121 – 212). If the number of observations increases to 100, then 2^{100} possible state sequences must be computed. To solve this optimization problem efficiently, a dynamic programming technique known as the Viterbi algorithm is employed (Viterbi 1967).

The Viterbi Algorithm

The Viterbi algorithm is a technique that reduces the optimization of a global problem to a sequential optimization of simpler sub-problems. This technique can be applied to the optimization of (7.5) since the problem can be broken into a sequence of optimal sub-problems. In effect, it can be noted that for each observation, the optimal path ending in each state can also be part of the final optimal path obtained for the full observation sequence. As an example, a three-state Viterbi optimization is illustrated in Fig. 7.1. There exists nine possible state sequences between time t_1 and t_2. The Viterbi algorithm computes the probability (7.5) for each sequence and then keeps the most likely path ending in each state. This result is then used by induction to compute the most likely sequences between times t_2 and t_3. As a result, the overall optimization problem is broken into T optimal sub-problems. As a final step, the state corresponding to the last observation is uncovered and then used to back estimate the complete state sequence maximizing (7.5).

The Viterbi algorithm reduces to $n^2 T$ the number of computations of the joint probability (7.5), making the algorithm a practical solution for problems with a limited number of states.

$$\delta_{1,1} = \rho_1 B_1(O_1)$$
$$\delta_{2,1} = \rho_2 B_2(O_1)$$
$$\delta_{3,1} = \rho_3 B_3(O_1)$$

$$\delta_{i,2} = Max \begin{pmatrix} \delta_{1,1} a_{1i} \\ \delta_{2,1} a_{2i} \\ \delta_{3,1} a_{3i} \end{pmatrix} B_i(O_2)$$

$$\delta_{i,3} = Max \begin{pmatrix} \delta_{1,2} a_{1i} \\ \delta_{2,2} a_{2i} \\ \delta_{3,2} a_{3i} \end{pmatrix} B_i(O_3)$$

$$End = Max \begin{pmatrix} \delta_{1,T} \\ \delta_{2,T} \\ \delta_{3,T} \end{pmatrix}$$
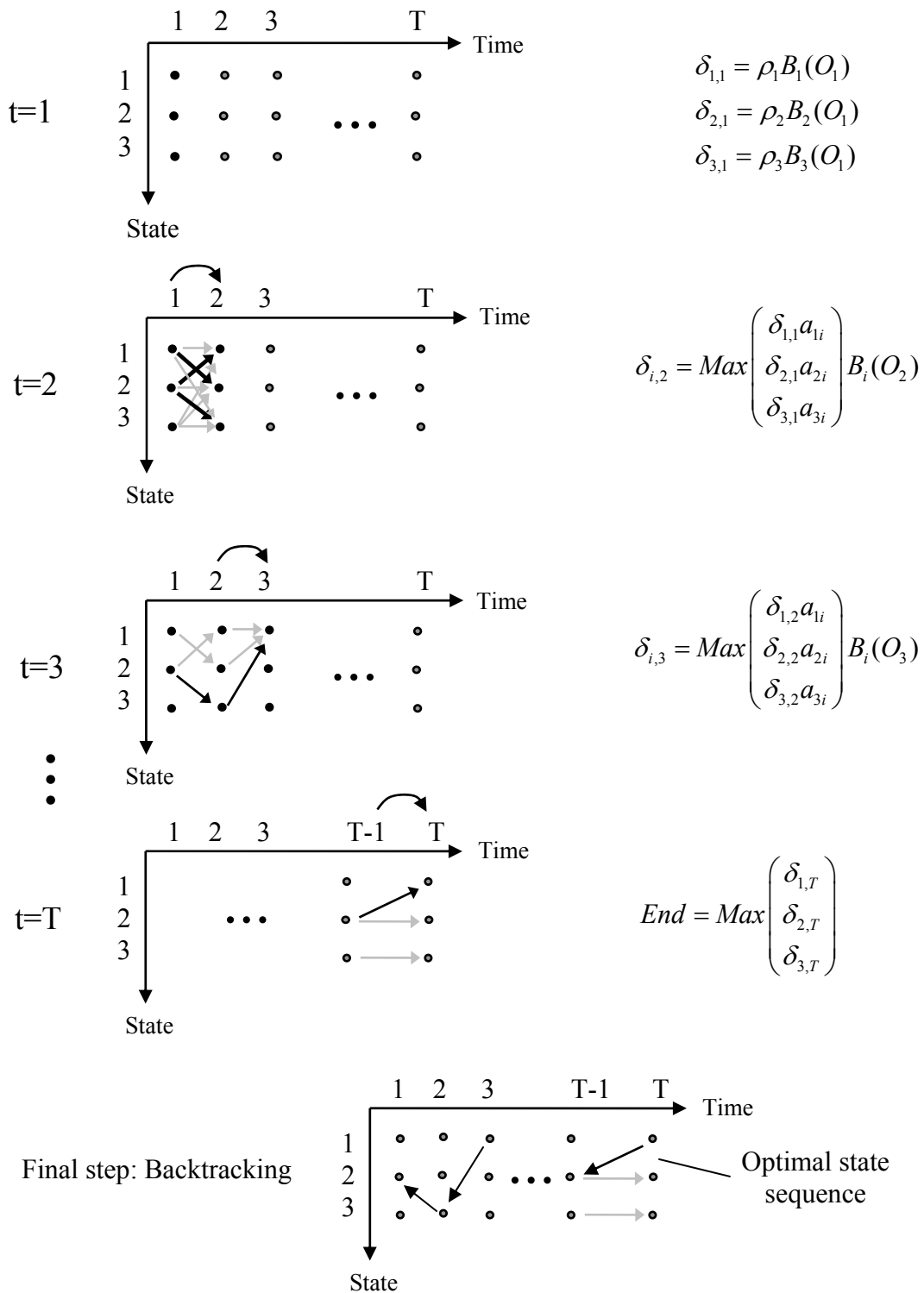
Figure 7.1: Implementation schematic of the Viterbi algorithm.

7.1.3 HMM Implementation

The implementation of an HMM requires the computation of the probabilistic quantities ρ, A and B introduced in (7.3). Two methods are commonly used in the literature: unsupervised training and supervised training. In unsupervised training, a learning algorithm is used to extract the three probability measures from unlabeled data sets. Several learning algorithms, such as the Baum-Welch method (Baum and Petrie 1966), are frequently used with HMMs. Unsupervised training methods are well-suited for applications possessing a large number of states (e.g., speech recognition). When the number of states is limited, supervised training techniques using labeled data can be more practical. These methods offer more control to the user and allows the decoupling of the learning problem: the task knowledge (i.e., ρ and A) can be set using one method, and the observation knowledge (i.e., B) can be set using another one, as described below.

Task knowledge:

The initial state probability vector ρ is generally known for a manipulation task since it is often assumed that the task starts in a non-contact state (i.e., free motion). As for the probability transition matrix, it can be obtained using the techniques described in 5.3. The elements of the matrix are computed by counting the number of occurrences of each transition given a large number of contact state sequences (i.e., large k in (5.7)).

<u>Observation knowledge:</u>

The observation probability distribution, B, represents the probabilistic map between the observations and the states. Several choices of observations can be used to character-ize the states (e.g., raw signals, processed signals). The observations that provide the most direct map to the contact states should be chosen. In the context of parameter-based contact state estimation, raw sensor signals (e.g., position, orientation, force and torque measurements) can be used to characterize the contact states; however, estimation residuals are better suited since a direct correspondence between a contact being active and the size of the residual exists. In effect, for each contact state, the residual of the estimation process is a scalar which depends only on sensor inputs $s(t)$ and the estimated time-independent parameters $\hat{p}$. As shown in equation (7.6), the residual corresponds to the sum of squares of the estimated nonlinear contact function $f(\hat{p}, s(t))$ computed inside an estimation window of length δ.

$$\varepsilon_p = \sum_{t=1}^{\delta} f(\hat{p}, s(t))^2 \tag{7.6}$$

The objective of the estimation phase is to find the parameter estimates that minimize (7.6). Thus, the magnitude of the residual is an indication of the goodness of the fit, assuming a well-conditioned data window (i.e., rich excitation). As a result, contact state models associated with small residuals are more likely to correspond to the actual state than models associated with large residuals.

In the HMM literature, the observation probability distribution is commonly ap-

proximated with mixtures of multivariate Gaussians (Rabiner 1989) as shown in (7.7). In this context, the distribution is characterized by its mean and covariance matrix. Since the residuals are nonlinear functions, these statistics can be difficult to obtain. However, they can be approximated analytically using first-order Taylor series, or they can be extracted using Monte Carlo simulations (Breipohl 1970).

$$B_i(O_t) = \sum_{j=1}^{J} \frac{s_{ij}}{\sqrt{(2\pi)^k |U_i|}} \exp\left\{-\frac{1}{2}(O_t - m_i)^T U_i^{-1}(O_t - m_i)\right\}, \qquad 1 \le i \le n;\ 1 \le t \le T$$

$$\sum_{j=1}^{J} s_{ij} = 1$$

(7.7)

where, k represents the maximum number of components of the signal O. Also, m_i and U_i are a $k \times 1$ vector of means and a $k \times k$ covariance matrix, respectively.

7.2 Experimental Contact State Estimation

In this section, the implementation of the contact state estimator illustrated in Fig. 6.1 is utilized during a manipulation task. As an example of a common assembly task, a peg-in-hole insertion is considered, as shown in Fig. 7.2. The expected sequence during the task can be reduced to four steps. First, the peg is slid towards the hole on the planar surface (Contact 2). As the peg enters the hole, it pivots on the rim of the hole (Contact 3) and typically maintains this contact until the other side of the hole is reached. It then stays in double contact with the rim and the inside of the hole (Contacts 3 and 4) until the peg is inserted far enough that the task can be easily completed.
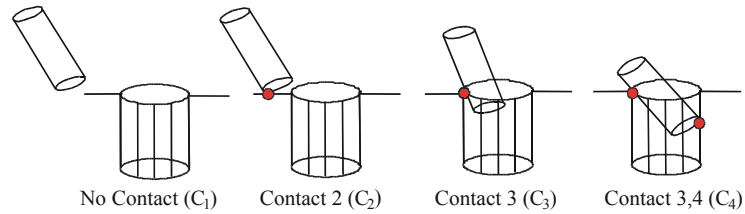
Figure 7.2: Possible sequence of contact states during peg-in-hole insertion

The goal of the experiment is to implement an HMM to estimate the sequence of contact states composing the task. The HMM presented in this experiment is based on an empirical selection of the HMM variables. A possible improvement of the approach is discussed at the end of the section.

7.2.1 System Configuration

A PHANToM® haptic device, as shown in Fig. 7.3, is used as the manipulating robot. The positions of the system's six joints are measured using high-resolution optical encoders. The kinematics of the robot are known, and a closed loop calibration technique (Hollerbach and Wampler 1996) is used to improve the absolute accuracy of the system.

A cylindrical peg is attached directly to the tip of the manipulator robot. The hole is drilled perpendicular to the surface of a rectangular aluminum block that is mounted on a three degree of freedom vise (roll-tilt-pan). The insertion is performed manually, using the manipulating robot to record the kinematic data.
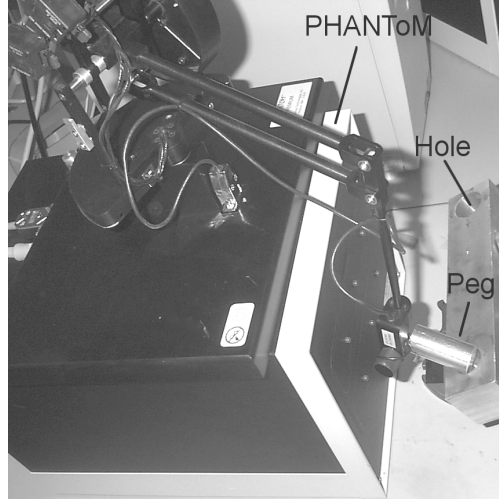
Figure 7.3: Experimental apparatus - PHANToM 1.5, cylindrical peg and orientable hole.

7.2.2 Contact State Equations

Pose equations are utilized to describe the contact states associated with the task. The technique developed in section 3.2.2 is used to represent the kinematic constraints associated with the contact state. Additional nonlinear constraints are needed to represent the position of the contact point on the peg's rim and hole's rim. Equation (7.8) corresponds to the pose equation associated with Contact 2. Equations for Contact 3 and Contact 4 takes similar form and can be found in Debus et al. (2004).

$$
\begin{cases}
\varepsilon_{p2} = \boldsymbol{K_2} + q_{14}\sin\boldsymbol{\beta_2} + q_{24}\cos\boldsymbol{\beta_2}\sin\boldsymbol{\beta_1} - q_{34}\cos\boldsymbol{\beta_1}\cos\boldsymbol{\beta_2} + \\
\qquad\quad + \boldsymbol{L_p}\left[-q_{33}\cos\boldsymbol{\beta_1}\cos\boldsymbol{\beta_2} + q_{23}\sin\boldsymbol{\beta_1}\cos\boldsymbol{\beta_2} + q_{13}\sin\boldsymbol{\beta_2} \right] \\
\qquad + \boldsymbol{R_p}\cos\boldsymbol{\alpha_2}\left[-q_{31}\cos\boldsymbol{\beta_1}\cos\boldsymbol{\beta_2} + q_{21}\sin\boldsymbol{\beta_1}\cos\boldsymbol{\beta_2} - q_{11}\sin\boldsymbol{\beta_2} \right] \\
\qquad + \boldsymbol{R_p}\sin\boldsymbol{\alpha_2}\left[-q_{32}\cos\boldsymbol{\beta_1}\cos\boldsymbol{\beta_2} + q_{22}\sin\boldsymbol{\beta_1}\cos\boldsymbol{\beta_2} - q_{12}\sin\boldsymbol{\beta_2} \right] \\
\\
where\ \ K_2 = H_z\cos\beta_1\cos\beta_2 - H_x\sin\beta_2 - H_y\cos\beta_2\sin\beta_1
\end{cases} \qquad (7.8)
$$

The bolded variables in this equation are the identifiable unknown parameters which

163

are listed in Table 7.1. Note that the terms forming K_2 are not individually identifiable since they do not multiply any input. In this case, they depend on the hole's center coordinates, which clearly cannot be identified in Contact 2. The q_{ij} are known functions of the robot's kinematic parameters and joint angles.

Table 7.1: Identifiable parameters.

R_p	Peg radius
L_p	Peg length
R_h	Hole radius
H_x, H_y, H_z	Hole's center coordinates
β_1, β_2	Orientation (pitch and yaw) of the plane
α_i	Angular coordinates locating the contact point on the rim of the peg for contact i
δ_i	Angular coordinates locating the contact point on the rim of the hole for contact i

7.2.3 Excitation Analysis

To investigate input excitation, the residuals for experimental data corresponding to the expected state sequence C_1 through C_4 of Fig. 7.2 are plotted in Fig. 7.4(a). While not depicted, the magnitude of the condition numbers corresponds to that of the residual values. Contact C_2 experiences a small residual ε_{p_2} when active and possesses the lowest condition number. In contrast, the residual ε_{p_3} for C_3 is large and poorly conditioned regardless of whether the contact state is active. The reason for this, as shown in Fig, 7.2, is that the possible robot configurations corresponding to contact C_2 are not as limited as the ones corresponding to contact C_3, since the robot pitch and yaw angles associated with C_2 are not constrained by the dimension of the hole.
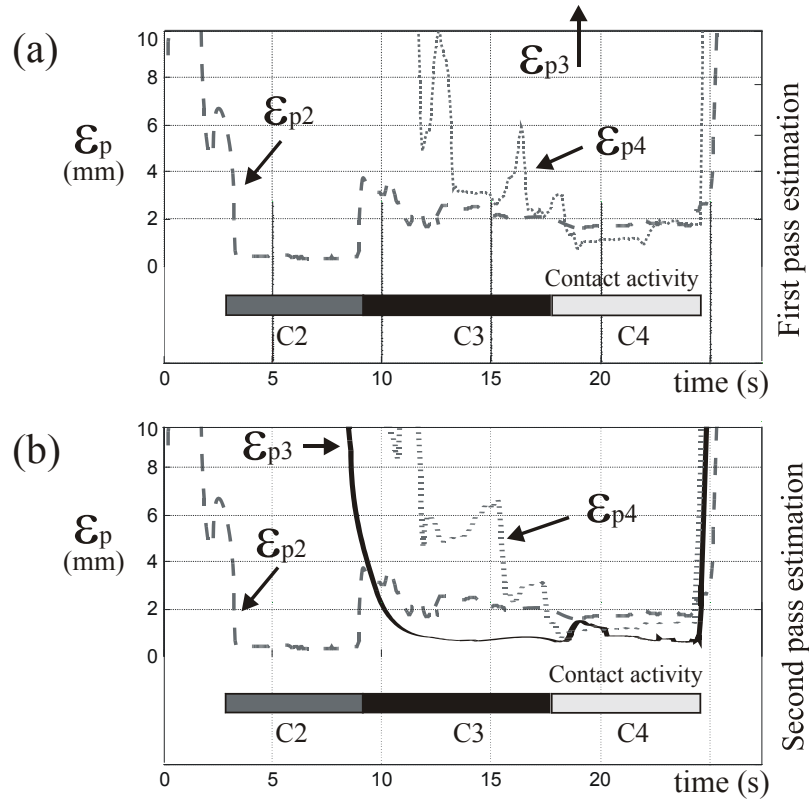
Figure 7.4: Multi-pass estimation. a) Initial estimation residuals, b) Estimation residuals computed using parameter estimates propagated from C_2.

A possible approach for improving the conditioning of poorly excited contact equations is to remove the parameters multiplying low-excitation inputs from the estimation process. Such elimination can be carried out by substituting parameter estimates from previously identified contact states into the estimation residuals to be used to estimate subsequent contact states. The assumption inherent in this approach is that the contact states occurring early in a task are less constrained and so experience high excitation and consequently exhibit low condition numbers. When this assumption is not met, an alternative method is multi-pass estimation. In this approach, the system first estimates those contact states for which high input excitation is most likely. After these

165

states are identified during task execution, their parameter estimates are used to estimate contact states occurring both prior to and subsequent to these states. If the well-conditioned states occur early in the task, then most of the estimation can be performed on line. If these states occur near the end of the task, then multi-pass estimation corresponds to post processing in its estimation of the early contact states. An example of the multi-pass technique is illustrated in Fig. 7.4. In the first pass, the parameters associated with the well-conditioned state C_2 are estimated (i.e., β_1, β_2, R_p and L_p). Then, in a second pass, the parameter estimates from C_2 are used to re-estimate the residuals for contact states occurring both before and after C_2. While the residual of C_4 is modestly affected, the residual of C_3 decreases substantially as shown in Fig. 7.4(b).

7.2.4 Contact State Network

As shown in Fig. 7.5(a), a state network can be used to model the sequence of contact states C_1-C_4 illustrated in Fig. 7.2. Connections between states are labeled with their state transition probabilities a_{ij}. As a second example, an alternate two-state network appears in Fig. 7.5(b). It is comprised of contact state C_2 and contact state C_0, representing all other possible contact states. These two networks can be used for the multi-pass approach described in the previous section. In the first pass, the state network of Fig. 7.5(b) is used to estimate the contact state C_2. Then, in a second pass, the four-state network of Fig. 7.5(a) is employed with the re-conditioned residuals obtained from the knowledge of C_2 to estimate the entire state sequence.
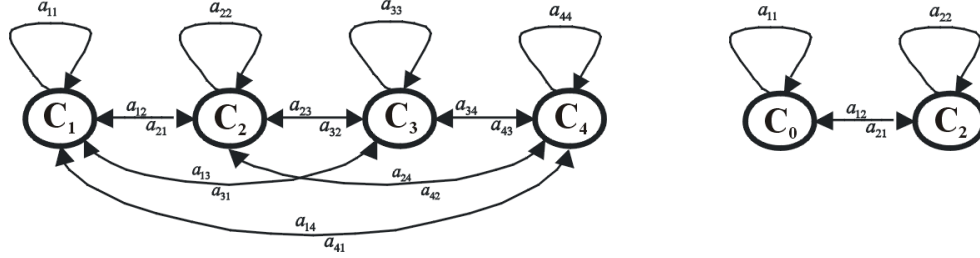
Figure 7.5: Contact state networks. a) Four-state network based on the contact states of Fig. 7.2, b) Two-state network for distinguishing contact state C_2 from all other possible contact states.

7.2.5 HMM Implementation

The multiple model estimation approach illustrated in Fig. 6.1 is used to estimate the contact state sequence. Orientation and position of the robot's tip are recorded at a rate of 25Hz, and contact state residuals (7.6) are computed at each time step using a 20-point moving data window. The residuals constitute the observation signal used as inputs to the HMM's:

$$O_t = \begin{bmatrix} \varepsilon_{p_2}(t) & \varepsilon_{p_3}(t) & \varepsilon_{p_4}(t) \end{bmatrix}^T \tag{7.9}$$

The two-state fully connected model of Fig. 7.5(b) is first utilized to estimate C_2 and its parameters. Then, the four-state, fully connected model of Fig. 7.5(a) is used, together with the parameter estimates from C_2, to estimate the remaining states and parameters.

The design of the HMM's associated with these two contact state networks reduces to the computation of the three probability measures ρ, A, and B defined in (7.3). Here, the task is comprised of a maximum of only four states, and so the HMM parameters can

167

be assigned manually using supervised training. The task knowledge and the observation knowledge associated with the experiment are described below.

Observation knowledge (B)

When a contact state is active, the associated residual is expected to be the smallest, given that the contact equations are well conditioned. This pattern, illustrated in Fig. 7.4(b), is encoded in a multivariate unimodal Gaussian distribution (i.e., equation (7.7) with $s_{i1} = 1$) for each state of the HMM. The mean and covariance matrix associated with each distribution are determined empirically using a two-step process. First, several contact sequences are manually segmented and the observations corresponding to the training sequences are gathered inside a training matrix $M_g \in \mathbb{R}^{T_g \times 3}$ for each contact state. Then the sample mean m_i and sample covariance U_i are extracted from M_g using (7.10) and (7.11), respectively.

$$m_i = \frac{1}{T_g} \sum_{t=1}^{T_g} O_t \tag{7.10}$$

$$U_i = \frac{1}{T_g - 1} \sum_{t=1}^{T_g} (O_t - m_i)(O_t - m_i)^T \tag{7.11}$$

As an example, the mean vector associated with the distribution of each contact state is described in (7.12). The rows represent the mean of the residuals ε_{p2} through ε_{p4}, while the columns correspond to the states C_1 though C_4. For example, $m_3(1) = 2$

168

implies that the expected mean of ε_{p2} is 2 when contact C_3 is active. Note that since C_4 is composed of contacts 3 and 4, it is expected that both ε_{p3} and ε_{p4} are low when the state is active.

$$m_1 = \begin{pmatrix} 10 \\ 90 \\ 80 \end{pmatrix}, \ m_2 = \begin{pmatrix} 0.5 \\ 40 \\ 90 \end{pmatrix}, \ m_3 = \begin{pmatrix} 2 \\ 1 \\ 5 \end{pmatrix}, \text{ and } m_4 = \begin{pmatrix} 2 \\ 1 \\ 1 \end{pmatrix} \tag{7.12}$$

The same technique is used to extract the statistics associated with the two-state network pictured in Fig. 7.5(b). The same training sequences are utilized; however, a two-state manual segmentation is performed instead of the four-state segmentation utilized to train the four-state network.

Task Knowledge (ρ, A)

To define A, the probability transition matrix, and ρ, the initial probability vector, the following task knowledge is used:

- State C_1 (no contact) occurs first: $\rho_1 > \rho_j$, $j = 2, 3, 4$.

- State transitions are short: $a_{ii} > a_{ij}$, $1 \le i, j \le 4$.

- Transitions between C_2 and C_4 are impossible: $a_{24} = a_{42} = 0$

For the two-state model of Fig. 7.4(b), the selection of the probability transition matrix is straightforward. The values were chosen such that the probability of remaining in the current state is much higher than the probability of leaving the state.

169

$$A = \begin{bmatrix} 0.99 & 0.01 \\ 0.01 & 0.99 \end{bmatrix} \tag{7.13}$$

Because there are only two states, this model does not encode any information about the likely sequence of contact states. In contrast, the four-state model of Fig. 7.5(a) does permit the inclusion of such information and the selection of its A affects what contact state sequences can be successfully estimated. This topic is explored in the following subsection.

7.2.6 Sensitivity of Contact State Estimation to Robot Path

While the state transition probability matrix encodes the probability of each contact state transition, the particular robot path employed in task execution may or may not correspond to the most likely sequence of transitions described by A. To be robust to variations in robot path, the matrix A must accommodate variations in contact state sequence. Such a matrix, A_f (f = flexible transition matrix), which was obtained empirically, is compared here with one which permits only the most likely state transitions, A_r (r = rigid transition matrix).

$$A_f = \begin{bmatrix} .7 & .1 & .1 & .1 \\ .15 & .7 & .15 & 0 \\ .1 & .1 & .7 & .1 \\ .15 & 0 & .15 & .7 \end{bmatrix} \quad (7.14) \qquad A_r = \begin{bmatrix} .99 & .01 & 0 & 0 \\ 0 & .99 & .01 & 0 \\ 0 & 0 & .99 & .01 \\ .01 & 0 & 0 & .99 \end{bmatrix} \quad (7.15)$$

These transition matrices are used to define two models, HMM_{2f} and HMM_{2r}, respectively. Employing two-pass estimation, a two-state model HMM_1 first estimates contact state 2 and provides estimates of its parameters. In a second pass, HMM_{2f} and HMM_{2r} estimate their four contact states using residuals computed with the parameters estimated during the first pass. For comparison, manual segmentation was performed by the operator who pressed a switch at each perceived state transition.

Figure 7.6 depicts the results for the most likely sequence of contact states in peg insertion, $\{C_1, C_2, C_3, C_4, C_1\}$. The two-state HMM_1 demonstrates agreement with manual segmentation. For the most likely sequence of states in Fig. 7.6, the additional transition flexibility of HMM_{2f} produces two short time segments in which the state is falsely identified. Nonetheless, both models successfully match manual segmentation for all contact states.

Figure 7.7 shows the results for a state sequence including some unexpected transitions, $\{C_1, C_3, C_2, C_3, C_4, C_1\}$. While the two-state model HMM_1 continues to perform well, the rigid state transition matrix of HMM_{2r} introduces many false transitions to satisfy the state transition matrix. For example, the first actual state change is from C_1 to C_3. The rigid model must pass through C_2 in order to make this transition. The next actual state change is from C_3 to C_2. The rigid model can only make this transition by the three state changes, $C_3 \rightarrow C_4 \rightarrow C_1 \rightarrow C_2$. The flexible state transition matrix of HMM_{2f} avoids all of these false transitions and successfully identifies large portions of the active states. It was found that this model was successful for a variety of state sequences. In addition,

state estimation was robust to variations in the flexible state transition matrix (7.14). These results show that a flexible state transition matrix can successfully accommodate a broad range of robot paths during task execution.
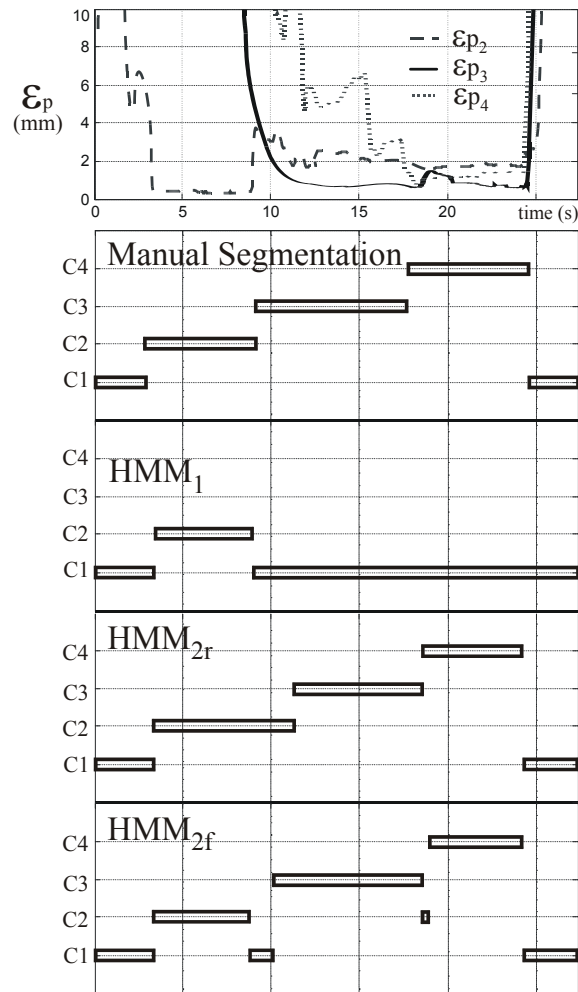
Figure 7.6: State estimation of the most likely insertion state sequence.
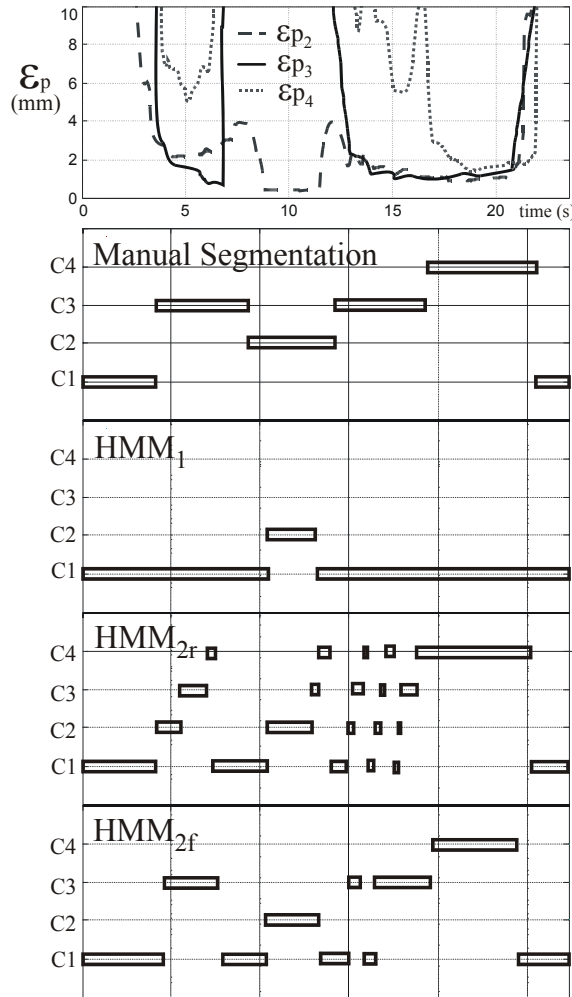
Figure 7.7: Segmentation of an atypical state sequence.

7.2.7 Alternate Formulation of the Observation Probability Distribution

In the preceding implementation, it is important to recognize that some ad hoc assumptions on the observation probability distribution were made that could limit the robustness of the approach. The distribution was assumed to be Gaussian; however, the validity of this assumption was not verified. A more satisfying approach, for example,

would be to identify the distribution using Monte Carlo simulations. Another approach would be to approximate the distribution using a first-order Taylor series. A sketch of this approach is presented below.

The residuals in (7.6) correspond to nonlinear functions having both estimated parameters and sensor values as inputs. Assuming a known Gaussian distribution of these inputs, the first-order linear approximation of the residuals is then also Gaussian. The mean and the covariance matrix associated with each state C_i, can be approximated as in Arras (1998). For example, the covariance matrix associated with the observation vector (7.9) can be written as follows:

$$
U_i = \begin{pmatrix} \sigma^2_{\varepsilon_{p2}} & \sigma_{\varepsilon_{p2}\varepsilon_{p3}} & \sigma_{\varepsilon_{p2}\varepsilon_{p4}} \\ \sigma_{\varepsilon_{p3}\varepsilon_{p2}} & \sigma^2_{\varepsilon_{p3}} & \sigma_{\varepsilon_{p3}\varepsilon_{p4}} \\ \sigma_{\varepsilon_{p4}\varepsilon_{p2}} & \sigma_{\varepsilon_{p4}\varepsilon_{p3}} & \sigma^2_{\varepsilon_{p4}} \end{pmatrix} = G\Sigma_i G^T, \qquad 1 \le i \le 4 \tag{7.16}
$$

where G and Σ_i represent the Jacobian matrix and the input covariance matrix respectively. Both matrices can be expressed as follows:

$$
G = \begin{pmatrix} \dfrac{\partial \varepsilon_{p2}}{\partial \hat{p}_1}\bigg|_{\hat{p}_1} & \cdots & \dfrac{\partial \varepsilon_{p2}}{\partial \hat{p}_n}\bigg|_{\hat{p}_n} & \dfrac{\partial \varepsilon_{p2}}{\partial s_1}\bigg|_{s_1} & \cdots & \dfrac{\partial \varepsilon_{p2}}{\partial s_m}\bigg|_{s_m} \\[3ex] \dfrac{\partial \varepsilon_{p3}}{\partial \hat{p}_1}\bigg|_{\hat{p}_1} & \cdots & \dfrac{\partial \varepsilon_{p3}}{\partial \hat{p}_n}\bigg|_{\hat{p}_n} & \dfrac{\partial \varepsilon_{p3}}{\partial s_1}\bigg|_{s_1} & \cdots & \dfrac{\partial \varepsilon_{p3}}{\partial s_m}\bigg|_{s_m} \\[3ex] \dfrac{\partial \varepsilon_{p4}}{\partial \hat{p}_1}\bigg|_{\hat{p}_1} & \cdots & \dfrac{\partial \varepsilon_{p4}}{\partial \hat{p}_n}\bigg|_{\hat{p}_n} & \dfrac{\partial \varepsilon_{p4}}{\partial s_1}\bigg|_{s_1} & \cdots & \dfrac{\partial \varepsilon_{p4}}{\partial s_m}\bigg|_{s_m} \end{pmatrix} \tag{7.17}
$$

$$
\Sigma_i =
\begin{pmatrix}
\sigma_{\hat{p}_1}^2 & \cdots & \sigma_{\hat{p}_1 \hat{p}_n} & \sigma_{\hat{p}_1 s_1} & \cdots & \sigma_{\hat{p}_1 s_m} \\
\vdots & \ddots & \vdots & \vdots & \ddots & \vdots \\
\sigma_{\hat{p}_n \hat{p}_1} & \cdots & \sigma_{\hat{p}_n}^2 & \sigma_{\hat{p}_n s_1} & \cdots & \sigma_{\hat{p}_n s_m} \\
\sigma_{s_1 \hat{p}_1} & \cdots & \sigma_{s_1 \hat{p}_n} & \sigma_{s_1}^2 & \cdots & \sigma_{s_1 s_m} \\
\vdots & \ddots & \vdots & \vdots & \ddots & \vdots \\
\sigma_{s_m \hat{p}_1} & \cdots & \sigma_{s_m \hat{p}_n} & \sigma_{s_m s_1} & \cdots & \sigma_{s_m}^2
\end{pmatrix}
\tag{7.18}
$$

The input covariance matrix Σ_i represents the prior knowledge associated with the inputs (i.e., $\hat{p}, s$). This matrix can be difficult to obtain; however, several simplifications can be considered to facilitate the construction of the matrix (the validity of which must be tested empirically afterwards). As a first simplification, independence of the inputs could be considered. As a result, the off-diagonal terms of the input covariance matrix can be set to zero. As a second (stronger) assumption, independence of the residuals could be considered. As a result, the off-diagonal terms of the input covariance matrix and the Jacobian matrix can be set to zero. This assumption would reduce the analytical complexity associated with the computation of the Jacobian matrix. Finally, while the covariance associated with the estimated parameters was assumed, this knowledge is not known a priori. To address this, covariance elements of small magnitudes can be assumed for the parameters associated with the active contact state, whereas covariance elements of high magnitudes must be guessed for the parameters associated with the non-active contact states.

7.3 Summary

This chapter discussed the implementation of a contact state estimator. The decision test was performed by a Hidden Markov Model (HMM), which combined a measure of how well each set of contact equations fit the sensor data with the probability of specific contact state transitions. The approach was illustrated for a three dimensional peg-in-hole insertion using a tabletop manipulator robot. At each sampling time, multiple model estimation coupled with an HMM was used to assess the most likely contact state. Using only position sensing, the contact state sequence was successfully estimated without knowledge of nominal parameter values.

Chapter 8

Conclusion

This thesis presents a complete and novel framework for achieving contact-based robot perception for manipulation tasks in poorly known environments. As a first step, the general problem was decomposed into seven design problems and two implementation problems, as shown in Fig. 1.4 and Fig. 1.5. An extensive literature review on contact state estimators pointed out the need for design tools. As a result, several analytical tools were developed to improve the design of contact state estimators.

This approach constitutes a contrast to the traditional method taken in the literature in which contact state estimators are first implemented with a limited design and then "tuned" to a specific application. In this research, tools were developed to ensure the a priori feasibility of contact estimation in poorly known environments so that standard estimation and detection algorithms could be used during the implementation phase.

8.1 Thesis Contributions

The major contributions of this thesis can be summarizes as follows:

1) The feasibility of contact state estimation in poorly known environments has been reduced to four design problems: contact state distinguishability, contact state observability, contact state identifiability, and data excitation. The first two problems address the feasibility of contact state detection, while the last two address the feasibility of the estimating the contact states' parameters.

2) The major technical contribution of this thesis is the development of analytical distinguishability and identifiability tools that can comment on the a priori implementation feasibility of a contact state estimator. This method, based on Taylor series expansion, provides a unified approach to testing the capability of candidate models to estimate both the parameters and the states. In this framework, identifiability is reduced to an existence problem while distinguishability is reduced to a uniqueness problem. Both problems are solved by comparing sets of algebraic equations based on the Taylor coefficients used to represent the structure of the contact models. In contrast to on-line, numerical methods presented in the literature, the Taylor series approach is an analytical method that replaces local results based on the sensor variable path with results which are global with respect to the space of sensor variables. Consequently, it can be used as a tool to select appropriate contact models and sensors in the design of a contact state estimator.

3) This thesis introduces the concept of contact state observability as a way of testing the feasibility of contact state estimation in a poorly known environment. The observability question is solved using a map between the distinguishable graph representing the task in the poorly known environment and the contact state graph representing the task in the structured environment. The mapping is defined as a forward projection on the parameter history associated with the execution of the task.

4) This thesis presents a first attempt to solve the difficult problem of data excitation for contact state estimation. A four-step estimation scheme is provided to solve explicitly for the parameters as a function of the sensor signals and their differentials. The central part of the procedure is based on finding a linear map between the Taylor coefficients characterizing the structure of the contact equation and the sensor variables. The effect of the sensor signals on the parameters is then analyzed by investigating the invertibility of the linear map. A necessary excitation condition on the sensor data is posed as a condition on the dimension of the nullspace associated with the linear mapping.

5) The contact estimator proposed in this thesis uses a two-step procedure: in the first step, the geometric parameters characterizing the contact states are estimated using a multiple-model estimation approach based on nonlinear least squares. In the second

step, the contact states corresponding to the sensor measurements are detected using HMMs. This approach has two advantages:

a. The nonlinear least squares algorithm is based on Levenberg-Marquardt, a technique shown to be robust to poorly known initial conditions. As a result, the estimation algorithm does not need accurate nominal parameter values, and large uncertainties in the parameters can be considered (i.e., poorly known environment).

b. The HMM presents a convenient framework to combine the estimation information coming from the multiple-model estimation and the prior information coming from the task knowledge (i.e., likelihood of transitions among the contact states). As a result of this combination, the detection capacity of the estimator is enhanced.

6) A collection of MATLAB$^{®}$ functions have been implemented to test the identifiability and distinguishability of arbitrary nonlinear algebraic models. These functions use the MATLAB Symbolic Math Toolbox to compute symbolically the Taylor coefficients corresponding to the contact equations, to build the nonlinear system of algebraic equations needed for the testing, and to solve these sets of equations for the time-independent unknowns parameterizing the contact states. Existence and uniqueness of a solution is then analyzed to comment on the identifiability and distinguishability of the contact models.

8.2 Future Research Directions

A thesis represents both a research ending point and a starting point. For every problem solved, another must be left unattempted and yet a third is uncovered. Several research directions that could enhance the design of contact state estimators in poorly known environments are described below:

- Uncertainty due to sensing noise was ignored in the design phase of the estimator. Sensor noise is, however, always present in real applications and can impact the distinguishability, identifiability, and observability of the contact states. Noise affects these three properties at different levels. Identifiability, for example, is not directly affected by noise since sensing uncertainties do not change the structural form of the contact equation. Nevertheless, noise can lower the quality of the estimation (i.e., large uncertainties on the estimates) and therefore reduce the benefit of the parameter history based observability technique presented in section 5.4. Distinguishability is the property most affected by sensor uncertainties since noise typically "blurs" the sensor-space partition resulting from the distinguishability testing. As a result, sensor noise cannot be ignored and additional design tools need to be built to take these uncertainties into consideration.

- Distinguishability and identifiability are intrinsic properties of contact state models. Therefore, these properties need to be established only once, regardless of the method. This thesis presents a general method to test for contact state

distinguishability and identifiability, and several examples were studied in section 4.3. A natural extension would be to use the developed method to create a contact database for polygonal and polyhedral contact states given different sensing modalities. This database could then be used regardless of the chosen estimation or detection algorithm.

- The problem of data excitation for contact state estimation has been introduced in this thesis. An excitation condition was developed for a pose equation using an explicit estimation scheme that resulted in a closed-form solution for the parameters of the equation. An interesting research direction would be to investigate the existence of optimal paths for contact state identifiability and distinguishability. These paths could be derived for each contact state and implemented in a compliant motion control package. As a direct application, a sequence of optimal paths could be run after each contact transition to facilitate the estimation and detection of the contact states and ultimately accelerate the task completion.

Appendix A

This appendix illustrates the derivation of the homogeneous transformation matrices T_f^m and T_m^f used to express the pose constraints presented in equations (3.6) and (3.7). Using the kinematic closure equations presented in equation (3.10), the components of T_f^m and T_m^f are expressed for planar and spatial transformations respectively.

A.1 Planar Pose Constraints

As shown in the kinematic closure equations (3.10), the matrices T_f^m and T_m^f depend on the three homogenous matrices: $T_w^g(t)$, T_g^m, and T_w^f. These three matrices can be written as follows in two-dimension:

$$T_w^g(t) = \begin{pmatrix} \cos\theta(t) & -\sin\theta(t) & x(t) \\ \sin\theta(t) & \cos\theta(t) & y(t) \\ 0 & 0 & 1 \end{pmatrix}, \ T_g^m = \begin{pmatrix} m_1 & -m_2 & m_3 \\ m_2 & m_1 & m_4 \\ 0 & 0 & 1 \end{pmatrix}, \ T_w^f = \begin{pmatrix} f_1 & -f_2 & f_3 \\ f_2 & f_1 & f_4 \\ 0 & 0 & 1 \end{pmatrix}$$

As a next step, these three matrices (and their inverse) are multiplied to obtain T_f^m and T_m^f.

A.1.1 $T_f^m = T_f^w T_w^g(t) T_g^m$

The three pose constraints associated with the computation of T_f^m can be written as follows:

- No rotation around the axis z_f:

$$T_f^m(1,2) = f_2\left(\sin(\theta)\,m_1 + \cos(\theta)\,m_2\right) + f_1\left(\cos(\theta)\,m_1 - \sin(\theta)\,m_2\right) = 0$$

- No translation around the axis x_f:

$$T_f^m(1,3) = f_2\left(y - f_4 + \sin(\theta)\,m_3 + \cos(\theta)\,m_4\right) + f_1\left(x - f_3 + \cos(\theta)\,m_3 - \sin(\theta)\,m_4\right) = 0$$

- No translation around the axis y_f:

$$T_f^m(2,3) = f_1\left(y - f_4 + \sin(\theta)\,m_3 + \cos(\theta)\,m_4\right) + f_2\left(-x + f_3 - \cos(\theta)\,m_3 + \sin(\theta)\,m_4\right) = 0$$

A.1.2 $T_m^f = T_m^g T_g^w(t) T_w^f$

The three pose constraints associated with the computation of T_m^f can be written as follows:

No rotation around the axis z_m:

- $T_m^f(1,2) = f_1\left(\sin(\theta)\,m_1 + \cos(\theta)\,m_2\right) + f_2\left(-\cos(\theta)\,m_1 + \sin(\theta)\,m_2\right) = 0$

- No translation around the axis x_m:

$$T_m^f(2,3) = \begin{pmatrix} m_2\left(x\cos(\theta) + y\sin(\theta) - \cos(\theta)\,f_3 - \sin(\theta)\,f_4 + m_3\right) \\ -m_1\left(y\cos(\theta) - x\sin(\theta) + \sin(\theta)\,f_3 - \cos(\theta)\,f_4 + m_4\right) \end{pmatrix} = 0$$

- No translation around the axis y_m:

$$T_m^f(1,3) = \begin{pmatrix} -\left(m_1\left(x\cos(\theta) + y\sin(\theta) - \cos(\theta)\,f_3 - \sin(\theta)\,f_4 + m_3\right)\right) \\ -m_2\left(y\cos(\theta) - x\sin(\theta) + \sin(\theta)\,f_3 - \cos(\theta)\,f_4 + m_4\right) \end{pmatrix} = 0$$

A.2 Spatial Pose Constraints

In three-dimension the three matrices $T_w^g(t)$, T_g^m, and T_w^f can be written as follows:

$$T_w^g(t) = \begin{pmatrix} \begin{pmatrix} \cos\alpha(t) & -\sin\alpha(t) & 0 \\ \sin\alpha(t) & \sin\alpha(t) & 0 \\ 0 & 0 & 1 \end{pmatrix} \begin{pmatrix} \cos\beta(t) & 0 & \sin\beta(t) \\ 0 & 1 & 0 \\ -\sin\beta(t) & 0 & \cos\beta(t) \end{pmatrix} \begin{pmatrix} 1 & 0 & 0 \\ 0 & \cos\gamma(t) & -\sin\gamma(t) \\ 0 & \sin\gamma(t) & \cos\gamma(t) \end{pmatrix} & \begin{matrix} x(t) \\ y(t) \\ z(t) \end{matrix} \\ 0 \qquad\qquad 0 \qquad\qquad 0 & 1 \end{pmatrix}$$

$$T_g^m = \begin{pmatrix} m_1 m_3 & -m_2 m_5 + m_1 m_4 m_6 & m_1 m_4 m_5 + m_2 m_6 & m_7 \\ m_2 m_3 & m_1 m_5 + m_2 m_4 m_6 & m_2 m_4 m_5 - m_1 m_6 & m_8 \\ -m_4 & m_3 m_6 & m_3 m_5 & m_9 \\ 0 & 0 & 0 & 1 \end{pmatrix}$$

$$T_w^f = \begin{pmatrix} f_1 f_3 & -f_2 f_5 + f_1 f_4 f_6 & f_1 f_4 f_5 + f_2 f_6 & f_7 \\ f_2 f_3 & f_1 f_5 + f_2 f_4 f_6 & f_2 f_4 f_5 - f_1 f_6 & f_8 \\ -f_4 & f_3 f_6 & f_3 f_5 & f_9 \\ 0 & 0 & 0 & 1 \end{pmatrix}$$

A.2.1 $\;\; T_f^m = T_f^w T_w^g(t) T_g^m$

The six pose constraints associated with the computation of T_f^m can be written as follows:

- No rotation around the axis x_f:

$$T_f^m(3,2) = 0 = m_3\, m_6 \left[\begin{array}{l} \cos(\beta)\cos(\gamma)\, f_3\, f_5 + \big(\cos(\gamma)\sin(\alpha)\sin(\beta) - \cos(\alpha)\sin(\gamma)\big)\big(f_2\, f_4\, f_5 - f_1\, f_6\big) \\ + \big(\cos(\alpha)\cos(\gamma)\sin(\beta) + \sin(\alpha)\sin(\gamma)\big)\big(f_1\, f_4\, f_5 + f_2\, f_6\big) \end{array} \right]$$

$$+ \big(-(m_2\, m_5) + m_1\, m_4\, m_6\big) \left[\begin{array}{l} -(\sin(\beta)\, f_3\, f_5) + \cos(\beta)\sin(\alpha)\big(f_2\, f_4\, f_5 - f_1\, f_6\big) \\ + \cos(\alpha)\cos(\beta)\big(f_1\, f_4\, f_5 + f_2\, f_6\big) \end{array} \right]$$

$$+ \big(m_1\, m_5 + m_2\, m_4\, m_6\big) \left[\begin{array}{l} \cos(\beta)\sin(\gamma)\, f_3\, f_5 + \big(\cos(\alpha)\cos(\gamma) + \sin(\alpha)\sin(\beta)\sin(\gamma)\big)\big(f_2\, f_4\, f_5 - f_1\, f_6\big) \\ + \big(-(\cos(\gamma)\sin(\alpha)) + \cos(\alpha)\sin(\beta)\sin(\gamma)\big)\big(f_1\, f_4\, f_5 + f_2\, f_6\big) \end{array} \right]$$

- No rotation around the axis y_f:

$$T_f^m(3,1) = 0 = \big(-(\sin(\beta)\, f_3\, f_5) + \cos(\beta)\sin(\alpha)\big(f_2\, f_4\, f_5 - f_1\, f_6\big) + \cos(\alpha)\cos(\beta)\big(f_1\, f_4\, f_5 + f_2\, f_6\big)\big) m_1\, m_3$$

$$+ \left[\begin{array}{l} \cos(\beta)\sin(\gamma)\, f_3\, f_5 + \big(\cos(\alpha)\cos(\gamma) + \sin(\alpha)\sin(\beta)\sin(\gamma)\big)\big(f_2\, f_4\, f_5 - f_1\, f_6\big) \\ + \big(-(\cos(\gamma)\sin(\alpha)) + \cos(\alpha)\sin(\beta)\sin(\gamma)\big)\big(f_1\, f_4\, f_5 + f_2\, f_6\big) \end{array} \right] m_2\, m_3$$

$$- \left[\begin{array}{l} \cos(\beta)\cos(\gamma)\, f_3\, f_5 + \big(\cos(\gamma)\sin(\alpha)\sin(\beta) - \cos(\alpha)\sin(\gamma)\big)\big(f_2\, f_4\, f_5 - f_1\, f_6\big) \\ + \big(\cos(\alpha)\cos(\gamma)\sin(\beta) + \sin(\alpha)\sin(\gamma)\big)\big(f_1\, f_4\, f_5 + f_2\, f_6\big) \end{array} \right] m_4$$

- No rotation around the axis z_f:

$$T_f^m(2,1) = 0 = m_1\, m_3 \Big[-(\sin(\beta)\, f_3\, f_6) + \cos(\alpha)\cos(\beta)\big(-(f_2\, f_5) + f_1\, f_4\, f_6\big) + \cos(\beta)\sin(\alpha)\big(f_1\, f_5 + f_2\, f_4\, f_6\big) \Big]$$

$$+ m_2\, m_3 \left[\begin{array}{l} \cos(\beta)\sin(\gamma)\, f_3\, f_6 + \big(-(\cos(\gamma)\sin(\alpha)) + \cos(\alpha)\sin(\beta)\sin(\gamma)\big)\big(-(f_2\, f_5) + f_1\, f_4\, f_6\big) \\ + \big(\cos(\alpha)\cos(\gamma) + \sin(\alpha)\sin(\beta)\sin(\gamma)\big)\big(f_1\, f_5 + f_2\, f_4\, f_6\big) \end{array} \right]$$

$$- m_4 \left[\begin{array}{l} \cos(\beta)\cos(\gamma)\, f_3\, f_6 + \big(\cos(\alpha)\cos(\gamma)\sin(\beta) + \sin(\alpha)\sin(\gamma)\big)\big(-(f_2\, f_5) + f_1\, f_4\, f_6\big) \\ + \big(\cos(\gamma)\sin(\alpha)\sin(\beta) - \cos(\alpha)\sin(\gamma)\big)\big(f_1\, f_5 + f_2\, f_4\, f_6\big) \end{array} \right]$$

- No translation around the axis x_f :

$$T_f^m(1,4) = 0 = x f_1 f_3 + y f_2 f_3 - z f_4 - f_1 f_3 f_7 - f_2 f_3 f_8 + f_4 f_9$$
$$+ m_7 \left(\cos(\alpha)\cos(\beta) f_1 f_3 + \cos(\beta)\sin(\alpha) f_2 f_3 + \sin(\beta) f_4 \right)$$
$$+ \left[\begin{array}{l} \left(-\left(\cos(\gamma)\sin(\alpha)\right) + \cos(\alpha)\sin(\beta)\sin(\gamma)\right) f_1 f_3 \\ + \left(\cos(\alpha)\cos(\gamma) + \sin(\alpha)\sin(\beta)\sin(\gamma)\right) f_2 f_3 - \cos(\beta)\sin(\gamma) f_4 \end{array} \right] m_8$$
$$+ \left[\begin{array}{l} \left(\cos(\alpha)\cos(\gamma)\sin(\beta) + \sin(\alpha)\sin(\gamma)\right) f_1 f_3 \\ + \left(\cos(\gamma)\sin(\alpha)\sin(\beta) - \cos(\alpha)\sin(\gamma)\right) f_2 f_3 - \cos(\beta)\cos(\gamma) f_4 \end{array} \right] m_9$$

- No translation around the axis y_f :

$$T_f^m(2,4) = 0 = z f_3 f_6 + x \left(-\left(f_2 f_5\right) + f_1 f_4 f_6 \right) + y \left(f_1 f_5 + f_2 f_4 f_6 \right)$$
$$- f_1 \left(f_4 f_6 f_7 + f_5 f_8 \right) + f_2 \left(f_5 f_7 - f_4 f_6 f_8 \right) - f_3 f_6 f_9$$
$$+ \left[\begin{array}{l} -\left(\sin(\beta) f_3 f_6\right) + \cos(\alpha)\cos(\beta)\left(-\left(f_2 f_5\right) + f_1 f_4 f_6 \right) \\ + \cos(\beta)\sin(\alpha)\left(f_1 f_5 + f_2 f_4 f_6 \right) \end{array} \right] m_7$$
$$+ \left[\begin{array}{l} \cos(\beta)\sin(\gamma) f_3 f_6 + \left(-\left(\cos(\gamma)\sin(\alpha)\right) + \cos(\alpha)\sin(\beta)\sin(\gamma)\right)\left(-\left(f_2 f_5\right) + f_1 f_4 f_6 \right) \\ + \left(\cos(\alpha)\cos(\gamma) + \sin(\alpha)\sin(\beta)\sin(\gamma)\right)\left(f_1 f_5 + f_2 f_4 f_6 \right) \end{array} \right] m_8$$
$$+ \left[\begin{array}{l} \cos(\beta)\cos(\gamma) f_3 f_6 + \left(\cos(\alpha)\cos(\gamma)\sin(\beta) + \sin(\alpha)\sin(\gamma)\right)\left(-\left(f_2 f_5\right) + f_1 f_4 f_6 \right) \\ + \left(\cos(\gamma)\sin(\alpha)\sin(\beta) - \cos(\alpha)\sin(\gamma)\right)\left(f_1 f_5 + f_2 f_4 f_6 \right) \end{array} \right] m_9$$

- No translation around the axis z_f :

$$T_f^m(3,4) = 0 = z f_3 f_5 + y \left(f_2 f_4 f_5 - f_1 f_6 \right) + x \left(f_1 f_4 f_5 + f_2 f_6 \right)$$
$$- f_1 f_4 f_5 f_7 - f_2 f_6 f_7 - f_2 f_4 f_5 f_8 + f_1 f_6 f_8 - f_3 f_5 f_9$$
$$+ \left(-\left(\sin(\beta) f_3 f_5\right) + \cos(\beta)\sin(\alpha)\left(f_2 f_4 f_5 - f_1 f_6 \right) + \cos(\alpha)\cos(\beta)\left(f_1 f_4 f_5 + f_2 f_6 \right) \right) m_7$$
$$+ \left[\begin{array}{l} \cos(\beta)\sin(\gamma) f_3 f_5 + \left(\cos(\alpha)\cos(\gamma) + \sin(\alpha)\sin(\beta)\sin(\gamma)\right)\left(f_2 f_4 f_5 - f_1 f_6 \right) \\ + \left(-\left(\cos(\gamma)\sin(\alpha)\right) + \cos(\alpha)\sin(\beta)\sin(\gamma)\right)\left(f_1 f_4 f_5 + f_2 f_6 \right) \end{array} \right] m_8$$
$$+ \left[\begin{array}{l} \cos(\beta)\cos(\gamma) f_3 f_5 + \left(\cos(\gamma)\sin(\alpha)\sin(\beta) - \cos(\alpha)\sin(\gamma)\right)\left(f_2 f_4 f_5 - f_1 f_6 \right) \\ + \left(\cos(\alpha)\cos(\gamma)\sin(\beta) + \sin(\alpha)\sin(\gamma)\right)\left(f_1 f_4 f_5 + f_2 f_6 \right) \end{array} \right] m_9$$

A.2.2 $\quad T_m^f = T_m^g T_g^w(t) T_w^f$

The six pose constraints associated with the computation of T_m^f can be written as follows:

- No rotation around the axis x_m:

$$T_m^f(3,2) = 0 = f_3\, f_6 \big(\cos(\beta)\cos(\gamma)\, m_3\, m_5 + \cos(\beta)\sin(\gamma)\big(m_2\, m_4\, m_5 - m_1\, m_6\big) - \sin(\beta)\big(m_1\, m_4\, m_5 + m_2\, m_6\big)\big)$$

$$+ \big(-(f_2\, f_5) + f_1\, f_4\, f_6\big) \begin{vmatrix} \big(\cos(\alpha)\cos(\gamma)\sin(\beta) + \sin(\alpha)\sin(\gamma)\big)m_3\, m_5 + \cos(\alpha)\cos(\beta)\big(m_1\, m_4\, m_5 + m_2\, m_6\big) \\ + \big(-(\cos(\gamma)\sin(\alpha)) + \cos(\alpha)\sin(\beta)\sin(\gamma)\big)\big(m_2\, m_4\, m_5 - m_1\, m_6\big) \end{vmatrix}$$

$$+ \big(f_1\, f_5 + f_2\, f_4\, f_6\big) \begin{vmatrix} \big(\cos(\gamma)\sin(\alpha)\sin(\beta) - \cos(\alpha)\sin(\gamma)\big)m_3\, m_5 + \cos(\beta)\sin(\alpha)\big(m_1\, m_4\, m_5 + m_2\, m_6\big) \\ + \big(\cos(\alpha)\cos(\gamma) + \sin(\alpha)\sin(\beta)\sin(\gamma)\big)\big(m_2\, m_4\, m_5 - m_1\, m_6\big) \end{vmatrix}$$

- No rotation around the axis y_m:

$$T_m^f(3,1) = 0 = -f_4 \big(\cos(\beta)\cos(\gamma)\, m_3\, m_5 + \cos(\beta)\sin(\gamma)\big(m_2\, m_4\, m_5 - m_1\, m_6\big) - \sin(\beta)\big(m_1\, m_4\, m_5 + m_2\, m_6\big)\big)$$

$$+ f_1\, f_3 \begin{vmatrix} \big(\cos(\alpha)\cos(\gamma)\sin(\beta) + \sin(\alpha)\sin(\gamma)\big)m_3\, m_5 + \cos(\alpha)\cos(\beta)\big(m_1\, m_4\, m_5 + m_2\, m_6\big) \\ + \big(-(\cos(\gamma)\sin(\alpha)) + \cos(\alpha)\sin(\beta)\sin(\gamma)\big)\big(m_2\, m_4\, m_5 - m_1\, m_6\big) \end{vmatrix}$$

$$+ f_2\, f_3 \begin{vmatrix} \big(\cos(\gamma)\sin(\alpha)\sin(\beta) - \cos(\alpha)\sin(\gamma)\big)m_3\, m_5 + \cos(\beta)\sin(\alpha)\big(m_1\, m_4\, m_5 + m_2\, m_6\big) \\ + \big(\cos(\alpha)\cos(\gamma) + \sin(\alpha)\sin(\beta)\sin(\gamma)\big)\big(m_2\, m_4\, m_5 - m_1\, m_6\big) \end{vmatrix}$$

- No rotation around the axis z_m:

$$T_m^f(2,1) = 0 = f_4 \big(\cos(\beta)\cos(\gamma)\, m_3\, m_6 - \sin(\beta)\big(-(m_2\, m_5) + m_1\, m_4\, m_6\big) + \cos(\beta)\sin(\gamma)\big(m_1\, m_5 + m_2\, m_4\, m_6\big)\big)$$

$$+ f_1\, f_3 \begin{vmatrix} \big(\cos(\alpha)\cos(\gamma)\sin(\beta) + \sin(\alpha)\sin(\gamma)\big)m_3\, m_6 + \cos(\alpha)\cos(\beta)\big(-(m_2\, m_5) + m_1\, m_4\, m_6\big) \\ + \big(-(\cos(\gamma)\sin(\alpha)) + \cos(\alpha)\sin(\beta)\sin(\gamma)\big)\big(m_1\, m_5 + m_2\, m_4\, m_6\big) \end{vmatrix}$$

$$+ f_2\, f_3 \begin{vmatrix} \big(\cos(\gamma)\sin(\alpha)\sin(\beta) - \cos(\alpha)\sin(\gamma)\big)m_3\, m_6 + \cos(\beta)\sin(\alpha)\big(-(m_2\, m_5) + m_1\, m_4\, m_6\big) \\ + \big(\cos(\alpha)\cos(\gamma) + \sin(\alpha)\sin(\beta)\sin(\gamma)\big)\big(m_1\, m_5 + m_2\, m_4\, m_6\big) \end{vmatrix}$$

- No translation around the axis x_m :

$$T_m^f(1,4) = 0 = m_1 m_3 \left(-\left(x\cos(\alpha)\cos(\beta)\right) - y\cos(\beta)\sin(\alpha) + z\sin(\beta)\right) - m_1 m_3 m_7 - m_2 m_3 m_8 + m_4 m_9$$

$$+ \left(\begin{array}{l} x\cos(\gamma)\sin(\alpha) - \left(z\cos(\beta) + y\sin(\alpha)\sin(\beta)\right)\sin(\gamma) \\ -\cos(\alpha)\left(y\cos(\gamma) + x\sin(\beta)\sin(\gamma)\right) \end{array}\right) m_2 m_3$$

$$- \left(\begin{array}{l} -\left(z\cos(\beta)\cos(\gamma)\right) - \sin(\alpha)\left(y\cos(\gamma)\sin(\beta) + x\sin(\gamma)\right) \\ +\cos(\alpha)\left(-\left(x\cos(\gamma)\sin(\beta)\right) + y\sin(\gamma)\right) \end{array}\right) m_4$$

$$+ f_9 \left(-\left(\sin(\beta) m_1 m_3\right) + \cos(\beta)\sin(\gamma) m_2 m_3 - \cos(\beta)\cos(\gamma) m_4\right)$$

$$+ f_8 \left(\begin{array}{l} \cos(\beta)\sin(\alpha) m_1 m_3 + \left(\cos(\alpha)\cos(\gamma) + \sin(\alpha)\sin(\beta)\sin(\gamma)\right) m_2 m_3 \\ -\left(\cos(\gamma)\sin(\alpha)\sin(\beta) - \cos(\alpha)\sin(\gamma)\right) m_4 \end{array}\right)$$

$$+ f_7 \left(\begin{array}{l} \cos(\alpha)\cos(\beta) m_1 m_3 + \left(-\left(\cos(\gamma)\sin(\alpha)\right) + \cos(\alpha)\sin(\beta)\sin(\gamma)\right) m_2 m_3 \\ -\left(\cos(\alpha)\cos(\gamma)\sin(\beta) + \sin(\alpha)\sin(\gamma)\right) m_4 \end{array}\right)$$

- No translation around the axis y_m :

$$T_m^f(2,4) = 0 = \left(\begin{array}{l} -\left(z\cos(\beta)\cos(\gamma)\right) - \sin(\alpha)\left(y\cos(\gamma)\sin(\beta) + x\sin(\gamma)\right) \\ +\cos(\alpha)\left(-\left(x\cos(\gamma)\sin(\beta)\right) + y\sin(\gamma)\right) \end{array}\right) m_3 m_6$$

$$+ \left(-\left(x\cos(\alpha)\cos(\beta)\right) - y\cos(\beta)\sin(\alpha) + z\sin(\beta)\right)\left(-\left(m_2 m_5\right) + m_1 m_4 m_6\right)$$

$$+ \left(\begin{array}{l} x\cos(\gamma)\sin(\alpha) - \left(z\cos(\beta) + y\sin(\alpha)\sin(\beta)\right)\sin(\gamma) \\ -\cos(\alpha)\left(y\cos(\gamma) + x\sin(\beta)\sin(\gamma)\right) \end{array}\right)\left(m_1 m_5 + m_2 m_4 m_6\right)$$

$$+ f_9 \left(\cos(\beta)\cos(\gamma) m_3 m_6 - \sin(\beta)\left(-\left(m_2 m_5\right) + m_1 m_4 m_6\right) + \cos(\beta)\sin(\gamma)\left(m_1 m_5 + m_2 m_4 m_6\right)\right)$$

$$+ f_7 \left(\begin{array}{l} \left(\cos(\alpha)\cos(\gamma)\sin(\beta) + \sin(\alpha)\sin(\gamma)\right) m_3 m_6 + \cos(\alpha)\cos(\beta)\left(-\left(m_2 m_5\right) + m_1 m_4 m_6\right) \\ +\left(-\left(\cos(\gamma)\sin(\alpha)\right) + \cos(\alpha)\sin(\beta)\sin(\gamma)\right)\left(m_1 m_5 + m_2 m_4 m_6\right) \end{array}\right)$$

$$+ f_8 \left(\begin{array}{l} \left(\cos(\gamma)\sin(\alpha)\sin(\beta) - \cos(\alpha)\sin(\gamma)\right) m_3 m_6 + \cos(\beta)\sin(\alpha)\left(-\left(m_2 m_5\right) + m_1 m_4 m_6\right) \\ +\left(\cos(\alpha)\cos(\gamma) + \sin(\alpha)\sin(\beta)\sin(\gamma)\right)\left(m_1 m_5 + m_2 m_4 m_6\right) \end{array}\right)$$

$$- m_1 \left(m_4 m_6 m_7 + m_5 m_8\right) + m_2 \left(m_5 m_7 - m_4 m_6 m_8\right) - m_3 m_6 m_9$$

- **No translation around the axis z_m:**

$$T_m^f(3,4) = 0 = \begin{pmatrix} -\left(z\cos(\beta)\cos(\gamma)\right) - \sin(\alpha)\left(y\cos(\gamma)\sin(\beta) + x\sin(\gamma)\right) \\ +\cos(\alpha)\left(-\left(x\cos(\gamma)\sin(\beta)\right) + y\sin(\gamma)\right) \end{pmatrix} m_3\, m_5$$

$$+\begin{pmatrix} x\cos(\gamma)\sin(\alpha) - \left(z\cos(\beta) + y\sin(\alpha)\sin(\beta)\right)\sin(\gamma) \\ -\cos(\alpha)\left(y\cos(\gamma) + x\sin(\beta)\sin(\gamma)\right) \end{pmatrix}\left(m_2\, m_4\, m_5 - m_1\, m_6\right)$$

$$+\left(-\left(x\cos(\alpha)\cos(\beta)\right) - y\cos(\beta)\sin(\alpha) + z\sin(\beta)\right)\left(m_1\, m_4\, m_5 + m_2\, m_6\right)$$

$$+f_7\begin{bmatrix} \left(\cos(\alpha)\cos(\gamma)\sin(\beta) + \sin(\alpha)\sin(\gamma)\right)m_3\, m_5 + \cos(\alpha)\cos(\beta)\left(m_1\, m_4\, m_5 + m_2\, m_6\right) \\ +\left(-\left(\cos(\gamma)\sin(\alpha)\right) + \cos(\alpha)\sin(\beta)\sin(\gamma)\right)\left(m_2\, m_4\, m_5 - m_1\, m_6\right) \end{bmatrix}$$

$$+f_8\begin{bmatrix} \left(\cos(\gamma)\sin(\alpha)\sin(\beta) - \cos(\alpha)\sin(\gamma)\right)m_3\, m_5 \\ +\left(\cos(\alpha)\cos(\gamma) + \sin(\alpha)\sin(\beta)\sin(\gamma)\right)\left(m_2\, m_4\, m_5 - m_1\, m_6\right) + \cos(\beta)\sin(\alpha)\left(m_1\, m_4\, m_5 + m_2\, m_6\right) \end{bmatrix}$$

$$+f_9\left(\cos(\beta)\cos(\gamma)\,m_3\, m_5 + \cos(\beta)\sin(\gamma)\left(m_2\, m_4\, m_5 - m_1\, m_6\right) - \sin(\beta)\left(m_1\, m_4\, m_5 + m_2\, m_6\right)\right)$$

$$-m_1\, m_4\, m_5\, m_7 - m_2\, m_6\, m_7 - m_2\, m_4\, m_5\, m_8 + m_1\, m_6\, m_8 - m_3\, m_5\, m_9$$

Appendix B

This appendix shows that a pure rotation path for a planar vertex-edge contact model can result in the partial explicit estimation of the contact parameters even though the excitation condition associated with the model is not satisfied.

B.1   Excitation Condition

As discussed in section 6.2.3, the excitation condition associated with the planar vertex-edge contact model illustrated in (6.12) requires that the dimension of the nullspace of the excitability matrix M is equal to one.

$$M = \begin{pmatrix} d\theta & dx & dy & 0 \\ d^2\theta & d^2x & d^2y & d\theta^2 \\ d^3\theta - d\theta^3 & d^3x & d^3y & 3d^2\theta d\theta \\ d^4\theta - 6d^2\theta d\theta^2 & d^4x & d^4y & 4d^3\theta d\theta + 3d^2\theta^2 - d\theta^4 \end{pmatrix} \quad \text{(B.1)}$$

The dimension of the nullspace of M is path dependent. For a pure rotation, as parameterized in (B.2), the dimension of the nullspace of M is equal to two.

$$\begin{cases} x(t) = x_0 + r\cos\big(\theta(t)+\theta_0\big) \\ y(t) = y_0 + r\sin\big(\theta(t)+\theta_0\big) \end{cases} \qquad\qquad (B.2)$$

<u>Proof</u>: $\dim\big(Ker(M)\big) = 2$

The determinant and the 3×3 minors of M are all equal to zero when substituting

(B.2) in (B.1). Therefore the dimension of the nullspace of M is equal to two. The

explicit computations of the determinant and the minors are not shown in this document;

however, they can easily be computed using a computer algebra package (e.g.,

Mathematica).

B.2   Partial Explicit Estimation

This section computes the closed-form solution for the parameters associated with the

planar vertex-to-edge contact (6.12) using the four-step technique summarized in (6.32).

The first two steps resulting in: 1) the expression of the model parameters as a function of

the Taylor coefficients, and 2) the excitability matrix M have already been presented in

(6.20) and (6.25) respectively. This section focuses on the two remaining steps.

B.2.1 Step3 - Taylor coefficients as a function of the nullspace of M

Since the nullspace of M is of dimension two, two Taylor coefficients are

independent of the nullspace components. These two free variables are chosen arbitrarily

to be f_y and $f_{\theta\theta}$. As shown in (B.3), the constraint equation on the Taylor Coefficients (i.e., $p_1^2 + p_2^2 = 1$) is used to constraint one of the free variables.

$$
\begin{cases}
\begin{pmatrix} f_\theta \\ f_x \\ f_y \\ f_{\theta\theta} \end{pmatrix} = \begin{pmatrix} N_{11} \\ N_{21} \\ 1 \\ 0 \end{pmatrix} f_y + \begin{pmatrix} N_{12} \\ N_{22} \\ 0 \\ 1 \end{pmatrix} f_{\theta\theta} \\[3em]
p_1^2 + p_2^2 = 1 \Rightarrow f_x^2 + f_y^2 = 1 \Rightarrow f_{\theta\theta} = \dfrac{-f_y N_{21} N_{22} \pm \sqrt{(1 - f_y^2) N_{22}^2}}{N_{22}^2}
\end{cases}
\tag{B.3}
$$

B.2.2   Step 4 – Nullspace of M as a function of the path variables

Using rows and columns manipulations, the matrix M can be rewritten in row echelon form as follows:

$$
M \sim \begin{pmatrix}
1 & 0 & \dfrac{-M_{13}M_{22} + M_{12}M_{23}}{-M_{22}M_{11} + M_{21}M_{12}} & \dfrac{-M_{14}M_{22} + M_{12}M_{24}}{-M_{22}M_{11} + M_{21}M_{12}} \\[1.5em]
0 & 1 & \dfrac{-M_{23}M_{11} + M_{21}M_{13}}{-M_{22}M_{11} + M_{21}M_{12}} & \dfrac{-M_{24}M_{11} + M_{21}M_{14}}{-M_{22}M_{11} + M_{21}M_{12}} \\[1.5em]
0 & 0 & 0 & 0 \\[0.5em]
0 & 0 & 0 & 0
\end{pmatrix}
\tag{B.4}
$$

The four components of the nullspace can be expressed using the row echelon form matrix (B.4), as shown in (B.5). The path equation (B.2) and the matrix (B.4) are utilized to express the nullspace of M as a function of the path variables.

$$N_{11} = \frac{-M_{13}M_{22} + M_{12}M_{23}}{M_{22}M_{11} - M_{21}M_{12}} = -\frac{r}{\cos(\theta + \theta_o)}$$

$$N_{12} = \frac{-M_{14}M_{22} + M_{12}M_{24}}{M_{22}M_{11} - M_{21}M_{12}} = \tan(\theta + \theta_o)$$

$$N_{21} = \frac{-M_{23}M_{11} + M_{21}M_{13}}{M_{22}M_{11} - M_{21}M_{12}} = -\tan(\theta + \theta_o)$$

$$N_{22} = \frac{-M_{24}M_{11} + M_{21}M_{14}}{M_{22}M_{11} - M_{21}M_{12}} = \frac{1}{r\cos(\theta + \theta_o)}$$

(B.5)

B.2.3 Explicit estimation

To obtain a closed-form solution for the parametersl, the Taylor coefficients obtained from the substitution of the nullspace values (B.5) into the Taylor coefficients (B.3) are substituted into the set of equations (6.20). This final substitution results in the explicit estimation of the parameters p_3 and p_4 shown in (B.6). The other parameters are not explicitly estimable since they depend on the unknown free variable f_y.

$$\begin{cases} p_1 = \pm\sqrt{1 - f_y^2} \\ p_2 = -f_y \\ p_3 = \dfrac{-\cos\theta - N_{12}\sin\theta}{N_{22}} \\ p_4 = \dfrac{\sin\theta - N_{12}\cos\theta}{N_{22}} \\ p_5 = \dfrac{\sqrt{(1 - f_y^2)N_{22}^2}(N_{22}x - 1) - f_y N_{22}(N_{21} + N_{22}y)}{N_{22}^2} \end{cases}$$

(B.6)

Bibliography

Ambler, A. and Popplestone, R. (1975). Inferring the Positions of Bodies from Specified Spatial Relationships. *Artificial Intelligence*, Vol. 6, No. 2, pp.157-174.

Armstrong, B. (1989). On Finding Exciting Trajectories for Identification Experiments Involving Systems with Nonlinear Dynamics. *The International Journal of Robotics Research,* Vol. 8, No. 6, pp. 28-48.

Arnold, V. (1989). *Mathematical Methods of Classical Mechanic*s. Springer-Verlag, New York.

Arras, K. (1998). An Introduction to Error Propagation: Derivation, Meaning, and Examples of Equation $C_Y = F_X C_X F_X^T$. *Technical Report EPFL-ASL-TR-98-01 R3*. Swiss Federal Institute of Technology.

Asada, H. (1990). Teaching and Learning of Compliance Using Neural Nets: Representation and Generation of Nonlinear Compliance. *Proceedings of the International Conference on Robotics and Automation*, pp. 1237-1244.

Asada, H., and Hirai, S. (1989). Towards a Symbolic-Level Force Feedback: Recognition of Assembly Process States. *Proceedings of the 5th International Symposium of Robotics Research*, pp. 341-346.

Atkeson, C., An, C., and Hollerbach, J. (1986). Estimation of Inertial Parameters of Manipulators Loads and Links. *The International Journal of Robotics Research*, Vol. 5, No. 3, pp. 101-119.

Ball, R. (1900). *A Treatise on the Theory of Screws*. Cambridge University Press.

Bates, D., and Watts, D. (1988). *Nonlinear Regression Analysis and its Applications.* Wiley, New York.

Baum, L. and Petrie, T. (1966). Statistical Inference for Probabilistic Functions of Finite State Markov Chains. *The Annals of Mathematical Statistics*, Vol. 37, pp. 1554-1563.

Breipohl, A., (1970). *Probabilistic Systems Analysis: An introduction to Probabilistic Models, Decisions, and Applications of Random Processes.* Wiley, New York.

Brost, R, and Mason, M, (1989). Graphical Analysis of Planar Rigid-Body Dynamics with Multiple Frictional Contacts. *Proceedings of the 5th International Symposium of Robotics Research,* pp. 293-300.

Bruyninckx, H. (1995). *Kinematics Models for Robot Compliant Motion with Identification of Uncertainties.* Ph.D Thesis, Katholieke Universiteit Leuven, Belgium.

Bruyninckx, H., Demey, S., Dutré, S., and De Schutter, J. (1995). Kinematic Models for Model-Based Compliant Motion in the Presence of Uncertainty. *The International Journal of Robotics Research*, Vol. 14, No. 5, pp. 465-482.

Cai, C., and Roth, B. (1987). On the Spatial Motion of a Rigid Body with Point Contact. *Proceedings of the International Conference on Robotics and Automation,* pp. 686-695.

Chapell, M., Godfrey, K., and Vajda, S. (1990). Global Identifiability of Non-Linear Systems with Specified Inputs: a Comparison of Methods. *Mathematical Biosciences*, Vol. 102, pp. 41-73.

De Schutter, J., and Van Brussel, H. (1988). Compliant Robot Motion I. A Formalism for Specifying Compliant Motion Tasks. *The International Journal of Robotics Research*, Vol. 7, No. 4, pp. 3-17.

De Schutter, J., Bruyninckx, H., Dutre, S., De Geeter, J., Katupitiya, J., Demey, S., Lefebvre, T. (1999). Estimating First Order Geometric Parameters and Monitoring Contact Transitions During Force Controlled Compliant Motion. *The International Journal of Robotics Research*, Vol. 18, No. 12, pp. 1161-1184.

Debus, T (2000). *Automatic Identification of Local Geometric Properties During Teleoperation.* Master Thesis, Boston University, Department of Aerospace and Mechanical Engineering.

Debus, T., Dupont, P., and Howe, R. (2004). Contact State Estimation using Multiple Model Estimation and Hidden Markov Models. *The International Journal of Robotics Research*, Vol. 23, No. 4/5, pp. 399-414.

Debus, T., Stoll, J., Howe, R. and Dupont, P. (2001). Combined Human and Machine Perception in Teleoperated Assembly. *Proceedings of the 7th International Symposium on Experimental Robotics, D. Rus and S. Singh (Eds.) Springer, New York*, pp. 51-60.

Denavit, J, and Hartenberg, R. (1955). A Kinematic Notation for Lower-Pair Mechanisms Based on Matrices. *Journal of Applied Mechanics*, Vol. 77, pp. 215-221.

Desai, R., and Volz, R. (1989). Identification and Verification of Termination Conditions in Fine Motion in Presence of Sensor Errors and Geometric Uncertainties. *Proceedings of the International Conference on Robotics and Automation*, pp. 800-807.

Donald, B., Jennings, J. (1991). Sensor Interpretation and Task-Directed Planning Using Perceptual Equivalence Classes. *Proceedings of the International Conference on Robotics and Automation*, pp. 190-197.

Dougherty, E. (1990). *Probability and Statistics for the Engineering, Computing, and Physical Sciences*. Prentice Hall, Englewood Cliff, N.J.

Duffy, J. (1990). The Fallacy of Modern Hybrid Control theory that is Based on "Orthogonal Complements" of Twist and Wrench Spaces. *Journal of Robotic Systems*, Vol. 7, No. 2, pp. 139-144.

Dupont, P., Schulteis, T., Millman, P., and Howe, R. (1999). Automatic Identification of Environment Haptic Properties. *PRESENCE: Teleoperators and Virtual Environments*, Vol. 8, No. 4, pp. 392-409.

Eberman, B. (1995). *Contact Sensing: A Sequential Decision Approach to Sensing Manipulation Contact Features*. Ph.D Thesis, M.I.T, Artificial Intelligence Laboratory.

Eberman, B. (1997). A Model-Based Approach to Cartesian Manipulation Contact Sensing. *The International Journal of Robotics Research*, Vol. 16, No. 4, pp. 508-528.

Eberman, B., and Salisbury, J. (1994). Application of Change Detection to Dynamic Contact Sensing. *International Journal of Robotics Research,* Vol. 13, No. 5, pp. 369-394.

Erdmann, M. (1986). Using Backprojections for Fine Motion Planning with Uncertainty. *The International Journal of Robotics Research*, Vol. 5, No. 1, pp. 19-45.

Farahat, A., Graves, B., and Trinckle., J. (1995b). Identifying Contact Formations in the Presence of Uncertainty. *Proceedings of the International Conference on Intelligent Robots and Systems,* pp. 59-64.

Farahat, A., Stiller, P., and Trinckle., J. (1995a). On the Geometry of Contact Formation Cells for Systems of Polygons. *IEEE Transactions on Robotics and Automation*, Vol. 11, No. 4, pp. 522-536.

Gautier, M, and Khalil, W. (1990). Direct Calculation of Minimum Set of Inertial Parameters of Serial Robots. *IEEE Transactions on Robotics and Automation*, Vol. 6, No. 3, pp. 368-373.

Gautier, M. and Khalil, W. (1992). Exciting Trajectories for the Identification of Base Inertial Parameters of Robots. *The International Journal of Robotics Research,* Vol. 11, No. 4, pp. 362-375.

Gill, P., Murray, W., and Wright, M. (1981). *Practical Optimization*. Academic Press, New York.

Glad, S., and Ljung, L. (1990). Model Structure Identifiability and Persistence of Excitation. *Proceedings of the 29th International Conference on Decision and Control*, pp. 3236-3240.

Grewal, M.S., and Glover, K. (1976). Identifiability of linear and nonlinear dynamical systems. *IEEE Transactions on Automatic Control*, Vol. 21, pp 833-837.

Hannaford, B., and Lee, P. (1991). Hidden Markov Modal Analysis of Force/Torque Information in Telemanipulation. *The International Journal of Robotics Research*, Vol. 10, No. 5, pp. 528-539.

Hirai, S. (1994). Identification of Contact States Based on a Geometric Model for Manipulative Operations. *Advanced Robotics*, Vol. 8, No. 2, pp. 139-155.

Hirai, S., and Asada, H. (1993). Kinematics and Statics of Manipulation Using the Theory of Polyhedral Convex Cones. *The International Journal of Robotics Research*, Vol. 12, No. 5, pp. 434-447.

Hirukawa, H., Papegay, Y., and Matsui, T. (1994). A Motion Planning Algorithm for Convex Polyhedra in Contact under Translation and Rotation. *Proceedings of the International Conference on Robotics and Automation,* pp. 3020-3027.

Hollerbach, M.., and Wampler, C. (1996). The Calibration Index and Taxonomy for Robot Kinematic Calibration Methods. *The International Journal of Robotics Research*, Vol. 15, No. 6, pp. 573-591.

Hovland, G., and McCarragher, B. (1998). Hidden Markov Models as a Process Monitor in Robotics Assembly. *The International Journal of Robotics Research,* Vol. 17, No. 2, pp. 153-168.

Hwang, Y., and Ahuja, N. (1992). Gross Motion Planning – A Survey. *ACM Computing Surveys*, Vol. 24, No. 3, pp. 219-291.

Khalil, W., Gautier, M., and Enguehard, C. (1991). Identifiable Parameters and Optimum Configurations for Robots Calibration. *Robotica*, Vol. 9, pp. 63-70.

Lawson, C. L., and Hanson, R. J. (1974). *Solving Least Squares Problems*. Prentice-Hall Series in Automatic Computation, Englewood Cliffs, N.J.

Lecourtier, Y., Walter, E., and Bertrand, P. (1982). Identifiability Testing for State-Space Models. *The 6th IFAC Symposium on Identification and System Parameter Estimation*, pp. 794-799.

Lefebvre, T., Bruyninckx, H., and De Schutter, J. (2003). Polyhedral Contact Formation Modeling and Identification for Autonomous Compliant Motion. *IEEE Transactions on Robotics and Automation*, Vol. 19, No. 1, pp. 26-41.

Lefebvre, T.; Bruyninckx, H.; DeSchutter, J. (2005). Polyhedral Contact Formation Identification for Autonomous Compliant Motion: Exact Nonlinear Bayesian Filtering. *IEEE Transactions on Robotics and Automation*, Vol. 21, No. 1, pp. 124-129.

Ljung, L. (1987). *System Identification: Theory for the User*. Prentice-Hall, Englewood Cliffs, NJ.

Ljung, L., and Glad, T. (1994). On Global Identifiability for Arbitrary Model Parametrizations. *Automatica*, Vol. 30, No. 2, pp. 265-276.

Lozano-Perez, T. (1981). Automatic Planning of Manipulator Transfer Movements. *IEEE Transactions on Systems, Man, and Cybernetics*, Vol. 11, No. 10, pp. 681-689.

Lozano-Perez, T. (1983). Spatial Planning: A Configuration Space Approach. *IEEE Transactions on Computers*, Vol. 32, No. 2, pp. 108-120.

Lozano-Perez, T., Mason, M., and Taylor, R. (1984). Automatic Synthesis of Fine-Motion Strategies for Robots. *The International Journal of Robotics Research*, Vol. 3, No. 1, pp. 3-24.

Luo, Q., Staffetti, E., and Xiao, J. (2004). On the Representation of Contact States Between Curved Objects. *Proceedings of the International Conference on Robotics and Automation*, Vol. 4, pp. 3589-3595.

Mason, M. (1981). Compliance and Force Control for Computer Controlled Manipulators. *IEEE Transactions on Systems, Man, and Cybernetics*, Vol. 11, No. 6, pp. 418-432.

McCarragher, B. (1996). Task Primitives for the Discrete Event Modeling and Control of 6-DOF Assembly Tasks. *IEEE Transactions on Robotics and Automation*, Vol. 12, No. 2, pp. 280-289.

McCarragher, B., and Asada, H. (1993). Qualitative Template Matching Using Dynamic Process Models for State Transition Recognition of Robotic Assembly. *ASME Journal of Dynamic Systems, Measurement, and Control*, Vol. 155, pp. 261-269.

McCarragher, B., and Asada, H. (1995a). The Discrete Event Control of Robotic Assembly Tasks. *ASME Journal of Dynamic Systems, Measurement, and Control*, Vol. 117, pp. 384-393.

McCarragher, B., and Asada, H. (1995b). The Discrete Event Modeling and Trajectory Planning of Robotic Assembly Tasks. *ASME Journal of Dynamic Systems, Measurement, and Control*, Vol. 117, pp. 394-400.

Montana, D. (1988). The Kinematics of Contact and Grasp. *The International Journal of Robotics Research*, Vol. 7, No. 3, pp. 17-32.

Murray, M., Li, Z., and Sastry, S. (1994). *A Mathematical Introduction to Robotic Manipulation*. Boca Raton: CRC Press.

Park, W. (1997). Minicomputer Software Organization for Control of Industrial Robots. *Proceedings of the Joint Automatic Control Conference*.

Pohjanpalo, H. (1978). System Identifiability based on the power Series Expansion of the Solution. *Mathematical Biosciences*, Vol. 41, pp 21-33.

Pook, P., and Ballard, D. (1993). Recognizing Teleoperated Manipulations. *Proceedings of the IEEE International Conference on Robotics and Automation*, Vol. 2, pp. 578-585.

Press, W., Teukoleski, S., Vetterling, T., and Flannery, B. (1992). *Numerical Recipes in C: The Art of Scientific Computing, Second Edition*. Cambridge University Press.

Rabiner, L. (1989). A Tutorial on Hidden Markov Models and Selected Applications in Speech Recognition. *Proceedings of the IEEE*, Vol. 77, No. 2, pp. 257-286.

Raksanyi, A., Lecourtier, Y., Walter, E., and Venot, A. (1985). Identifiability and Distinguishability Testing Via Computer Algebra. *Mathematical Biosciences*, Vol. 77, pp. 245-266.

Rosell, J., Suárez, R, and Basañez, L. (2001). Path Validation in Constrained Motion with Uncertainty. *Proceedings of the International Conference on Intelligent Robots and Systems,* pp. 2270-2275.

Schröer, K., Uhl, L., Albright, S., and Huttenhofer, M. (1992). Ensuring Solvability and Analyzing Results of the Nonlinear Robot Calibration Problem. *Proceedings of the 2nd International Symposium on Measurement and Control in Robotics*, pp. 851-858.

Sheu, S., and Walker, M. (1989). Basis Sets for Manipulator Inertial Parameters. *Proceedings of the International Conference on Robotics and Automation*, pp. 1517-1522.

Simunovic, S. (1979). *An Information Approach to Part Mating*. Ph.D thesis, M.I.T.

Skubic, M., and Volz, R. (2000). Identifying Single-Ended Contact Formations from Force Sensor Patterns. *IEEE Transactions on Robotics and Automation*, Vol. 16, No. 5, pp. 597-603.

Swevers, J., Ganseman, C., Tukel, D.B., De Schutter, J., and Van Brussel, H. (1997). Optimal Robot Excitation and Identification. *IEEE Transactions on Robotics and Automation*, Vol. 13, No. 5, pp.730-740.

Vajda, S., Godfrey, K., and Rabitz, H. (1989). Similarity Transformation Approach to Identifiability Analysis of Nonlinear Compartmental Models. *Mathematical Biosciences*, Vol. 93, pp 217-248.

Walter, A., Lecourtier, Y., Raksanyi, A. (1985). On the Distinguishability of Parametric Models with Different Structures. *Mathematics and Computers in Biomedical Applications, IMACS, J. Eisenfeld and C. DeLisi (editors), Elsevier Science Publishers B.V.*, pp 145-160.

Walter, E., Lecourtier, Y., and Happel, J. (1984). On the Structural Output Distinguishability of Parametric Models, and its Relations with Structural Identifiability. *IEEE Transactions on Automatic Control*, Vol. 29, No. 1, pp. 56-57.

Walter, E., Pronzato, L. (1996). On the Identifiability and Distinguishability of Nonlinear Parametric Models. *Mathematics and Computers in Simulation*, Vol. 42, pp. 125-134.

Whitney, D. (1982). Quasi-Static Assembly of Compliantly Supported Rigid Parts. *Journal of Dynamic Systems, Measurement, and Control*, Vol. 104, pp. 65-77.

Wilson, R. (1985). *Introduction to Graph Theory*. Third Edition, Longman, Harlow, Essex, England.

Xiao, J. (1993). Automatic Determination of Topological Contacts in the Presence of Sensing Uncertainties. *Proceedings of the International Conference on Robotics and Automation*, pp. 65-70.

Xiao, J., and Ji, X. (2001). On Automatic Generation of High-level Contact State Space. *The International Journal of Robotics Research*, Vol. 20, No. 7, pp. 584-606.

Xiao, J., and Lianzhong, L. (1998). Contact States: Representation and Recognizability in the Presence of Uncertainties. *Proceedings of the International Conference on Intelligent Robots and Systems*, Vol. 2, pp. 1151-1156.

Xiao, J., and Zhang, L. (1997). Contact Constraint Analysis and Determination of Geometrically Valid Contact Formations from Possible Contact Primitives. *IEEE Transactions on Robotics and Automation,* Vol. 13, No. 3, pp. 456-466.

Vita

Thomas Debus
thomas.debus@gmail.com
87 Waltham ST, Apt#4, Boston, MA 02118

EDUCATION

Boston University, College of Engineering, Boston, MA   May 2005
Ph.D., Mechanical Engineering, Dynamics and Control
Dissertation: "Modeling by Manipulation – Enhancing Robot Perception through Contact State Estimation"
Advisor: Pierre E. Dupont

Boston University, College of Engineering, Boston, MA   January 2000
M.S., Mechanical Engineering, Dynamics and Control
Thesis: "Automatic Identification of Local Geometric Properties During Teleoperation"
Advisor: Pierre E. Dupont

University of Versailles, Versailles, France   June 1996
M.S., Robotics and Automation
Thesis: "Design, Realization and Control of a Light Manipulator Arm"
Advisor: Nasser K. M'Sirdi

University of Versailles, Versailles, France   June 1995
B.S., Mechanical Engineering

AWARDS and HONORS

- Research Fellowship, Boston University, 2000-2005.
- Teaching Fellowship, Boston University, 1998-2000.

RESEARCH EXPERIENCE

Graduate Research Assistant, Boston University, Boston, MA   May 2005

Developed a novel framework for achieving contact-based robot perception in manipulation tasks in a project sponsored by the National Science Foundation. This framework is the most flexible and versatile for contact state estimation in poorly known environments.

- Designed analytical tools to test the feasibility of robotic assembly tasks in poorly known environments.
- Developed sensor-based algorithms for man-machine cooperation in unstructured assembly tasks.
- Designed and implemented statistical estimators to identify object properties during tele-manipulation.
- Tested the complete framework for a teleoperated connector insertion task.
- Developed kinematic, velocity and force models of contact formations between manipulated objects.
- Evaluated the effects of a multi-channel vibrotactile display for teleoperated assembly tasks.

Research Assistant, Harvard BioRobotics Laboratory,   Summer, 1998 – 2001
Harvard University, Cambridge, MA

Responsible for the design and implementation of several teleoperation control schemes.

- Developed a C library for the control of a Barrett Whole Arm Manipulator robot.
- Implemented a force reflecting controller for a teleoperation system composed of two PHANToM® robots.

Teaching Assistant in Control Theory and Mechanics of Materials   1998 to 2001
Boston University, Boston, MA

- Taught a half-semester of graduate state-space control theory.
- Tutored undergraduate students in control theory and mechanics of materials.

Control Engineer, Naval Institute Laboratory ENSIETA, Brest, France   1996 to 1997

- Designed a multivariable sliding mode controller for an autonomous underwater vehicle.

Mechanical Engineer Intern, Robotics Laboratory of Paris, Summer 1996
Velizy, France

Responsible for the design, realization, and control of a three-link serial robotic arm with flexible distal joint.

- Built the arms using carbon fiber parts.
- Implemented a gravity compensator, motion controller, and feedforward dynamic compensator.
- Developed the robot-human interface using Matlab/Simulink under Dspace environment.

Mechanical Engineer Intern, Robotics Laboratory of Paris, Summer 1995
Velizy, France

- Kinematic and dynamic analysis of a climbing robot using a solid dynamic package (SDS from Solid Dynamics).

PUBLICATIONS

1. Thomas Debus, Pierre Dupont, and Robert Howe (2005). "Distinguishability and Identifiability Testing of Contact State Models," *Advanced Robotics, Special Issue on Compliant motion*, to appear June 2005.

2. Thomas Debus, Pierre Dupont, and Robert Howe (2004). "Contact State Estimation using Multiple Model Estimation and Hidden Markov Models," *The International Journal of Robotics Research,* Vol. 23, no. 4-5, pp. 399-413.

3. Thomas Debus and Pierre Dupont (2004). "Distinguishability and Identifiability of Contact States," *Proceedings of the IEEE International Conference on Robotics and Automation*, New Orleans, pp. 1135-1140.

4. Thomas Debus, Pierre Dupont, Tae-Jeong Jang, and Robert Howe (2004). "Multi-channel Vibrotactile Display for Teleoperated Assembly," *International Journal of Control, Automation, and Systems*, Vol.2, no.3, pp. 390-397.

5. Thomas Debus, Pierre Dupont, and R. Howe (2003). "Contact State Estimation using Multiple Model Estimation and Hidden Markov Models," *Experimental Robotics VIII, Springer Tracts in Advanced Robotics*, Vol. 5, B. Siciliano and Paolo Dario (Eds.), Springer, New York, pp. 517-526.

6. Thomas Debus, Pierre Dupont, Tae-Jeong Jang, and Robert Howe (2002). "Multichannel Vibrotactile Display for Teleoperated Assembly," *Proceedings of the IEEE International Conference on Robotics and Automation*, Washington D.C., pp. 592-597.

PUBLICATIONS (Continued)

7. Thomas Debus, Theresia Becker, Pierre Dupont, Tae-Jeong Jang, and Robert Howe (2001). "Multichannel Vibrotactile Display for Sensory Substitution During teleoperation," *Telemanipulator and Telepresence Technologies VIII Conference, Proceedings of the SPIE Vol. 4570*, Newton, MA, pp. 42-49.

8. Thomas Debus, Jeff Stoll, Robert Howe, and Pierre Dupont (2000). "Cooperative Human and Machine Perception in Teleoperated Assembly," *Experimental Robotics VII, Lecture Notes in Control and Information Sciences,* Vol. 271, D. Rus and S. Singh (Eds.), Springer, New York, pp. 51-60.

9. Thomas Debus, Pierre Dupont, and Robert Howe (2000). "Automatic Identification of Local Geometric Properties During Teleoperation," *IEEE International Conference on Robotics and Automation*, San Francisco, pp. 3428-3434.

10. Robert Howe, Thomas Debus, and Pierre Dupont (1999). "Twice the Fun: Two Phantoms as a High-Performance Telemanipulation System," *Proceedings of the Fourth Annual PHANTOM Users Group Workshop*, Dedham, MA, pp. 56-58.

11. Thomas Debus, Pierre Dupont, and Robert Howe (1999). "Automatic Property Identification via Parameterized Constraints," *Proceedings of the IEEE International Conference on Robotics and Automation*, Detroit, MI, pp. 1876-1881.

12. Robert Howe, Thomas Debus, and Pierre Dupont (1998). "Haptic Identification of Remote Environment Properties," *SPIE International Symposium on Intelligent Systems and Advanced Manufacturing, Proceedings of the SPIE Vol. 3524*, Boston, MA, pp. 123-130.